Designing Green Walls: An Early-Design Framework to Estimate the Cooling Impact of Indirect Green Walls on Buildings in Six Different Climates

HARVARD UNIVERSITY
Graduate School of Design

THESIS ACCEPTANCE CERTIFICATE

The undersigned, appointed by the Doctor of Design Program, have examined a dissertation entitled

Designing green walls: An early-design framework to estimate the cooling impact of indirect vining green walls on buildings in six different climates

Presented by

Arta Yazdanseta

candidate for the Doctor of Design degree and hereby certify that it is worthy of acceptance.

Signature ______________________
Professor Ali Malkawi

Signature ______________________
Professor Holly Samuelson

Signature ______________________
Professor David Tilley

Date: October 27, 2017

Designing Green Walls: An Early-design Framework to Estimate the Cooling Impact of Indirect Green Walls on Buildings in Six Different Climates

A dissertation presented

by

Arta Yazdanseta

to

The Harvard University Graduate School of Design

In partial fulfillment of requirements for the degree of

Doctor of Design

Harvard University Graduate School of Design

Cambridge, Massachusetts

October 2017

Advisors:
Professor Ali Malkawi
Professor Holly Samuelson
Professor David Tilley

Author: Arta Yazdanseta

Designing Green walls: An Early-design Tool to Estimate the Cooling Impact of Indirect Green Walls on Buildings in Six Different Climates

Abstract

Green walls are a component of urban green infrastructure and if designed properly, require only moderate human intervention and maintenance during their lifespans (Cameron, Taylor, & Emmett, 2014). The benefits of green walls are numerous for both building and urban scales.

Green walls reduce building heat gain by providing shade (Ip, Lam, & Miller, 2010) and increasing surface albedo (Holm, 1989). They offer thermal insulation for buildings by acting as wind screens and cavity walls (Susorova, Azimi, & Stephens, 2014) and improve indoor air quality by trapping airborne pollutants (Ottelé, van Bohemen, & Fraaij, 2010). Furthermore, they negate the urban heat island effect through solar radiation interception and transpiration (McPherson, Nowak, & Rowntree, 1994). Green walls are also an effective solution for storm water management, provide ecosystem services, and improve the quality of human life (Meier, 1990).

A literature review from this field highlighted three major problems: (a) lack of an effective method for making research findings useful to practitioners, (b) limited understanding of the morphological and biophysical characteristics of vines, and (c) lack of a standardized research methodology across the field.

The objective of this research is to provide practitioners with a series of matrices to easily and quickly evaluate the cooling efficacy of indirect green walls during the early phase of a project. These matrices

account for the biophysical traits of the plants used, canopy geometry, and environmental variables for six climatic scenarios.

The climate scenarios are based on summer conditions (e.g., ambient temperatures, precipitation, and relative humidity) and are broken down into the following climates: cool and humid, cool and dry, warm and humid, warm and dry, hot and humid, and hot and dry.

Special attention is given to plant biophysics and performance evaluation methods used in fields such as biophysical ecology and agronomy. The cooling effect of green walls is broken down into two major components: transpiration (W/m^2) and solar radiation interception, or shading (W/m^2).

A modified version of the FAO 56 method was used to evaluate the cooling power produced. FAO 56 is a method developed by the Food and Agriculture Organization of the United Nations to estimate the transpiration rate of crop fields. Additionally, a library of stomatal resistances for 97 vine species expanding through 13 countries was created from measurements from existing field studies.

Variables impacting the transpiration rate were reviewed and possible green wall designs corresponding with the maximum cooling power for each climate condition were investigated. The results show that canopies with a resistance of lower than 100 s/m, a height of 3 to 6 m, and Leaf Area Index (*LAI*) of 3 or larger produce the maximum possible cooling power. Taking into account the aforementioned design considerations (*LAI* and height), and average stomatal resistance, it is estimated that the largest cooling power (300 W/m^2) corresponds with the hot and dry climate. The smallest cooling power (50 W/m^2) corresponds with the cool and dry climate.

Similarly, variables impacting the shading effect of indirect green walls are reviewed. A technique for estimating the extinction coefficient of a canopy by combing empirical and statistical methods is introduced. The predicted solar interception calculations show good agreement with field study measurements, with only ±10% margins of error.

Three sets of matrices for designers are introduced. The first two sets provide designers with the cooling power values (W/m^2) of various green wall designs in six climatic scenarios through transpiration and solar radiation reduction. These values show good agreement with the findings of other studies. The results show an average summer cooling power of 42 W/m^2 for the cool and dry climate and 176 W/m^2 for the hot and dry climate. These two sets of matrices are intended to provide designers with back-of-the-envelope estimations of the cooling power of green walls during the early design phase of a project.

The last set of matrices provides designers with the cooling effects of green walls through transpiration and solar radiation interception as a percentage of total incident solar radiation received by the canopy in each climatic scenario.

The cooling power from transpiration accounts for 20% to 30% of the cooling effect of green walls for cool and dry, cool and humid, and warm and humid climates. The contribution from transpiration increases to 48% for warm and dry climates, and 52% for hot and humid climates. The largest contribution from transpiration occurs in hot and dry climates (99%) due to the oasis effect.

For almost all climates, the cooling effect of solar radiation interception was approximately 70%, 80%, and 90% for Leaf Area Indices of 3, 4, and 5, respectively.

The results show that the total cooling power of green walls exceeds 100% for all climates. The canopy not only provides shading, but also acts as a heat sink by storing solar radiation energy in water and releasing it to the environment as vapor via latent heat transfer.

The largest cooling power values correspond with the hot climate, followed by the warm and cool climates. The percentage of cooling power from transpiration in dry climates is larger than that in humid climates. The exception is the cool and dry climate. This exception is due to the high canopy resistance associated with the cool and dry climate.

Table of Contents

Abstract ..... *iii*

Table of Contents ..... *vi*

Acknowledgements ..... *viii*

List of Symbols ..... *ix*

List of Tables ..... *xi*

List of Figures ..... *xiii*

1. Introduction *1*

2. Research Objectives and Questions *3*

3. Literature Review *4*

3.1. Vegetative Façade Types **4**

3.2. The Thermal Impact of Green Walls on Buildings **5**

3.3. Research Methodology Review **8**

3.4. Climate and Site Considerations **10**

3.5. Design Considerations **10**

3.5.1. Building Design and Material 10
3.5.2. Support Structure & Container Design 13
3.5.3. Air Cavity Design 14
3.5.4. Plant Biophysical Trait and Energetics Considerations 16

3.6. Discussion and Conclusions **19**

4. Background *21*

4.1. Plant Biophysical Ecology **21**

4.1.1. Leaf Scale Energy Balance 21
4.1.2. Radiation Influence on Leaf Temperature 22
4.1.3. Convection Influence on Leaf Temperature 26
4.1.4. Transpiration Influence on Leaf Temperature 29
4.1.5. Plant Energetics 33

4.2. Climbers Types, Morphology, and Biomechanics **35**

4.2.1. Climber Types 35
4.2.2. Vines Anatomy and Stem Morphology 37
4.2.3. Vines Biomechanics Types 38
4.2.4. Vines Structural Support 41

4.3. Indirect Green Walls Design Considerations....43

4.3.1. 2D Indirect Green Walls....43
4.3.2. 3D Indirect Green Walls....44
4.3.3. Planter Locations....44

5. Cooling from Indirect Green Walls.... 46

5.1. Cooling from Canopy Transpiration....46

5.1.1. Introduction....47
5.1.2. Model Development....48
5.1.3. Stomatal Resistance Library....61
5.1.4. Model Sensitivity Analysis....64
5.1.5. Model Verification-Climatic Scenario Studies....70
5.1.6. Design Optimization - Aerodynamic and Canopy Resistances Sensitivity Analysis....73

5.2. Cooling from Canopy Solar Interception....88

5.2.1. Introduction....88
5.2.2. Methodology....90
5.2.3. Leaf Area Index....90
5.2.4. Extinction Coefficient....91
5.2.5. Sensitivity Analysis....104
5.2.6. Scenario Study....105
5.2.7. Statistical vs. Empirical Extinction Coefficient Evaluation....118

6. Matrix for Designers.... 122

6.1. Transpiration Matrix—Cooling Power Production for Six Climatic Scenarios....125

6.2. Solar Interception Matrix—Heat Gain Reduction for Six Climate Scenarios....134

6.3. A Simplified Matrix for Designers....139

7. Contributions and Discussion.... 144

7.1. Areas for Further Investigations....145

7.2. Instructions for Use of Matrices....147

7.2.1. A Case Study – Seasonal Cooling Performance Evaluation....148
7.2.2. A Case Study – Monthly Cooling Performance Evaluation....150

References.... 153

Appendix.... 169

Acknowledgements

I am indebted to my supervisors: Professor Ali Malkawi, who generously provided support and mentorship from the very beginning through the final steps of this research, and Professor Holly Samuelson, who kept me steady by continuously reminding me not to lose sight of the bigger picture. I would also like to thank Professor David Tilley for his time and expertise.

I would like to express my gratitude to Professor Leslie Norford at MIT, who kindly and patiently helped me to unpack and understand some of the most challenging parts of this research.

I am grateful to Professor Salmon Craig for many challenging discussions that have inspired me to think outside the box and question our existing design paradigm.

I am thankful to my parents and sister for their unwavering support, encouragement, and patience. Kheyli mamnoonam, azizanam.

Last but not least, I am thankful to Collin Vierra, my partner in crime, for his emotional and intellectual support throughout each step during the past three years. Merci, Khers-e-man!

List of Symbols

C	energy transferred by convection [MJ/m^2.h, MJ/m^2.d]
C_p	specific heat of dry air at constant pressure [MJ/kg°C]
d	zero plane displacement height [m]
d_m	number of days in a month
d_r	inverse relationship Earth-Sun distance
$e_{(T)}$	saturation vapor pressure at the air temperature T [kPa]
e_a	actual vapor pressure [kPa]
e_a	actual vapor pressure [kPa]
e_{Tmax}	saturation vapor pressure at monthly maximum temperature [kPa]
e_{Tmin}	saturation vapor pressure at monthly minimum temperature [kPa]
G_{sc}	solar constant, 0.0820 [MJ/m^2.min]
h	height of the canopy [m]
I	total incident radiation, flux density at the surface, irradiance passing through a canopy [W/m^2]
I_0	flux density normal to the beam, irradiance at the top of the canopy [W/m^2]
I_a	absorbed incident radiation [W/m^2]
I_r	reflected incident radiation [W/m^2]
$I_{s(max)}$	the maximum shortwave radiation [W/m^2]
I_{st}	the irradiance t hours after the sunrise [W/m^2]
I_t	transmitted incident radiation [W/m^2]
J	number of days in a year
k	extinction coefficient [-]
K	amount of daylight time in a month [s]
K_{time}	a unit time conversion, equal to 86,400 s/day for mm/day and 3,600 s/h for mm/h
k_{von}	Von Kaman's constant, 0.41 [-]
LAI	Leaf Area Index [-]
LAI_{Sunlit}	sunlit Leaf Area Index (LAI) [-]
N	the daylight hours [hr]
N_h	number of daylight hours in the 15th day of a month
P	atmospheric pressure [kPa]
Q_a	amount of energy absorbed by the surface [MJ/m^2.h, MJ/m^2.d]
r	total leaf diffusion resistance to water vapor [s/m]
R	radiation emitted from the leaf
r_a	canopy aerodynamic resistance [s/m]
R_a	extraterrestrial radiation [MJ/m^2.day]
r_c	the canopy resistance [s/m]
r_{ct}	leaf cuticular resistance [s/m]
RH_{max}	monthly maximum relative humidity [%]
RH_{min}	monthly minimum relative humidity [%]
r_i	leaf intercellular air-space resistance [s/m]
r_l	leaf resistance/Bulk stomatal resistance [s/m]
$r_{l,a}$	leaf aerodynamic resistance [s/m]
R_n	net radiation absorbed by the canopy [MJ/m^2.h, MJ/m^2.d]
R_{nl}	net outgoing long wave radiation [[MJ/m^2.h, MJ/m^2.d]
R_{ns}	net short wave radiation [MJ/m^2.h, MJ/m^2.d]
R_s	shortwave radiation [MJ/m^2.day] (for this study the values were simulated using *Diva for Rhino* software)
R_{so}	clear-sky radiation [MJ/m^2. day]

r_{st}	leaf stomatal resistance [s/m]
t	hour after the sunrise [hr]
T	air temperature [°C]
T_{max}	maximum monthly air temperature [°C, K]
T_{mean}	mean monthly air temperature [°C]
T_{min}	minimum monthly air temperature [°C, K]
TR	canopy transpiration rate [mm/h, mm/d]
U	wind speed
u_z	wind speed at height Z [m/s]
VPD	apor pressure deficit of air [kPa]
w_s	sunset hour angle [rad]
Z	elevation above sea level [m]
Z_0	roughness length height taken as 0.13xh[m]
Z_{0h}	roughness length governing transfer of heat and vapor [m]
Z_{0m}	roughness length governing momentum transfer [m]
Z_h	height of humidity measurement [m]
Z_m	height of wind measurements [m]
Z_w	height of the measurement of wind speed, 2 m

α	the angle between the beam and the normal to the surface (Zenith)
β	solar elevation angle (solar altitude) [°]
γ	the Psychrometric constant [kPa/°C]
δ	solar declination [rad]
Δ	the slope of saturation vapor pressure vs. temperature [kPa/°C]
ε	ratio molecular weight of water vapor/dry air, 0.622
θ	the azimuth difference between the leaf and the sun's azimuth
λ	the latent heat of vaporization of water [MJ/kg]
λE	energy exchange by transpiration [$MJ/m^2.h$, $MJ/m^2.d$]
ρ	the density of dry air [kg/m^3]
σ	Stefan-Boltzmann constant [4.903 x 10^-9 $MJ/K^4.m^2.day$)
ϕ	latitude [rad]

List of Tables

Table 1. Considered six climate scenarios 61

Table 2. Geographical distribution of the recoded vines 62

Table 3. Average, high and low values of the stomatal resistances of grapevines and urban vibes for various climates 64

Table 4. Considered values of variables for P-M model sensitivity analysis 65

Table 5. Six climatic scenarios and the considered corresponding U.S cities 70

Table 6. Considered biophysical variables for climatic scenario studies 71

Table 7. Extinction coefficient, k, as function of solar altitude, β, for various leaf angle distributions. (a: where x is the ratio of the horizontal to the vertical axis of the elliptical and A≈ (x + 1.774 (x + 1.182) - 0.733)/x, (Jones 1992)) 90

Table 8. Leaf inclination angles for various vines 100

Table 9. Extinction coefficients, k, for various leaf inclinations, α, and solar altitudes, β 100

Table 10. Comparative study of extinction coefficient, k. values using the detailed, Lumeur and Blad (1974), and general, Equation (29, methods for New York City and Miami from 6 a.m. to 6 p.m. of the 15th of each summer month. 102

Table 11. Simulated solar radiation values for the six United States cities representative of each climatic condition. 106

Table 12. Monthly average extinction coefficient, k_{avg}, for each summer month for six climatic scenario. B_{max}: solar noon elevation. 107

Table 13. a) Calculated average daily extinction coefficients from the 15th of each summer month (see Section 5.2.6 for the method of calculation). b) Calculated ratios between k values according to the baseline; i.e., themonth of August at a latitude of 40°. c) The adjusted extinction coefficient values for the summer months of various latitudes according to the baseline of the month of August at a latitude of 40° 121

Table 14. Estimated average transpiration cooling power for cool climatic scenarios for well-watered, south- and west-facing canopies for each June, July, and August. Assumed design variables: LAI of 3, height of 3 m, no wind condition (0.1 m/s), and average leaf resistances (r_l s/m) obtained for each climate. (For a detailed discussion of the assumed vine biophysical traits and climate scenario selections, see the section on Cooling from Canopy Transpiration.) 126

Table 15. Estimated average transpiration cooling power for warm climatic scenarios for well-watered, south- and west-facing canopies for June, July, and August. Assumed design variables: LAI of 3,

height of 3 m, no wind condition (0.1 m/s), and average leaf resistances (r_l s/m) obtained for each climate. (For a detailed discussion of the assumed vine biophysical traits and climate scenario selections, see chapter on Cooling from Canopy Transpiration.) 127

Table 16. Estimated average transpiration cooling power for hot climate scenarios for well-watered, south- and west-facing canopies for June, July, and August. Assumed design variables: LAI of 3, height of 3 m, no wind condition (0.1 m/s), and average leaf resistances (r_l s/m) obtained for each climate. (For detailed discussion of the assumed vine biophysical traits and climate scenario selections, see section on Cooling from Canopy Transpiration.) 127

Table 17. Solar radiation reduction (w/m^2 and %) for cool climates (latitude of 48°) for each summer month, for south- and west-facing orientations, and LAI values of 3, 4, and 5 (for a detailed discussion of the extinction coefficient, k, see Section 5.2.4) 137

Table 18. Solar radiation reduction (w/m^2) for warm climates (latitude of 40°) for each summer month, for south- and west-facing orientations, and LAI values of 3, 4, and 5 (for a detailed discussion of the extinction coefficient, k, see Section 5.2.4) 137

Table 19. Solar radiation reduction (w/m^2) for hot climates (latitudes of 32° and 25°) for each summer month, for south- and west-facing orientations, and LAI values of 3, 4, and 5 (for a detailed discussion of the extinction coefficient, k, see Section 5.2.4) 138

Table 20. Percentage of cooling power from the transpiration and shading effects of various LAIs (3, 4, and 5) of south- and west-facing green walls for cool climates. Assumed variables: height of 3 m, average canopy resistance, no wind condition. 140

Table 21. Percentage of cooling power from the transpiration and shading effects of various LAIs (3, 4, and 5) of south-and west-facing green walls for warm climates. Assumed variables: height of 3 m, average canopy resistance, no wind condition. 140

Table 22. Percentage of cooling power from the transpiration and shading effects of various LAIs (3, 4, and 5) of south- and west-facing green walls for hot climates. Assumed variables: height of 3 m, average canopy resistance, no wind condition. 140

List of Figures

Figure 1. Diagrammatic representation of green facades and the canopy relation to a building façade....... 4

Figure 2. Exchange of energy between a plant and its surrounding environment through radiation, convection, and conduction 21

Figure 3. Typical spectral properties of a broad leaf. Reproduced from Gates (1980)............................. 25

Figure 4. Flow types in fluids. Left, laminar flow boundary layer. Right, turbulent dl flow boundary layer 27

Figure 5. Typical leaf structure 30

Figure 6. Exchange of CO_2 and H_2O from stomata of a leaf 32

Figure 7. Number of considered vines per climate 62

Figure 8. Number of occurrences of irrigation patterns for each climate condition 63

Figure 9. Stomatal resistance, r_l, averages and ranges per climate conditions for grapevine and urban vines (non-agricultural vines)... 64

Figure 10. Transpiration as a function of Vapor Pressure Deficit and Radiation (see Table 4 for considered variables). Considered variables unless otherwise indicated; u = 0.8 m /s, Rn = 100 W/m^2, Air temperature = 20 °C, Relative humidity = 50%, Stomatal conductance = 4 mm /s....................... 66

Figure 11. Transpiration as a function of Radiation and Wind Velocity (see Table 4 for considered variables), Considered variables unless otherwise indicated; u = 0.8 m /s, Rn = 100 W/m^2, Air temperature = 20 °C, Relative humidity = 50%, Stomatal conductance = 4 mm /s....................... 67

Figure 12. Transpiration as a function of Wind Speed and Radiation (see Table 4 for considered variables), Considered variables unless otherwise indicated; u = 0.8 m /s, Rn = 100 W/m^2, Air temperature = 20 °C, Relative humidity = 50%, Stomatal conductance = 4 mm /s 68

Figure 13. Transpiration as a function of Canopy/Surface Resistance and Wind Speed (see Table 4 for considered variables), Considered variables unless otherwise indicated; u = 0.8 m /s, Rn = 100 W/m^2, Air temperature = 20 °C, Relative humidity = 50%, Stomatal conductance = 4 mm /s 69

Figure 14. Summer daily average canopy transpiration rates from the developed model and published field experiments 72

Figure 15. Summer average monthly cooling power values per climatic condition.................................. 72

Figure 16. Cooling power as a function of canopy surface resistance (r_c, s/m) and aerodynamic resistance (r_a, s/m) for the month of July. Dashed lines indicate the average, low, and high r_c values of grapevines and urban vines. See Table 5 for environmental variable values. 77

Figure 17. r_c (s/m) as a function of r_l (s/m) and LAI per climate scenario 78

Figure 18. Cooling power as a function of LAI for month of July, r_a =12.3 s/m. See Table 5 for environmental variable values. 79

Figure 19. Aerodynamic resistance (r_a) as a function of canopy height (h) and wind speed (u) 80

Figure 20. Month of June cooling power of south facing canopy in various climates as a function of canopy resistance (r_c) and aerodynamic resistance (r_a) for various canopy heights (3 m, 6 m, and 9 m) and wind speeds (0.1m/s and 2 m/s). The pink bar represents the average r_c values per climate with 10% possible changes. The highlighted cooling power values correspond with 6 m canopy height..... 82

Figure 21. Month of June cooling power of west facing canopy in various climates as a function of canopy resistance (r_c) and aerodynamic resistance (r_a) for various canopy heights (3 m, 6 m, and 9 m) and wind speeds (0.1 m/s and 2 m/s). The pink bar represents the average r_c values per climate with 10% possible changes. The highlighted cooling power values correspond with 6 m canopy height. 83

Figure 22. Month of July cooling power of south facing canopy in various climates as a function of canopy resistance (r_c) and aerodynamic resistance (r_a) for various canopy heights (3 m, 6 m, and 9 m) and wind speeds (0.1 m/s and 2 m/s). The pink bar represents the average per climate with 10% possible changes. The highlighted cooling power values correspond with a 6 m canopy height. 84

Figure 23. Month of July cooling power of west facing canopy in various climates as a function of canopy resistance (r_c) and aerodynamic resistance (r_a) for various canopy heights (3 m, 6 m, and 9 m) and wind speeds (0.1m/s and 2 m/s). The pink bar represents the average r_c values per climate with 10% possible changes. The highlighted cooling power values correspond with a 6 m canopy height. . 85

Figure 24. Month of Aug cooling power of south facing canopy in various climates as a function of canopy resistance (r_c) and aerodynamic resistance ($_{ra}$) for various canopy heights (3 m, 6 m, and 9 m) and wind speeds (0.1 m/s and 2 m/s). The pink bar represents the average r_c values per climate with 10% possible changes. The highlighted cooling power values correspond with 6 m canopy height. 86

Figure 25. Month of Aug cooling power of west facing canopy in various climates as a function of canopy resistance (r_c) and aerodynamic resistance (r_a) for various canopy heights (3 m, 6 m, and 9 m) and wind speeds (0.1m/s and 2 m/s). The pink bar represents the average r_c values per climate with 10% possible changes. The highlighted cooling power values correspond with 6 m canopy height..... 87

Figure 26. High cordon system using a non-VSP shoot arrangement (Erwin Elsner, 2014)...................... 93

Figure 27. Guyot training system using a VSP shoot arrangement (Erwin Elsner, 2014).......................... 93

Figure 28. A leaf orientation defined in a spherical system coordinate. β: Solar altitude angle, α: the angle between a projection normal to the leaf surface and the zenith, which is equal to the angle between the leaf and the horizon, θ: the azimuth difference between the leaf and the sun's azimuth (redrawn from R. Lumeur and B. Blad, 1974) 97

Figure 29. Extinction coefficient, k, as a function of solar elevation, β 101

Figure 30. Fraction of light transmittance through a canopy as a function of the extinction coefficient, k, for various Leaf Area Indices (LAI values). The dotted lines are k values obtained from empirical and statistical methods. See Section 5.2.4 for a detailed discussion. 105

Figure 31. The monthly average extinction coefficients of summer months for various climates. (C&D: cool and dry, C&H: cool and humid, W&D: warm and dry, W&H: warm and humid, H&D: hot and dry, H&H: hot and humid) 108

Figure 32. Solar radiation transmitted through the canopy, I, as a function of extinction coefficient, k, for various LAI values for a south-facing green wall in the month of June. The dotted lines are the referenced k values from the empirical and statistical methods (see Section 5.2.4 for details). The highlighted pink texts show the transmitted radiation for a green wall with an LAI of 5 and corresponding daily average extinction coefficient. 110

Figure 33. Solar radiation transmitted through the canopy, I, as a function of extinction coefficient, k, for various LAI values for a west-facing green wall in the month of June. The dotted lines are the referenced k values from the empirical and statistical methods (see Section 5.2.4 for details). The highlighted pink texts show the transmitted radiation for a green wall with an LAI of 5 and corresponding daily average extinction coefficient. 111

Figure 34. Solar radiation transmitted through the canopy, I, as a function of extinction coefficient, k, for various LAI values for a south-facing green wall in the month of July. The dotted lines are the referenced k values from the empirical and statistical methods (see Section 5.2.4 for details). The highlighted pink texts show the transmitted radiation for a green wall with an LAI of 5 and corresponding daily average extinction coefficient. 112

Figure 35. Solar radiation transmitted through the canopy, I, as a function of extinction coefficient, k, for various LAI values for a west-facing green wall in the month of July. The dotted lines are the referenced k values from the empirical and statistical methods (see Section 5.2.4 for details). The highlighted pink texts show the transmitted radiation for a green wall with an LAI of 5 and corresponding daily average extinction coefficient. 113

Figure 36. Solar radiation transmitted through the canopy, I, as a function of extinction coefficient, k, for various LAI values for a south-facing green wall in the month of August. The dotted lines are the referenced k values from the empirical and statistical methods (see Section 5.2.4 for details). The highlighted pink texts show the transmitted radiation for a green wall with an LAI of 5 and corresponding daily average extinction coefficient. 114

Figure 37. Solar radiation transmitted through the canopy, I, as a function of extinction coefficient, k, for various LAI values for a west-facing green wall in the month of August. The dotted lines are the referenced k values from the empirical and statistical methods (see Section 5.2.4 for details). The highlighted pink texts show the transmitted radiation for a green wall with an LAI of 5 and corresponding daily average extinction coefficient. 115

Figure 38. Percentage of solar transmittance as a function of various latitudes for south- and west-facing green walls in the month of June. The k values obtained from the statistical method (Table 12) were used for calculations. 117

Figure 39. Percentage of solar transmittance as a function of various latitudes for south- and west-facing green walls in the month of July. The k values obtained from the statistical method (Table 12) were used for calculations. 117

Figure 40. Percentage of solar transmittance as a function of various latitudes for south- and west- facing green walls in the month of August. The k values obtained from the statistical method (Table 12) were used for calculations. 118

Figure 41. Average cooling power for south-facing green wall. Assumed variables: well-watered condition, LAI of 3, height of 3 m, average leaf resistance per climatic scenario, no wind condition. 129

Figure 42. Average cooling power for west-facing green wall. Assumed variables: well-watered condition, LAI of 3, height of 3 m, average leaf resistance per climatic scenario, no wind condition. 129

Figure 43. Transpiration cooling power of south-facing green walls as a function of average monthly solar radiation. Assumed variables: well-watered condition, LAI of 3, height of 3 m, average leaf resistance per climatic scenario (r_l m/s), no wind condition. 132

Figure 44. Transpiration cooling power of south-facing green walls as a function of average monthly solar radiation. Assumed variables: well-watered condition, LAI of 3, height of 3 m, leaf resistance of 100 s/m, no wind condition. 134

Table 23. Boston, MA summer months climate conditions. 148

1. Introduction

Several recent projects emphasize the crucial role of green infrastructure for the future of our cities and buildings: the 2015 Milan World Expo, Paris 2050, Million Trees NYC project and the Liuzhou Forest City project in China. Arguably, one can trace this new trend to Chicago's 1994 Urban Forest Project by E. McPherson et al. (JONNES, 2011). This project revolutionized urban forest research by estimating the monetary value of a tree in terms of energy savings and environmental benefits (McPherson & Rowntree, 1993; McPherson et al., 1997; Nowak et al., 1996).

Vegetative surfaces lower surrounding temperatures by providing shading and transpiration. Much work has been done to quantify the impact of green infrastructure on remediating the urban heat island (UHI) effect, reducing the energy loads of buildings, and reducing CO2 emissions. For example, Huang et al. (1987) estimated that a 25% increase in urban canopy cover with optimally located trees could reduce peak load electrical consumption by 44% in Los Angeles, California. Their analysis showed that most of the savings would be attributed to evapotranspiration, and that only 10% to 40% of the total savings would be due to shading.

Green infrastructure contributes to the reduction of CO2 emissions by substituting vegetative cooling for electricity use, primarily by reducing the need for air conditioning during summer months and peak load times. Vegetative surfaces can reduce peak load demands by 8% to 12% (McPherson & Rowntree, 1993). Thus, green infrastructure can reduce both CO2 emissions and burdens on utility companies (Hacker & Holmes, 2007).

Green walls are a particularly promising component of green infrastructure (Cameron et al., 2014). They are cost effective and, if designed properly, require minimal human intervention and maintenance over their lifespans (Hunter et al., 2014; Mitsch & Jorgensen, 2003; Mitsch, 2012). While it takes 5 to 15 years for a tree to grow large enough to provide energy savings (McPherson & Rowntree, 1993), vines can cover large spaces in only a few years (Tilley, Price, Matt, & Marrow, 2012).

Furthermore, green walls have small footprints compared to trees. Thus, they are a perfect solution for dense urban areas. Indirect green walls are highly robust and customizable too, because vines can be easily trained to different support structures.

The environmental advantages of green walls are numerous. In hot weather, green walls reduce the urban heat island effect by providing shading and transpiration (Akbari, Kurn, Bretz, & Hanford, 1997; McPherson et al., 1994; Nowak et al., 1996). In cold weather they insulate buildings by acting as wind screens and cavity walls (Köhler, 2008; Pérez, Rincón, Vila, González, & Cabeza, 2011). Green walls both attenuate noise and improve air quality by trapping airborne pollutants (Ottelé et al., 2010). They also help capture storm water surges and provide ecological services (Buccola & Spolek, 2011; Rowe, 2011).

Research on urban forests is extensive, but research on the impact of green walls on the energy consumption of buildings is limited. There are no comprehensive methodologies that allow designers to evaluate the efficacy of green walls for specific projects during the early design phase.

The main problem is that current studies aim to define the performance of green walls on a short temporal scale (mostly hourly timeframes). Taking measurements at this scale of resolution is both time and labor intensive. As a result, these investigations are primarily useful only to academics. To be useful to practitioners, the temporal scale of resolution must be expanded. Any method for estimating the cooling power of green walls must be sufficiently quick and simple to be of any use to designers.

2. Research Objectives and Questions

The objective of this dissertation is to develop an early-design-phase decision-making framework for estimating the cooling effects of indirect green walls on buildings in different climates. The primary and secondary research questions this dissertation aims to answer are as follows:

Primary:

- Is it possible to evaluate the cooling performance of green walls during the early design phase of a project with a fast and relatively simple method?
- Is it possible to create a green wall performance matrix that can account for climatic conditions, biophysical plant traits, green wall design, and building façade thermal properties?

Secondary:

- How precise must such a matrix be to be useful to designers during the early phase of a project?
- What are the appropriate practical methods for evaluating the cooling of a green wall from the shading and transpiration of a green wall?

3. Literature Review

3.1. Vegetative Façade Types

Vegetative facades can be categorized into three main types: living walls, direct green walls, and indirect green walls (Cameron et al., 2014; Hunter et al., 2014; Perini, Ottelé, Haas, & Raiteri, 2011). (See Figure 1.) Living walls are a relatively new design solution. They consist of plants hosted in artificial substrates. Hydroponic technology is used for irrigation and nutrient diffusion. A variety of living wall systems are available in the market, including in-situ living wall panels, prefabricated living walls, foam-based systems, and planter box systems (Perini et al., 2011). Living walls are attractive but expensive, require heavy maintenance, and have relatively short lifespans compared to green walls (Green Roofs for Healthy Cities, 2008).

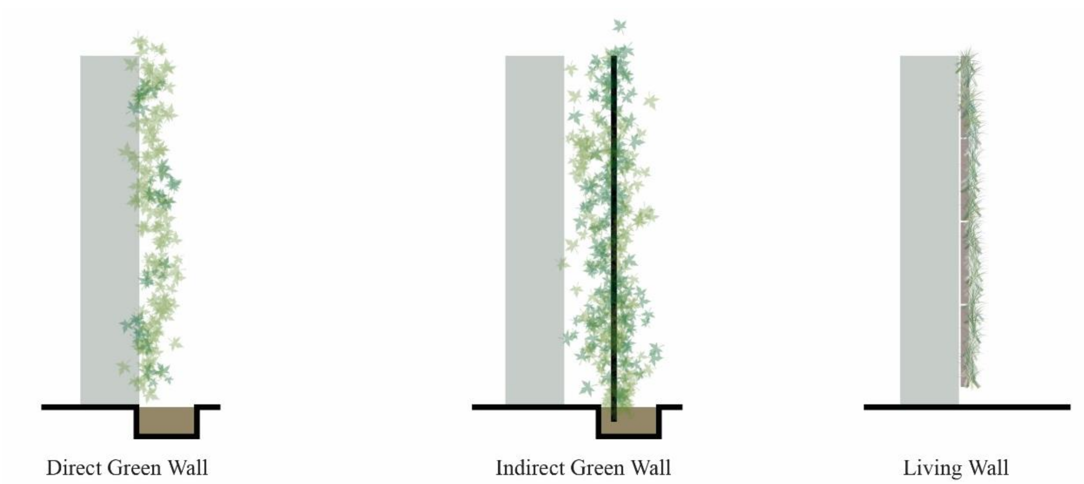

Figure 1. Diagrammatic representation of green facades and the canopy relation to a building façade

Direct green walls utilize clinging climbers—plants with adventitious roots and adhesive disk tendrils—to create a vegetative surface (Isnard & Silk, 2009). Some of the most common plant types for direct green walls are English ivy (*Hedera helix*), Boston ivy (*Parthenocissus tricuspidata*), and Virginia creeper (*Parthenocissus quinquefolia*). These high-climbing plants (up to 20 m) are hardy, drought tolerant, and require minimal maintenance (Cameron et al., 2014; Hunter et al., 2014). Direct green walls are the least costly of the three systems under discussion because they are supported by buildings, and the vines they utilize are vigorous. However, the aggressive nature of the useable vines limits the usefulness of direct green walls to masonry buildings.

Indirect green walls also use vines. These systems utilize climbing vines such as twining plants, leaf climbers, and tendril bearers, and provide independent structures to support the vegetative canopy (Cameron et al., 2014). Because the support structure is affixed to a building façade, indirect green walls can be used for different building construction types. The resulting cavity between the green wall and the building façade enhances the energy performance of the building by acting as an insulating layer (Hunter et al., 2014; Perini et al., 2011).

Furthermore, the geometry of the vegetative canopy of an indirect green wall can be adjusted to control the thermal performance of the overall structure (Schumann, 2007). Thus, indirect green walls provide a robust design system.

3.2. The Thermal Impact of Green Walls on Buildings

Green walls impact the energy performance of buildings. However, the extent of this impact depends on (a) the thermal and spectral properties of the façade (Šuklje, Medved, & Arkar, 2016; Tilley et al., 2012); (b) the design, plant health, biophysical characteristics, and orientation of the green wall (Tilley et al., 2012); and c) the climatic conditions of the site (Cameron et al., 2014; Hunter et al., 2014).

During the summer, green walls reduce the solar heat gain of buildings by intercepting solar radiation (Coma et al., 2017; Eumorfopoulou & Kontoleon, 2009; Holm, 1989; Hoyano, 1988; Kontoleon & Eumorfopoulou, 2010; Pérez, Coma, Sol, & Cabeza, 2017). Green walls also reduce building infiltration rates by reducing natural and forced convection flows. They create an insulating air layer between the façade and the vegetative layer (Hunter et al., 2014; Perini et al., 2011; Šuklje et al., 2016) and cool the microclimates around buildings via evapotranspiration (Alexandri & Jones, 2008; Hoelscher, Nehls, Jänicke, & Wessolek, 2016; Koyama, Yoshinaga, Hayashi, Maeda, & Yamauchi, 2013; Tan, Wong, Tan, Ismail, & Wee, 2017; Yin et al., 2017).

The cooling effects of green walls from solar radiation interception or shading (in terms of the reduction in façade surface temperatures) is well documented (Ip et al., 2010; Pérez et al., 2011; Susorova et al., 2014; Wang, 1999).

In Berlin, Germany (latitude 50°), M. Hoellsher et al. (2016) found that south-, southwest-, and east-facing direct green walls reduced façade temperatures by up to 11.3 °C. In Ljubljana, Slovenia (latitude 46°), a south-facing indirect green wall reduced façade temperatures by up to 29 °C (Šuklje et al., 2016).

In Chicago, IL (latitude 41°), north-, south-, west-, and east-facing direct green walls reduced façade temperatures by up to 1.8 °C, 3.0 °C, 11.1 °C, and 12.6 °C respectively (Susorova et al., 2014). In Lleida, Spain (latitude 41°), a south facing green wall reduced façade temperatures by up to 15.18 °C (Pérez et al., 2011).

Di & Wang investigated the cooling effect of an ivy layer on a west-facing façade in Beijing, China (latitude 39°). They reported an average 4.5 °C surface temperature reduction during the summer months (Wang, 1999). A. Hayona (1988) measured the cooling effect of a west-facing vine layer on a residential building in Tokyo, Japan (latitude 35°) during the summer months, and reported an 18 °C surface temperature reduction.

There have been limited investigations into the impact of green walls on a building's infiltration rate. Vegetative walls act as wind barriers and reduce air infiltration caused by pressure differences between the interior and exterior of buildings. Considering that remediating air infiltration contributes 33% of a building's total energy consumption in cold climates, green walls can significantly reduce building energy consumption (Susorova et al., 2014).

Only a few studies have investigated the cooling power of green walls through transpiration. Most plants cannot survive leaf surface temperatures higher than 40°C (Gates, 1980). Therefore, to cope with excess heat, leaf temperatures are regulated through transpiration; and, in case of drought, wilting (Gates, 1980; Jones, 1992). As a plant transpires it converts excess solar gains to latent heat. As a result, the air surrounding a leaf typically has a lower temperature and higher humidity than it would otherwise (Koyama et al., 2013).

W. Stec et al. (2005) investigated the thermal impact of a green wall located in a double skin façade compared to a similar cavity with white blinds. Compared to the control, the green wall reduced the air temperature of the cavity by 20 °C.

Although cooling from the transpiration of green walls is well understood as a general phenomenon, there is much confusion as to the expected possible cooling from transpiration for different climates. M. Hoelsher et al. (2016) observed no ambient temperature reduction from the transpiration of direct and indirect green walls during the summer in Berlin, Germany. However, using a sap flow measurement technique, they reported that up to 39.9% of the incoming solar radiation was converted to latent heat via canopy transpiration.

In Reading, UK, Cameron et al. (2014) measured up to a 3 °C air temperature reduction from indirect green walls. In Chicago, IL, Susorova et al. (2014) reported an average temperature decrease of 0.8 °C to 2.1 °C near a direct green wall façade, as well as a 2% to 4% increase in relative humidity.

During the hot summer days in Maryland, MD, Tilley et al. (2012) reported a 1.4 °C to 1.8 °C reduction in air temperatures from transpiration of indirect green walls. In Hong Kong, China, C. Jim (2015), reported that indirect green walls reduced ambient air temperatures by 5 °C.

Only a few studies have tried to separate and quantify the cooling effects from transpiration and solar radiation interception in green walls (Cameron et al., 2014; Hoelscher et al., 2016; Koyama, Yoshinaga, Maeda, & Yamauchi, 2015; Susorova et al., 2014; Tilley et al., 2012; Wang, 1999). However, directly comparing the cooling contribution of these two components from existing studies is difficult due to differences between green wall designs, climates, and methodologies employed in those studies.

3.3. Research Methodology Review

The methodologies adopted for green wall research studies can be broken down into three major categories: observational, experimental, and modeling (Hunter et al., 2014).

Observational study—wherein data is gathered from an existing green wall—is the most common methodology (Alexandri & Jones, 2008; Bolton, Rahman, Armson, & Ennos, 2014; Eumorfopoulou & Kontoleon, 2009; Hoelscher et al., 2016; Perini et al., 2011; Perini et al., 2011; Susorova, Angulo, Bahrami, & Stephens, 2013; Susorova et al., 2014; Wang, 1999; Yin et al., 2017). Hunter et al. (2014) stated that the observational study is the weakest methodology because data from observational studies is highly impacted by the building's particular construction and current use, developmental conditions of the plan, and the surrounding urban geometry. For example, Perini et al. (2011) compared the air flow and temperature of three building facades with three different types of existing green walls. However, not only were these walls located in three different towns (Rotterdam, Delf, and Benthuizen), but they also had different solar orientations.

A possible way of addressing this issue is to compare the observational data with a few randomly selected control sites before and after installation of the vegetated surface. One would expect that the temporal data between the control sites and the experimental site would vary in time independent of one another. However, the changes common to the two sites could be used to identify the impacts attributable to the vegetative surface (Hunter et al., 2014).

Experimental studies rely on field data. This method provides more control when setting up experiments. However, with the exception of three studies (Ip et al., 2010; Koyama et al., 2013; Tilley et al., 2012), all experimental studies on green walls "lack adequate replication, having only a single replicate with which to address their research question" (Hunter et al., 2014). Hunter et al. suggests that introducing redundancies in experiments can address this problem. For example, a comparative study of two south facing green walls (instead of one) to a bare wall introduces more effective control for an experiment.

Furthermore, most experimental studies have been conducted over short time durations. For example, Susorova et al. (2014) conducted an experiment for only nine days, and Di and Wang (1999) for only one day. To collect reliable data on the thermal impact of green walls, the plants must be well established at the site and the experiments should be conducted over the course of at least one year (Hunter et al., 2014; Pearcy, 1989).

In most cases, the locations of the instruments that were used are also not clearly described (Hunter et al., 2014). The Koyama et al. (2013) experiment, designed to identify key plant traits contributing to the cooling impact of green façades, did not identify the environmental conditions (sunlight exposure, irrigation regime, soil and nutrient conditions) under which the plants developed.

Eight studies have evaluated the energetics and thermal effects of green walls on buildings through numerical modeling: (Alexandri & Jones, 2008; Eumorfopoulou & Kontoleon, 2009; Holm, 1989; Stec et al., 2005; Šuklje et al., 2016; Susorova et al., 2013; Tilley et al., 2012; Wang, 1999). Neither Holm (1989) nor Eumorfopoulou (2009) considered canopy transpiration.

Other than Alexandri, all numerical studies have evaluated their models using observational or experimental studies. Stec et al. (2005) developed a lump-capacitance model and evaluated it using laboratory setting experiments. Susorova et al. (2013) developed a similar model wherein the empirical leaf surface temperature was based on generic plant properties.

Tilley et al. (2012) developed a numerical model that showed a good fit compared to field study measurements. However, they observed hourly time step errors owing to poor estimates of transpiration and cloud cover. T. Šuklje et al. (2016) developed a numerical model using a finite difference method to estimate the temperatures of the canopy surface, cavity, and external wall surface. Their model also showed a good fit with field study measurements. The inputs for the model were Leaf Area Index (*LAI*), canopy transmissivity, and view factors (sky view) of the canopy and the exterior wall behind it. *LAI* is the ratio of the projected leaf area to the wall area.

3.4. Climate and Site Considerations

More than most passive strategies, the success of green walls depends on local climatic conditions. Nevertheless, much of the literature on this topic assumes that green walls can thrive similarly in all climatic conditions. Alexandri et al. (2008) developed a numerical model and considered scenarios where vegetated surfaces covered the full envelopes (walls and roof) of multi-story buildings in urban canyons in different climates, from hot and arid to sub-arctic. They claimed that all the surfaces in urban areas can "easily be covered with vegetation and alter the microclimate of the built environment" (Alexandri & Jones, 2008).

In response, Hunter et al. (2014) argued that Alexandri et al. (2008) failed to recognize the physiological limits of climbing plants and carelessly assumed that the thermal effects of green walls can be scaled up linearly from a single building to a complex urban geometry.

Understanding plant biophysics can drastically reduce misinformed conclusions. For example, the transpiration rate of a canopy is intimately dependent upon solar radiation and water availability. Therefore, climates with summer monsoons or summer drought conditions cannot expect high cooling effects through evapotranspiration (Graaf & Ende, 1981; Rana & Katerji, 2000; Rose & Sharma, 1984).

3.5. Design Considerations

The environmental conditions highlighted above constitute variables outside a researchers' control. In contrast, this section focuses on variables the values of which a researcher can modify. Not all the design variables listed below can be tested within a single research study. However, it is important to consider them when designing research questions so that their impacts can be anticipated and adjusted for, if necessary.

3.5.1. Building Design and Material

Šuklje et al. (2016) found that regardless of the exterior wall type, a green wall reduced the peak heat flux of a façade by 77%. The magnitude of this heat flux reduction depended on the thermal resistance of the wall. Similar observations have been made by other researchers (Susorova et al., 2013; Tilley et al., 2012).

Both Holm (1989) and Wang (1999) demonstrated that buildings with high mass construction and an ivy layer maintained cooler daytime surface temperatures compared to bare control walls. However, at night, the ivy-covered wall stayed warmer because the vegetated layer blocked both wind and the escape of long-wave radiation from the wall surface.

There are no comprehensive studies on the optimal mass and spectral properties of an ivy-covered wall in various climatic conditions. Holm (1989) experimented with the spectral properties of two ivy-covered walls. He found that black and white surface temperatures were roughly equivalent throughout the vegetated period. As the foliage decreased, however, the black wall surface temperature rose more than did the white wall surface temperature. This effect can be applied to enhance the thermal performance of an ivy-covered wall during cold seasons.

With the exception of two studies, Davis and Hirmer (2015) and Stec et al. (2005), there have been no investigations into integrated design solutions involving green walls. Stec et al. (2005) used the latent heat of a green wall to reduce the cavity temperature of a double glazed façade. Davis and Hirmer (2015) reduced interior temperatures by moving the air behind the wetted substrate of a living wall.

The use of vegetation in vernacular construction has persisted throughout the history of architecture. Each climatic condition has inspired the invention of climate-specific design solutions to take advantage of the cooling effect of plant evapotranspiration. However, all these solutions share a universal principle: they all bring cooled air into a building via natural ventilation. For example, traditional Japanese buildings, in a hot and humid climate, use movable shoji screens that maximize air movement into buildings. Persian and Spanish buildings, in hot and dry climates, bring cooled air from courtyards and gardens inside through either cross- or buoyancy-driven ventilation strategies (American Society of, 1984; Brown, 2014).

Although these techniques have proven successful, the surrounding landscapes and vegetation designs have mostly been governed by aesthetic principles. It was not until the 1950s that several studies aimed to quantify the impacts of landscaping on the natural ventilation of buildings (White, 1954). Wind tunnel experiments proved that wind speed increases beneath the "crowns of trees that have branches pruned from ground to part of the bole" (American Society of, 1984). Therefore, if trees are pruned just above window height along the path of primary wind direction, they can strengthen cross ventilation into buildings (White, 1954).

During the 1970s and 1980s many publications on energy conservation landscaping hypothesized design methods to enhance the natural ventilation of buildings through "precision landscaping" (Parker J.H., 1983). For instance, A. Moffat and M. Schiller suggested that planting trees in a funnel shape toward a building could both cool and increase the velocity of entering wind (Moffat, 1981). However, none of the design strategies has been quantified or verified (American Society of, 1984).

Most of the design strategies suggested by A. Moffat and M. Schiller and their contemporaries recommended cross-ventilation and the placement of vegetation either below or to the side of window openings so as not to interrupt the wind path. A. Spirn (1981) advanced these design solutions by introducing porous or movable green walls in front of windows, but none of her design proposals have been tested.

Although it is clear that vegetative surfaces introduce resistance along the path of the wind, the particularities of mass and heat transfer inside plant canopies is still under investigation. H. Jones, a plant biophysicist, argues that the main difficulties in this investigation are (a) the erratic turbulent structures within plant canopies and the complexities introduced by the distribution of sources and sinks for heat, and (b) the mass and momentum within canopy structures (Jones, 1992).

Nevertheless, clear wind patterns exist for dense versus porous canopies. As expected, dense canopies introduce higher resistances and reduce wind velocity compared to more porous canopies (Jones, 1992).

K. Perini et al. measured the wind speed within a canopy structure and the air cavity inside an indirect green wall. The objective of the experiment was to evaluate the insulating properties of different green wall systems. Measurement showed that, the wind velocity was decreased inside both the canopy and the air cavity (between the green wall and the building façade). However, the wind velocity inside the canopy was reduced further (0.55 m/s) compared to the air cavity (0.29 m/s) (Perini et al., 2011).

So far, there has not been a comprehensive study demonstrating the relationship between the porosity of green wall surfaces and the resultant wind coefficient discharge. Yet both variables are essential to the design of an integrated green wall coupled to the natural ventilation of a building.

3.5.2. Support Structure & Container Design

There have been limited investigations into the impact of support structure designs of green walls (Tilley et al. (2012), Schumann et al. (2007)).

Ip et al. (2010) developed and verified an empirical model for the shading properties of Virginia creeper. They reported that because the support structure was not considered carefully in relation to the vigorous growing habits of the Virginia creeper, the experiment was constrained due to the overly-dense plant coverage. This lack of attention to the support structure, substrate, container design, and irrigation regimes of green walls is common to the majority of the reviewed studies in this area (Hunter et al., 2014).

The various climbing mechanisms of vines reveal the ecological needs of the plant in question (F. E. Putz & Mooney, 1991). C. Darwin (1865) observed that the manner in which a plant climbs indicates both the maximum possible diameter of the supporting structure and the necessary distribution of individual supports.

Extensive and detailed investigations of support structures of climbers have been conducted by ecologists and botanists (F. Putz, 2014; F. E. Putz & Mooney, 1991). However, in most studies on green walls, information about the supporting structures used is not listed, and limited comprehensive studies on variations among support structure designs exist (Cameron et al., 2014; Hunter et al., 2014).

The growing conditions of a climbing plant—such as soil condition, container design, and irrigation regime—directly influence the relative growth rate, growth habit, total leaf area, and health of a plant. All of these factors impact the thermal performance of a green wall. To replicate experiments and predict plant performance, these variables must be tested and comprehensively documented (Hunter et al., 2014).

None of the reviewed research discusses variables specifically relevant to soil-grown climbing plants, such as soil structure and texture, air-filled porosity, water holding capacity, bulk density, or saturated hydraulic conductivity. Other than Tilley et al. (2012) and Koyama et al. (2015), no study describes the irrigation regime used in the experiment.

3.5.3. Air Cavity Design

Many studies on green walls have observed cooler temperatures around the canopies. In Reading, United Kingdom (latitude of 51°), south-facing green walls reduced ambient temperatures up to 3 °C during the summer months (Cameron et al., 2014). In Maryland, (latitude of 39°), indirect green walls reduced ambient air temperatures by 1.4 °C to 1.8 °C during the hot summer days (Tilley et al., 2012). In the subtropical climate of Hong Kong, China (latitude of 22°), green walls reduced ambient temperature by 5 °C (Jim, 2015).

What is less clear are the relative impacts of transpiration and shading on the temperatures within the air cavities of green walls. A. Antonyova et al. (2017) measured the humidity and temperature of a 4 cm air gap of a south-facing green wall located at a latitude of 49° during the summer months. They found that the air gap temperature remained lower than the ambient temperature until 9 a.m., after which the temperature increased above the ambient temperature by up to 8 °C until 7 p.m. The humidity levels in the air gap remained continuously above the ambient humidity levels throughout the experiment.

In contrast, both Hoelscher et al. (2016) at a latitude of 50°, and Šuklje et al. (2016) at a latitude of 46°, found higher-than-ambient air temperatures within the cavities of green walls during both day and night. Both attribute this finding to the insulating effect of green walls.

In Chicago, Illinois, at a latitude of 41°, Susorova et al. (2014) observed up to a 2.1 °C temperature reduction in the air around a direct green wall. However, they measured an increase of 1.0 °C to 1.5 °C behind the vegetated layer. Similarly, they attributed this to the reduction in both the outgoing long-wave radiation and the convective heat transfer from the building façade.

J. Coma et al. (2017) observed a similar difference between cavity and ambient air temperatures for a south-facing indirect green wall in Llidia, Spain at a latitude of 41°. In contrast, Wang (1999) measured an approximately 2 °C temperature reduction behind the vegetated canopy of a direct west-facing green wall in Beijing, China (latitude of 39°). Similar to others, he reported higher-than-ambient air temperatures behind the canopy during the night.

At a latitude of 35° in Nagoya, Japan, Koyoma et al. (Koyama et al., 2013) measured the cavity temperature of a south-facing indirect green wall covered with the high-transpiring Zudzu vine. They reported a cavity temperature similar to the ambient temperature for a 45 cm cavity. They hypothesized that the cooling power produced through transpiration was dissipated to the surrounding environment due to the large size of the cavity.

Finally, at a latitude of 22° in Hong Kong, China, C. Jim (2015) reported that indirect green walls lowered the ambient temperature by 5 °C. However, the temperature of the cavity was cooler than ambient by only 3 °C to 4 °C. He hypothesized that the air inside the cavity became warmer due its adjacency to the heated façade behind the green wall.

The literature review above illustrates the vast differences between reported cavity temperatures in different climates. Therefore, it is difficult to ascertain a meaningful trend. However, most studies show that cavity temperature rises due to the limiting effect of the green wall on outgoing long-wave radiation and convective heat transfer.

More research is required to evaluate the variables that impact the hydrothermal effect of the cavity between the vegetative layer and the building façade. Depending on the wall type, the insulating effect of green walls can impact the thermal performance of a building. Further investigation of the effects of the cavity size, wall thermal and spectral properties, transmitted solar radiation, and latent heat of the canopy is recommended to quantify the insulating impact of green wall canopies. A. Hunter et al. (2014), in their thorough review of research methods currently employed in studying green walls, similarly highlighted the limited research that has been done on this topic.

3.5.4. Plant Biophysical Trait and Energetics Considerations

The energy balance of leaves is complex and variable. The energetic component is divided into transpiration, reflection, long-wave emission, transmission, and photosynthesis (Gates, 1980; Jones, 1992; J. Monteith & Unsworth, 2013). The surrounding environmental conditions of a plant dictate the energetic status of a plant, which in turn can be observed and measured through plant temperatures. Temperatures of plant leaves and stems rapidly change, as leaves and stems have minimal thermal mass and therefore low heat capacities. In contrast, tree trunks and branches have higher heat capacities and therefore respond more slowly to environmental changes (Gates, 1980; Jones, 1992).

Energy is transmitted to and from leaves through radiation, convection, and transpiration. Each heat transfer phenomenon is described through different variables such as radiation fluxes, air temperature, wind speed, and water vapor density. Their combined influence can be measured by monitoring leaf temperatures (Gates, 1980; Jones, 1992).

A leaf is coupled to radiation fluxes through its spectral properties. If a leaf were to absorb all received incident radiation, its temperature would be highly coupled to the external radiation field. In contrast, if a leaf were to reflect all incident radiation, it would be completely decoupled from radiation fluxes (Gates, 1980; J. Monteith & Unsworth, 2013).

Other variables such as a leaf's shape, orientation, color, and even its growth stage, can impact its reflectivity. For example, broad, light-colored leaves that grow parallel to the ground have higher albedo compared to the needle-shaped, dark-colored leaves of conifers. It is safe to assume that most broad green leaves absorb 50% of total received radiation fluxes and the rest is either reflected from or transmitted through the leaves (Gates, 1980).

Most leaves are strongly coupled to ambient temperatures through convection. The rate at which heat is transferred to or from a leaf is measured through the convective heat coefficient. A high convective coefficient indicates a high heat transfer rate between a leaf and the surrounding air. Small leaves have high convective heat coefficients. As a result, their temperatures do not deviate from ambient temperatures by more than 2 °C to 3 °C. Broad leaves have relatively low convective heat coefficients and their temperature can vary up to 15 °C from ambient air temperatures. Therefore, leaf morphology is highly coupled with thermal convection (Gates, 1980; Grace, 1977).

Additionally, the concentration of various gases in a leaf is coupled to the concentrations in the surrounding air. Water vapor, carbon dioxide, and oxygen are the most influential gases exchanged between a leaf and its environment. However, other gases and pollutants are also exchanged. Transpiration reduces leaf temperature because water requires 2.43×10^6 J/kg of energy, in the form of heat, to vaporize. Through this vaporization leaves provide evaporative cooling for plants, which maintain plant temperatures within an acceptable range (Gates, 1980; Jones, 1992).

The amount of transpiration varies between species and is directly dependent on the water vapor diffusion resistance of leaves, light intensity, and the relative humidity of the air. A plant with high diffusion resistance transpires less compared to a plant with low diffusion resistance. The temperature of a leaf with low diffusion resistance is highly dependent upon the water vapor density of the air outside the leaf. On the other hand, the temperature of a leaf with high diffusion resistance is less influenced by the relative humidity of the air, and is instead mainly controlled through stomatal behavior (Gates, 1980; Grace, 1977; J. L. Monteith, 2008).

For example, Graaf et al. (1981) measured and compared transpiration rates of sweet pepper, tomato, and lettuce plants in a greenhouse. They observed that the tomato plant had the highest average transpiration rate, 5 mm/day. The lettuce plant had the lowest average transpiration rate, 1 mm/day. The sweet pepper plant's average transpiration was 3 mm/day (Graaf & Ende, 1981).

M. Gates noted that

> a large leaf with very low diffusion resistance can have its temperature reduced as much as 30 °C when transpiring vigorously under intense radiation. Other plants with high diffusion resistances may have their leaf temperatures affected less than 5 °C under intense radiation in still air. (Gates, 1980)

In general, an increase in light intensity will increase a leaf's temperature, which in turn boosts its transpiration rate.

Surprisingly, there have been limited investigations into the biological and developmental traits of climbing plant species (Hunter et al., 2014). These traits are fundamental factors affecting the thermal performance of a vegetated surface (Koyama et al., 2013). This gap might be caused by the limited information available on temperate climate vines, because vines only account for 1.3% of temperate forest species (Leicht-Young, Hormaza, Boufford, & Rose, 2014).

Cameron et al. (2014) measured the cooling effect of six different plants (four shrubs and two ivies) on 1.2 m high break walls. The objective of the experiments was to compare the cooling effects of different species as well as to identify to what degree the cooling occurred through shading vs. transpiration. The experiments were conducted in a temperate maritime climate in Reading, United Kingdom.

The results showed that the cooling effect of each plant differed. Cameron et al. (2014) reported that Hedra, Lonicera, and Jasminum provided the most cooling through shading, whereas Fuchsia had the largest cooling effect through evapotranspiration. Prunus and Stachys had medium-range cooling effects from both shading and evapotranspiration. Cameron et al. observed a 3 °C lower air temperature around the vegetative surfaces during the warmest days.

The experiment can only be considered as proof of a concept because the plants were not mature and established. The age of the plant is an important variable impacting the transpiration rate because a plant's transpiration rate increases until plant maturity (Hunter et al., 2014). Only at that point does it reach a steady state (Graaf & Ende, 1981).

The selected plants were short, as they were designed to cover only 1.2 m high brick walls. The height of the canopy has an inverse relationship with the transpiration rate (Jones, 1992). This is because the internal resistance of a plant becomes larger when water needs to travel a longer distance from the root system to the leaves (F. E. Putz & Mooney, 1991).

Better understanding of the biophysical and morphological traits of plants is essential for the development of robust research design problems in this area. Therefore, interdisciplinary cooperation between experts in "plant biology, ecology, horticultural and soil science" is strongly recommended (Hunter et al., 2014).

3.6. Discussion and Conclusions

Two major knowledge gaps are observed in this field: (a) a limited understanding of the morphological and biophysical characteristics of vines, and (b) a lack of a standardized research methodology to evaluate the performance of green walls.

The first is due to the limited attention designers have given to fields such as plant biophysics, agronomy, and botany. To that end, this dissertation evaluates the performance of green wall designs with an eye toward the biomechanics and biophysical traits of vines. It is important to note that the number of grapevine studies, is extensive, but there are few studies of urban vines.

These fields have standardized methods where the variables impacting plant performance have been clearly identified. As a result, it is possible to compare various studies. In contrast, the lack of a standardized methodology in the relatively young field of green wall performance evaluation has limited the ability of researchers to replicate and evaluate existing research.

This research will address the second issue by using methods already used in the fields of agronomy and plant biophysics. The goal is to highlight a set of key standardized variables impacting green wall performance, and to provide designers with a methodology for designing green walls with these variables in mind.

4. Background

4.1. Plant Biophysical Ecology

The literature review demonstrated the importance of engaging with other scientific fields such as botany, agronomy, and biophysical ecology to develop robust research design questions. This section will develop a detailed background knowledge on leaf scale biophysical traits. The next sections will review the biomechanical behaviors of vines.

4.1.1. Leaf Scale Energy Balance

The effect of climate on a plant is shown in Figure 2. The right image illustrates total environmental energy gains and the left image illustrates the energy losses of a leaf throughout a day. During the day a leaf receives energy though (a) direct solar radiation, (b) diffused solar radiation from atmospheric scattering, (c) reflected radiation from clouds and the surrounding environment, and (d) long wave thermal radiation from the atmosphere and its surroundings.

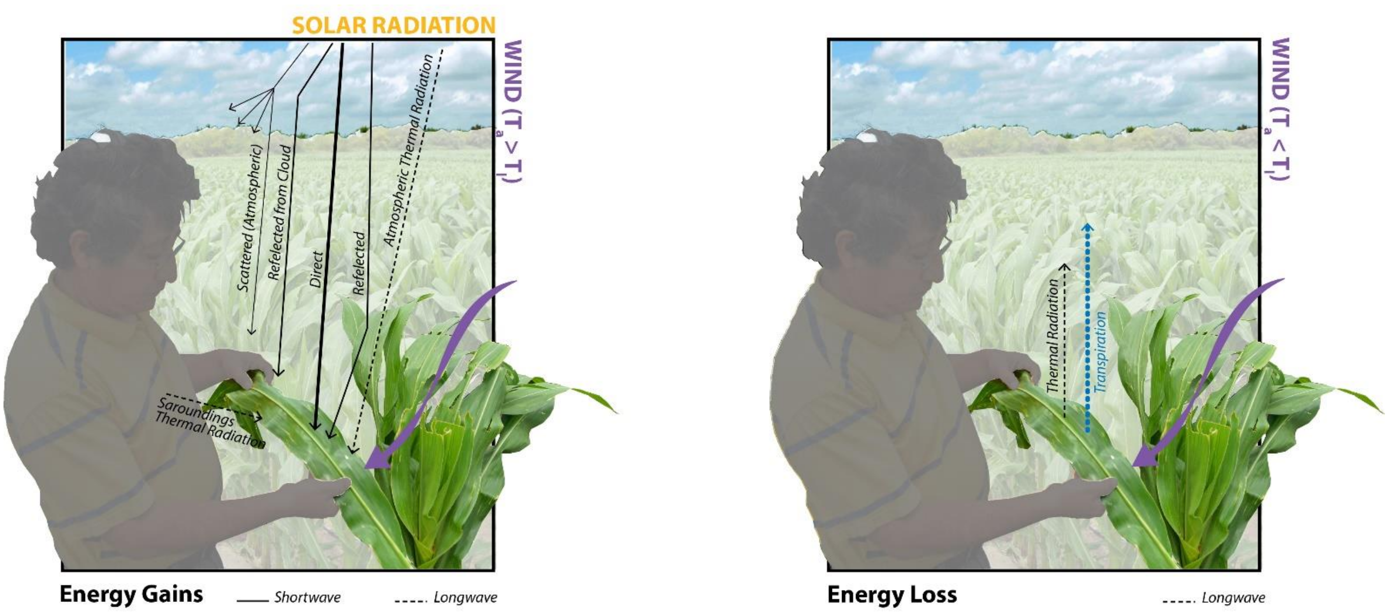

Figure 2. Exchange of energy between a plant and its surrounding environment through radiation, convection, and conduction

Wind can either deposit or extract energy from a leaf surface. If the wind temperature is larger than the surface temperature of a leaf, it will deposit energy to the leaf. If the wind temperature is lower than the surface temperature of a leaf, it will contribute to the loss of energy from the leaf. A leaf regulates its temperature through transpiration—the release of water vapor from the stomata of a leaf—and outgoing longwave thermal radiation. Only a negligible portion of the energy gains is used for photosynthesis. A plant leaf has no significant amount of energy transferred to or from it by conduction.

According to the First Law of Thermodynamics, the total energy gains should equal the total energy losses by a leaf (Gates, 1980). Hence, the energy balance of a leaf can be written as:

$$Q_a = R_{nl} + C + \lambda E \quad (1)$$

Where

Q_a amount of energy absorbed by the surface

R_{nl} net radiation emitted from the leaf

C energy transferred by convection

λE energy exchange by transpiration

A leaf absorbs a certain amount of the received radiation energy and partitions the rest through three outgoing flows of energy: radiation, convective heat transfer with the surrounding air, and transpiration. To better examine these three outgoing streams of energies, each is separately considered. Later their combined effect is described.

4.1.2. Radiation Influence on Leaf Temperature

The electromagnetic radiation wavelengths of plant biophysics lies between 300 nm to 100 µm. This range is comprised of Ultraviolet (UV), Photosynthetically Active Radiation (PAR), which is generally similar to the visible range, and Infrared (IR) spectrums. The UV range is categorized as UV-C (< 280 nm), UV-B (280–315 nm), and UV-A (315–400 nm). The IR spectrum is further broken down into near IR (NIR, 700–

1,000 nm), mid-IR (MIR, 1,000–4,000 nm), thermal IR (TIR, 4,000–15,000 nm), and far IR (15,000–100,000 nm) (Jones, 1992).

From the total incident radiation I that falls upon an object such as a leaf, a part may be reflected (I_r), transmitted (I_t), and absorbed (I_a). The exact magnitude of each phenomenon depends on the spectral properties of the object. However, the sum of the amount that is reflected, transmitted, and absorbed is always equal to the total amount of radiation received by the object:

$$I = I_r + I_t + I_a \tag{2}$$

The amount of radiation energy received, transmitted, or emitted from a surface per unit time [W] is termed *radiation flux*. The net radiation flux through a unit surface area is *radiation flux density* [W/m^2]. The flux incident on a surface is called irradiance [W/m^2] and the flux incident leaving the surface is termed emittance [W/m^2] (Gates, 1980; Jones, 1992).

I, the irradiance received on a surface, is a function of its orientation toward the radiant beam I_0. The revived irradiance can be quantified by Lambart's cosine law: (Jones, 1992)

$$I = I_0\, Cos\alpha = I_0\, Sin\beta = I_0\, \frac{Beam\ Area}{Surface\ Area} \tag{3}$$

Where

I flux density at the surface [W/m^2]

I_0 flux density normal to the beam [W/m^2]

α the angle between the beam and the normal to the surface (zenith)

β solar elevation angle (solar altitude)

The amount of solar radiation received on a surface depends on its geographical location as well as the day and time of the year. Generally, the maximum shortwave irradiance (at noon) for much of the earth surface falls between 800 W/m^2 to 1,000 W/m^2 during the growing seasons (Jones, 1992). The irradiance during a clear day can be approximated by:

$$I_{st} = I_{s(max)} Sin\,(\frac{\pi t}{N}) \qquad (4)$$

Where

I_{st} the irradiance t hours after the sunrise [W/m^2]

$I_{s(max)}$ the maximum shortwave radiation [W/m^2]

t hour after the sunrise [hr]

N the daylight hours [hr]

Equation (4) represents an idealized scenario without any consideration of the climatic conditions of a site. Currently, various simulation software such as Diva for Rhino, Lady Bug, and Climate Consultant can be used for a more detailed understanding of the received solar irradiance of a particular site. The *U*.S. Solar Radiation Resource Maps created by the National Renewable Energy Laboratory provides information on solar radiation received in the United States and its territories.

4.1.2.1. Leaf Spectral Properties

The spectral properties of leaf surfaces are generally alike. However, "for most species the details vary with thickness, age, water content, surface morphology, and orientation" (Jones, 1992). Figure 3 illustrates the spectral properties of a Cottonwood leaf. Although the magnitude of the reflectance (albedo) and transmittance curves might be slightly different from one leaf to another, the absorbance curve is typical of all broad green leaves. With the exception of the wavelength corresponding to the green color (about 0.51 μm), a leaf has a high absorptivity on ultraviolet and most of the visible wavelengths. High absorption in this range is due to the presence of leaf pigments such as chlorophyll (Gates, 1980).

However, there is an abrupt decrease of absorptivity, and the consequential increase of transmittance and reflectance, in the range between 0.7 μm to 1.4 μm. This allows a broad green leaf to decouple from near-infrared radiation. The high absorptivity of the leaf returns at wavelengths greater than 2.0 μm.

All good absorbers of radiation are good emitters at the same wavelength. Because a leaf's temperature is mostly close to the ambient temperature—between 270 °K and 300 °K—it emits radiation effectively in the far-infrared range. As illustrated in Figure 3, the absorptance of a leaf lies in the far-infrared ranges between 0.95 and 0.97, meaning that a leaf can dump its excess heat (emissivity of 0.95 to 0.97) within the same wavelengths.

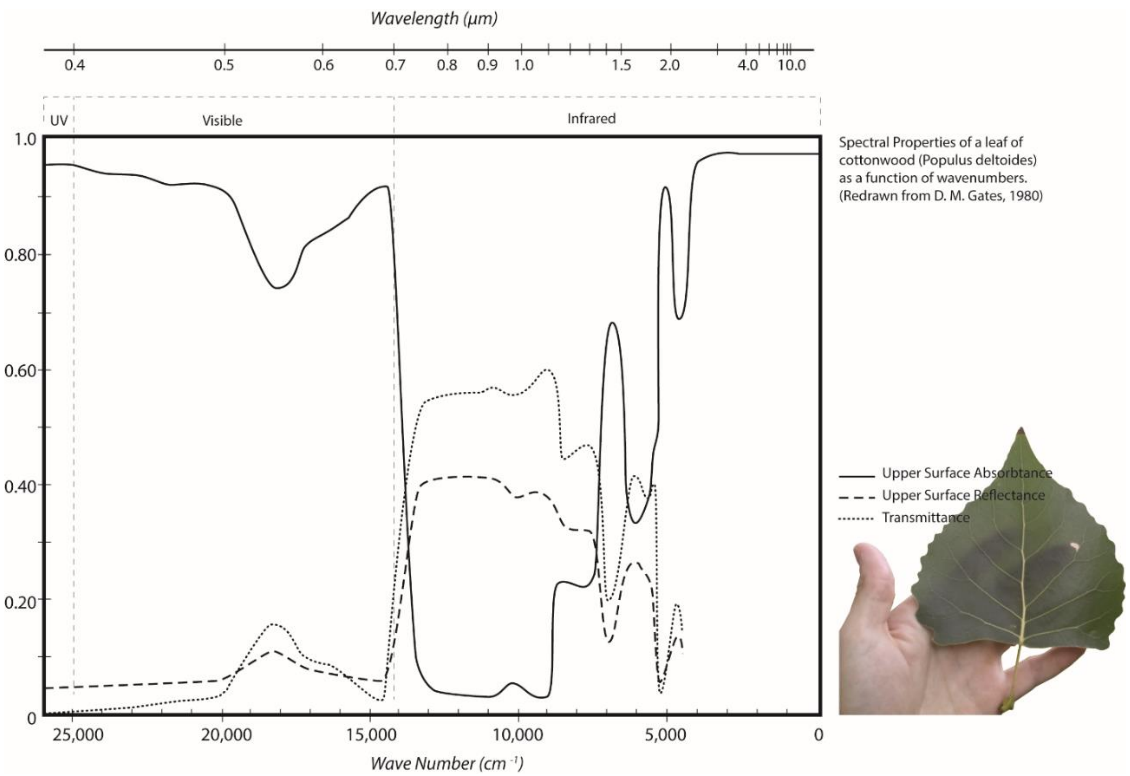

Figure 3. Typical spectral properties of a broad leaf. Reproduced from Gates (1980)

4.1.2.2. Impact of Solar Radiation on the Transpiration of Leaves

Solar radiation is the most important environmental variable. The transpiration rate of a plant is directly proportional to the magnitude of received solar irradiance. High solar gains promote high rates of photosynthesis and warmer leaf temperatures, which in turn trigger high transpiration rates. However, the maximum transpiration rate varies from one species to another and it is controlled by plant stomata and internal resistance (Gates, 1980).

For instance, D. Bell and A. Teramura measured the transpiration rates of three temperate vines in Maryland. They reported that Virginia creeper was consistently the lowest transpiring vine, with a maximum value of 1.3 mmol/m^2s. The highest transpiring vine was Frost Grape with 10.2 mm/m^2s. The Honeysuckle Vine was in the middle with a maximum transpiration rate of 5.2 mmol/m^2s (Bell, Forseth, & Teramura, 1988).

4.1.3. Convection Influence on Leaf Temperature

4.1.3.1. Convective Heat Transfer

Convection is the transfer of energy through a moving medium such as gas or liquid flowing across an object. The transfer of energy in a flowing fluid is due to conduction and enthalpy in the system. Enthalpy is the total internal energy of the fluid and is the product of the pressure and volume of the fluid.

4.1.3.2. Free vs. Forced Convection and Boundary Layer

In free convection, fluid flow is induced by density differences caused by temperature differences within the fluid. For example, a current of warm air rises from a heated radiator and the cool surrounding air replaces it, only to warm up and rise again.

On the other hand, in forced convection, the fluid moves due to an external source such a fan. As a fluid moves along a surface, the particles close to the surface are slowed down due to the viscosity of the fluid. Full velocity is restored again at some distance from the surface. This transition zone is called the boundary layer. If there is a temperature difference between the fluid and the surface, the boundary layer becomes a transition zone for thermal transfer (thermal boundary layer). As the boundary layer thickness is reduced the rate of heat transfer is increased. In other words, the temperature gradient is much larger when the boundary layer is small (Figure 4).

4.1.3.3. Laminar vs. Turbulent flow

There are two primary types of flows in fluids: laminar and turbulent. In laminar flow the particles are flowing orderly one over the other. If there is a temperature difference between the surface and the fluid, heat is transferred by molecular conduction within the fluid starting at the interface of the fluid and the surface. The temperature and velocity profiles for laminar flow are shown in Figure 4.

The thickness of the boundary layer grows as the fluid moves downstream. At a critical distance *x,* shown in Figure 4, the fluid transitions into a turbulent flow. This type of flow is different from laminar flow in that the highly ordered character of the flow is broken down into eddies and irregularities generated as the fluid passes over the surface.

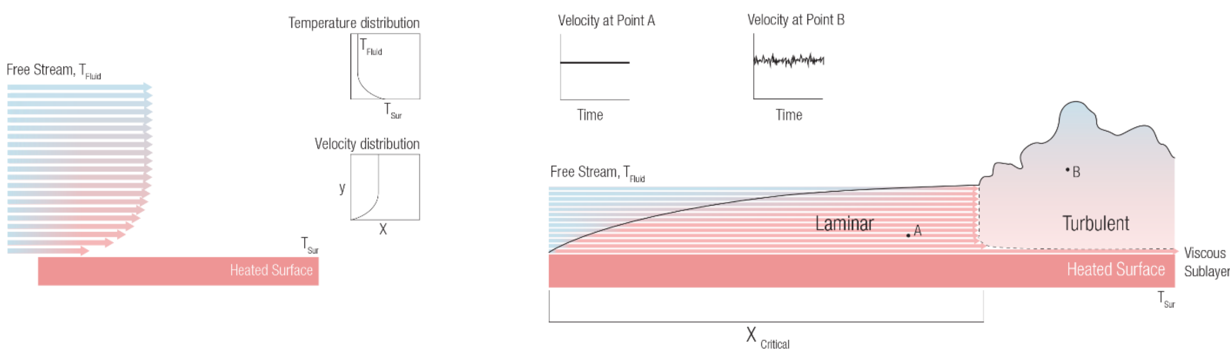

Figure 4. Flow types in fluids. Left, laminar flow boundary layer. Right, turbulent dl flow boundary layer

The behavior of turbulent flows is highly randomized and difficult to predict. Turbulent flows, as compared to laminar flows, are highly efficient in transferring heat and momentum. Note that turbulent eddies are suppressed at the viscous sublayer along the surface. The temperature and velocity profiles for turbulent flow are shown in Figure 4.

4.1.3.4. Impact of Free and Forced Convection on a Leaf Energy Budget

The contribution of free convection on the energy budget of a leaf is small. Consequently, its influence on surface temperature of a leaf is minimal. It has been observed that forced convection equal or lower than 0.1 m/s has a similar convective heat coefficient as free convection (Gates, 1980).

> Generally, it is simplest to apply the forced convection formulation to all conditions and consider the lower limit forced convection to be the amount of air movement at which the convective heat transfer coefficient for forced convection equal those for free convection. (Gates, 1980)

4.1.3.5. Impact of Wind on Leaves

Following solar radiation, wind is the second most important variable impacting the energy budget of a leaf. Plants blocked from the wind experience higher leaf temperatures, and their growth rate is reduced compared to their counterparts with windbreaks (Grace, 1977). To avoid overheating, plants in hot climates have evolved with small leaves. This reduction of size allows leaves to be strongly coupled to the ambient temperature. Experiments have shown that the leaves of desert plants continuously remain within 2.5 °C of the ambient temperature (Gates, 1980).

As the size of a leaf increases, the impact of wind on the leaf temperature is reduced. For example, a leaf with area of 0.2m x 0.2m, experiencing 1 m/s wind speed, can have a temperature difference up to 12 °C to 15 °C from the ambient temperature. That is because leaves with greater surface areas have larger thermal boundaries and as a result, a smaller convective heat coefficient (Gates, 1980).

In most cases, leaf temperatures higher than 50 °C can cause permanent damage to leaves and threaten a plant's livelihood. Therefore, broad leaves geometry and structure evolved to take the most advantage of wind. S. Vogel (1968) compared the temperatures of sun and shade leaves of the white oak (Quercus Alba L.) in a low-speed wind tunnel. The experiment showed that the smaller, lobed shaped sun leaves are evolved to facilitate a greater convection coefficient. He concluded that "the difference between ambient and leaf temperature is about 20% less for the sun leaves than for the shade leaves in either still or a gentle upward current."

S. Vogel, D. Gates, and J. Grace have demonstrated that convective heat coefficient of leaves with dimensions between 0.01 m to 0.1 m could reach twice as large as the predicted equations developed for free convection from equivalent flat rectangular plates. The adaptation of the size and shape of a leaf to its climate shows the significance of convective heat transfer on the energy balance of a leaf.

4.1.3.6. Impact of Wind on the Transpiration of Leaves

Wind is another important variable impacting the transpiration rates of a leaf. Low wind speeds increase the rate of transpiration. However, there is still much confusion about the impact of wind at speeds greater than two meters per second. Some studies show lower rates of transpiration as wind speed increases (Dixon & Grace, 1984; Drake, Raschke, & Salisbury, 1970). Others predict that transpiration increases only under conditions of high wind velocity and low available solar energy, and that in conditions with low available solar energy, transpiration rates decrease (Tyree & Ewers, 1991).

Most recent studies have observed that, regardless of the plant species, evapotranspiration rates increase in high wind velocities (up to 8 m/s). Surprisingly, the thermal boundary layer conductance—which is dictated by the geometry and size of the leaves—has minimal impact on transpiration rates. Instead, the main factor is the internal resistance of the leaves (leaf conductance) to losing water vapor.

The transpiration rates of well-watered plants with high stomatal conductances vary linearly with wind speed. However, the transpiration rates of plants with low stomatal conductances increase and then level off as wind speed increases. It has been observed that in low wind velocities (up to 3 m/s), they exhibit high transpiration rates. As the wind velocity further increases, the transpiration rate plateaus and stays unchanged (Tyree & Ewers, 1991).

4.1.4. Transpiration Influence on Leaf Temperature

4.1.4.1. Leaf Structure

A leaf blade is composed of several layers. Epidermises are cells that are located on the top and bottom of a leaf. This transparent outermost tissue includes leaf hairs, cuticle (a waxy protective layer), and guard cells. Guard cells are located at the entry of stomata and control the exchange of gases and water vapor between a leaf and its environment. The size, location, distribution, and resistance of stomata vary per species.

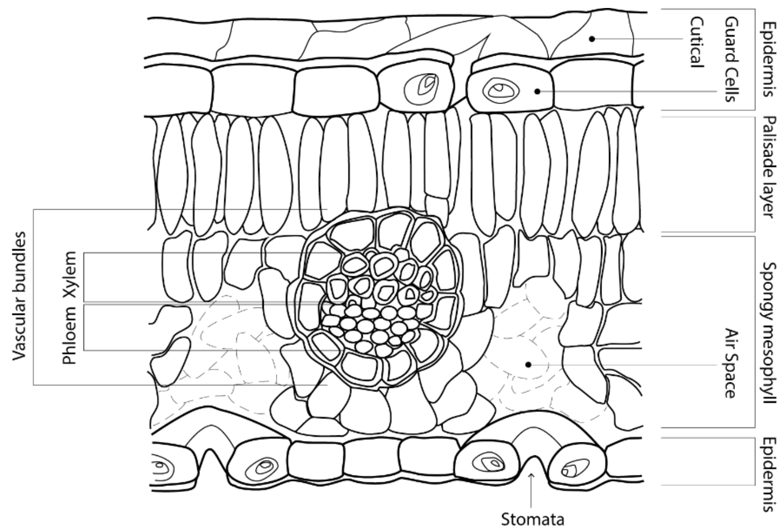

Figure 5. Typical leaf structure

The palisade layer is composed of one or more layers of tightly packed, elongated cells that are arranged in parallel normal to a leaf surface. These cells are filled with chloroplasts containing chlorophyll that capture solar energy and conduct photosynthesis processes.

Vascular bundles consist of xylem and phloem tissues. Xylem tissue is responsible for the transport of water and minerals to the leaf. Phloem tissue removes synthesized food from a leaf. A spongy mesophyll layer is located below the palisade layer and includes loosely packed irregular shaped cells that store sugar and amino acids produced from photosynthesis processes. During the day, these cells release oxygen and water vapor to the surrounding air space and absorb the existing carbon dioxide within these spaces.

4.1.4.2. Leaf Resistances

The rate of water vapor diffusion from a leaf to its environment depends on two types of resistances: leaf resistance r_l, and aerodynamic resistance $r_{l,a}$. Leaf resistance is a function of intercellular air-space resistance, stomatal resistance, and cuticular resistance of a leaf. The range of values for leaf resistance can vary drastically between species.

Leaf aerodynamic resistance describes the boundary layer along the surface of a leaf. Equation (5) can be used for the average value of the total leaf resistances r (Gates, 1980) .

$$r = r_l + r_{l,a} = \frac{(r_i + r_{st})r_{ct}}{r_i + r_{st} + r_{ct}} + r_{l,a} \tag{5}$$

Where

r total leaf diffusion resistance to water vapor [s/m]

r_l leaf resistance/bulk stomatal resistance [s/m]

$r_{l,a}$ leaf aerodynamic resistance [s/m]

r_i leaf intercellular air-space resistance [s/m]

r_{st} stomatal resistance [s/m]

r_{ct} leaf cuticular resistance [s/m]

It is important to note that in some literature the phrase *stomatal resistance* is used interchangeably with *leaf resistance*. For example, the Food and Agricultural Organization of the United Nations (FAO) defines r_l as the bulk stomatal resistance, which "is the average resistance of an individual leaf." Similarly, in this dissertation, r_l defines the leaf resistance. However, r_l will be referred to as bulk stomatal resistance.

4.1.4.3. Transpiration by Leaves

Transpiration of a leaf might be the consequence of leaves taking in CO_2 through their stomata. However, since the molecular weight of CO_2 is much larger than H_2O, a greater amount of H_2O molecules are lost compared to the number of CO_2 molecules that are taken in through stomata (Figure 6).

Water must pass through a plant's root hairs, epidermis, stem, and xylem to get to the leaf. Once the water reaches the mesophyll cells, it vaporizes and leaves the leaf through stomata. This vaporization of water through the leaf creates a drop in water potential in the leaf, which acts as a driving force to pull more water through the plant.

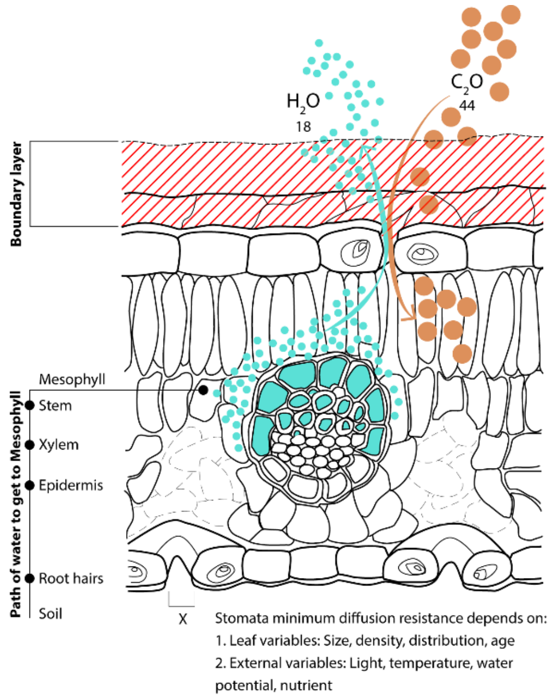

Figure 6. Exchange of CO_2 and H_2O from stomata of a leaf

The transpiration rate of a leaf, which is highly controlled by stomates, depends on several factors such as light, temperature, CO_2, water, and the relative humidity of the air. Stomates need to synchronize between the demand for CO_2 by the metabolic centers in the leaf, and the loss of water vapor to the sarroundings. It seems that stomates prioritize conservation of water in relation to the CO_2 intake. If the relative humidity of the ambient air is low, or the plant is exposed to high wind velocity, the stomata close to prevent rapid water loss (Gates, 1980).

Furthermore, transpiration reduces the temperature of a leaf, which in turn exerts a negative-feedback effect upon water loss through the reduction of water vapor pressure in the leaf. In general the impact of leaf temperature on stomata is not clear. Raschke (1975) reports, "if stomata respond to the change in environmental factors, it is uncertain which feedback loop will determine the ultimate stomatal aperture because CO_2 exchange and water vapor loss are always simultaneously affected by stomatal movement."

4.1.5. Plant Energetics

The surrounding environmental conditions of a plant dictate the energetic status of a plant. By measuring the temperature of a plant its energetic status is revealed. The temperature of leaves and stems rapidly change as they have minimal thermal mass and therefore low heat capacity. In contrast, trunks and branches of trees have higher heat capacity and respond slowly to environmental changes, sometimes even by several hours.

Energy is transmitted to and from leaves through radiation, convection, and transpiration. Each heat transfer phenomenon is described through different variables such as radiation fluxes, air temperature, wind speed, water vapor density, and Vapor Pressure Deficit (VPD). Their combined influence can be measured through monitoring leaf temperature. VPD is the difference between the theoretical pressure exerted by water vapor held in saturated air (100% RH at a given temperature) and the pressure exerted by the water vapor that is actually held in the air being measured at the same given temperature.

A leaf is coupled to radiation fluxes through its spectral properties. If a leaf absorbed all received incident radiation, its temperate would be highly coupled to the external radiation field. If a leaf reflected all incident radiation, it would be completely decoupled from radiation fluxes. Other variables such as a leaf's shape, orientation, color, and even growth stage can impact its reflectivity. For example broad, light-colored leaves that grow parallel to the ground have higher albedo when compared to needle-shaped, dark-colored leaves of conifers. It is safe to assume that most broad green leaves absorb 50% of the total received radiation fluxes and that the rest is either reflected from or transmitted through the leaves (Gates, 1980; Jones, 1992).

Most leaves are strongly coupled to the ambient temperature through convection. The rate at which heat is transferred to or from a leaf is measured through the convective heat coefficient. A high convective coefficient indicates a high heat transfer rate between the leaf and the surrounding air. Small leaves have high convective heat coefficients. As a result their temperature does not deviate from the ambient temperature by more than 2 °C to 3 °C. Broad leaves have a relatively low convective heat coefficient and their temperature can vary up to 15 °C from that of the ambient air. Therefore, leaf morphology is highly coupled with thermal convection (Gates, 1980).

The concentration of various gases in a leaf is coupled to the concentrations in leaf's surrounding air. Water vapor, carbon dioxide, and oxygen are the most influential gases that are exchanged between a leaf and its environment; however, other gases and pollutants may be involved. Transpiration reduces leaf temperature because water requires 2.43 x 10^6 J/kg of energy at 30 °C, in the form of heat, to vaporize. Through vaporization the leaf provides evaporative cooling for the plant in order to maintain its temperature in an acceptable range.

The amount of transpiration varies between species and is directly dependent on the leaf's water vapor diffusion resistance, air relative humidity, and light intensity. A plant with high diffusion resistance transpires less compared to a plant with low diffusion resistance. The temperature of leaves with low diffusion resistance is highly coupled to the water-vapor density of the air outside the leaf. On the other hand, the temperature of leaves with high diffusion resistance is less influenced by air relative humidity and is mainly controlled through stomatal behaviors.

M. Gates (1980) notes that

> a large leaf with very low diffusion resistance can have its temperature reduced as much as 30 °C when transpiring vigorously under intense radiation. Other plants with high diffusion resistances may have their leaf temperatures affected less than 5 °C under intense radiation in still air.

In general, an increase in light intensity will increase the temperature of a leaf, which in turn boosts its transpiration rate.

A negligible amount of energy is used for photosynthetic processes and a small amount of energy is released due to these chemical reactions. However, except for a few species, the thermal impact of such processes can be ignored (Gates, 1980; Jones, 1992).

4.2. Climbers Types, Morphology, and Biomechanics

A general understanding of the characteristics of vines is required as they are the medium/material of indirect green wall design. The following section provides an overview of the anatomy of climbing plants, stem morphology, and the climbing biomechanics of vines. Later, in section 4.3, the discussion is brought back to design by reviewing the systems and building scale design solutions.

4.2.1. Climber Types

According to their ecology and morphology, climbers are divided into four distinct categories.

4.2.1.1. Herbaceous epiphyte

These exotic plants mostly cling to the trunk and branches of their host through advantageous roots. They do not require contact with the ground to become established. Almost all of the herbaceous epiphyte (e.g., Orchidaceous and bromeliad) species are native to tropical forests.

4.2.1.1.1. Woody Hemiepiphytes

These plants start as epiphytes. To further establish themselves and become mature, they soon send down roots to the ground and connect to the earth. Some of the woody Hemiepiphytes, such as strangler fig (*Ficus watkinsiana*), can kill their hosts by encircling and girdling it.

4.2.1.2. Lianas

Lianas are relatively thick-stemmed, woody climbers that start from seedlings and can grow into a mature forest. They contribute up to 25% (Leicht-Young et al., 2014) of tropical forest biodiversity and have been called "the single most important physiognomic feature differentiating tropical from temperate forests" (F. E. Putz & Mooney, 1991). Furthermore, they are an important structural component of tropical forests as they tie the trees together. Very few lianas have adapted to temperate zone forests. Only 1.3% of the native plants of North and South Carolina forests are composed of lianas (Leicht-Young et al., 2014).

Lianas compete for light, water, and nutrients with other trees. However, the health of the forest is directly linked to this competition because lianas create a highly selective process where weaker trees are eliminated. Other contributions of lianas include providing food and shelter for a diverse range of forest animals (F. E. Putz & Mooney, 1991).

4.2.1.3. Vines

In compared to lianas, vines are thin-stemmed climbers that can start from seedlings and grow in disturbed habitats or at the forest edge (F. E. Putz & Mooney, 1991). Vines can be divided into woody/sub-woody and herbaceous types. Similar to lianas, vine species diversity is more prominent in tropical forests.

There are many common attributes between North American vines and their Asian relatives. Wisteria, Clematis, Vitis, and Celastrus are a few examples of vines that are present on both continents. In most cases, when compared to their American relatives, Asian and Asian-hybrid species are more aggressive, fertile, and tolerant of extreme environmental conditions such as drought and soil types (Putz and Mooney 1991; Leicht-Young et al., 2014).

Asian vines such as Oriental Bittersweet (*Celastrus orbiculatus*) and Japanese honeysuckle (*Lonicera japonica*) were mostly introduced to North America for their ecological benefits or horticultural properties. However, their natural controls—herbivores and pathogens—were no longer present in the new ecosystem. These vines were allowed to grow more prolifically and finally led to them being an invasive species.

The majority of lianas and vines are vigorous climbers and can impose stress on their hosts. The negative impact of vines can be numerous. The fast growing habits of vines allow them to compete with their hosts for resources above, below, and at ground level. They compete for sunlight by reaching the canopy of the main host and expand further by moving from one canopy to another. As they become more mature, their weight can contribute to destruction and breakage of the canopy of the host; and in turn, may damage many more neighboring trees. The extensive and deep root structure of vines allows them to access underground water tables before their hosts. Also, they compete for fertile ground and can damage the trunk and branches of the host through biomechanical exertion (Putz, 2014).

It is apparent that understanding the biological needs and control strategies for vines are required for a successful green wall design. In most cases designers ignore vines anatomy, stem morphology, and biomechanics (Alexandri & Jones, 2008; Eumorfopoulou & Kontoleon, 2009; Jim, 2015). However, these topics are tightly bound to the success of a green wall system. Therefore, the following sections provide an overview of these topics prior to the introduction of the structural support of vines.

4.2.2. Vines Anatomy and Stem Morphology

Compared to their self-supporting counterparts such as trees, vines and lianas grow at a much higher rate because they do not invest in their support structure. The stem cross-section of climbing plants is very tree-like except that they possess large diameter vessels and more soft tissues in the xylem (F. Putz, 2014).

These wide vessels are a crucial characteristic of vines because they allow for sufficient transportation of nutrients and water to the leaves. As a result, vines have more hydraulic power to support larger leaf areas. E. Putz reports that "a liana 10 cm in diameter may have as much leaf area (or leaf mass) as a tree five times as large" (F. E. Putz, 1983).

The combination of large vessels and narrow stems can induce the formation of air bubbles (embolism) within the stem during the cold months (Leicht-Young et al., 2014). If these embolisms block the flow of water and nutrients to the leaves, the vine will not survive. As a result, vines have consequently developed mechanisms to overcome this problem. For example, grapes (Vitis spp.) create a positive pressure at the root to force out air bubbles trapped in the stem. Oriental Bittersweet (Celastrus orbiculatus) replaces the old damaged xylems with new ones during the spring (Leicht-Young et al., 2014).

Furthermore, lianas and vines are notable for anomalous structure, which result from cambial variants. Cambium is a cellular plant tissue that is responsible for the generation of phloem, xylem, and cork. Cambium irregularities are not unique only to lianas and vines. However, some of the most complex forms of cambial variants is exclusive to lianas (F. E. Putz & Mooney, 1991).

It is has been observed that the anomalous structural variants in vines and lianas develop after the development of the climbing mechanism. The combination of high soft tissue in xylem and cambial variants result in flexibility of the vine stems, minimizes the possibility of mechanical damage, and aids the process of fast healing (Isnard & Silk, 2009; F. E. Putz & Mooney, 1991).

4.2.3. Vines Biomechanics Types

Lianas and vines propagate through seeds and root sprouts. The climbing mechanics of vines and lianas have a direct relation to their ecology.

However, these climbing mechanisms do not manifest until the seedling has reached the height of one half meter to four meters; until then, the seedling is self-supporting. The cylindrical wood in juvenile stems provides the needed stiffness for a seedling to support itself. As the seedling matures the development of flexible stem and irregular cambium begins (Isnard & Silk, 2009; F. E. Putz & Mooney, 1991).

In 1875 Charles Darwin, in his seminal book *On the Movements and Habits of Climbing Plants*, divides vines' climbing mechanisms into five distinct categories: leaf climbers, twining plants, clinging climbers, and hook climbers. In the following section, each climbing mechanism is introduced and their functional perspective is discussed.

4.2.3.1. Twining Plants

Twining plants/Stem Twiners utilize their stems to wind around a support by forming a spiral grip. They do so by sending out a search shoot that is straight and vertical at the base, straight but horizontal at its apex, and curved in a plane (Isnard & Silk, 2009). Darwin named this circular movement—when observed from atop the plant—circumnutation. Through circumnutation the plant increases its chance of finding a support for its growth. Once a support is located its movement pattern changes from two revolutions to more than nine (Isnard & Silk, 2009).

Once the stem is securely wrapped around the support it twists along it axis opposite to the direction of circumnutation (antidromous twist). It is observed that as the surface roughness of the support increases the antidromous twist is exaggerated.

The direction of the spiral can vary. The majority of twining plants are right-handed helices: When observed from the top they wind in a counter-clockwise direction. Fewer species such as Humulus spp., Wisteria Frutescens, and Cannabaceae, are left-handed helices.

As the stem reaches the top of the support, it becomes a search shoot again and resumes circumnutation to find another support nearby. These search shoots can extend vertically up to six feet, and can be observed above tree canopies in a tropical forest.

The biomechanics of twining plants are still under investigation. The stem creates a squeezing force normal to its support through various means. Friction plays a key role in stabilizing the twining. Fluid pressure inside the stem, as well as a slight thickening of the stem against its support, provide a tighter grip for the plant. As a result, twining plants are extremely resistant to gravitational forces (Isnard & Silk, 2009; F. E. Putz & Mooney, 1991). A few examples of stem twiners are Dutchman's pipe (*Aristolochia*), Bittersweet (*Celastrus scandens*), and Moonflower (*Ipomoea*).

4.2.3.2. Leaf Climbers

Leaf climbers, also known as leaf bearers or petiole climbers, utilize sensitive petioles that can wrap around a support after contact. As the contact is made the petiole become woody and develop a structure similar to stems. When compared to twining plants, they circumnutate at faster rates. Sensitive hooks are also grouped under leaf climbers because (similar to sensitive petioles) they thicken to hold to their support (Isnard & Silk, 2009). Some of the popular leaf climbers are Clematis, Climbing nasturtium (*Tropaeolum polyphyllum*), and Rhodochiton

4.2.3.3. Tendril Bearers

"Tendrils are structures that are formed through modifications of the stem, leaves, leaf tips, or stipules (outgrowth at the base of the leaf)" (Leicht-Young et al., 2014). Their length varies from 1.5 inches to 15.7 inches. Compared to leaf climbers and twining plants, they have faster circumnutation movement and they move in an "irregular ellipsoidal" manner (Isnard & Silk, 2009).

Tendrils can be divided into three groups: tendrils that behave similar to search shoots and circumnutate to increase the chance of finding a support, tendrils that are irritable and coil when contact to the support structure is made, and tendrils that coil without any contact with a support. (Jaffe & Galston, 1968)

When a tendril contacts a support it creates two equal helixes but with opposite directions. This spring-like coiling method increases the plant's resistance against wind and external loads, and pulls the plant closer to the support. Tendril bearers can only wrap around thin support structures. Some of the popular vines are Grapes (*Vitis spp*) and porcelain berry (*Ampelopsis brevipedunculata*) (Isnard & Silk, 2009; Leicht-Young et al., 2014).

4.2.3.4. Clinging Climbers

Clinging climbers attach to their host either by secreting viscid fluid or burrowing through the host's surface irregularities. Clinging climbers can be further broken down into two categories: adventitious roots and adhesive disk tendril.

Adventitious roots normally grow alongside of vines and lianas stems. The width and length of these rootlets varies depending on the species. Once these rootlets contact the support structure, the glandular secretion is released from the rootlet tips. The rootlets later absorb the "watery part, and ultimately leave a cement" (Darwin, 1865). The created bond between the plant and the host is very strong. The exact makeup of the viscid fluid is still under research (Leicht-Young et al., 2014).

Tendrils of clinging climbers are different then tendril bearers in that they are modified with small, pad-like disks at their tips. Similar to adventitious roots, the glandular secretion is released from the tip of the adhesive disks when it contacts the support. The secretion creates a strong bond with the surface.

Clinging climbers can attach themselves to almost any support system. However, this method of climbing limits the plant to only one main host. Some popular species are Euonymus, English ivy *(Hedera helix*), and Climbing hydrangea (*Hydrangea petiolaris*).

4.2.3.5. Hook Climbers

Hook climbers, as the name suggests, climb with the aid of hooks. "These recurved structures, which can occur along stems, leaves, or modified inflorescences, vary in size from several millimeters to upwards of centimeters" (F. E. Putz & Mooney, 1991).

Compared to other climbing mechanisms, hook climbers are less specialized, but they demonstrate morphological change when they contact support structures. The hooks that have contacted a support become thicker and woodier in comparison to the ones that are free. The maturity of the hooks are related to both contact simulation and the stresses that are exerted on the hook due to supporting the plant itself (Leicht-Young et al., 2014; F. E. Putz & Mooney, 1991)

4.2.4. Vines Structural Support

The climbing mechanisms of vines reveal the ecological needs of the climbing plants. Darwin observed that the manner in which a plan climbs describes both the maximum diameter of the supporting structure as well as the needed distribution of the support (Darwin, 1865; F. E. Putz & Mooney, 1991).

Investigations of the support structures of lianas and vines suggest that as long as the host is strong enough to carry their mass, there is no minimum required diameter for the support structure. In other words, there is no lower limit on a trellis's thinness (F. E. Putz, 1984).

This observation explains the distribution of lianas and vines in forests. The majority of climbing plants are found at the forest edge where trees are smaller. On the other hand, the population of climbing plants drops significantly within the interiors and mature sections of a forest where the tree trunks are large (F. E. Putz, 1984).

Tendril bearers require the smallest trellis diameter. Their support structure diameter should not exceed 7 cm (2.7 inches). Finding a thin host in a forest can be a daunting task for tendril bearers. Therefore, compared to other climbers, they invest very little in their stems and roots so that they can grow fast when the appropriate support structure is located (Darwin, 1865; F. E. Putz, 1984).

Stem twiners can utilize larger diameter support structures than tendril bearers. The maximum trellis diameter for twiners is 16 cm (6.3 inches). However, most twiner species cannot utilize support structures with diameters exceeding 7 cm (2.7 inches). "The rigidity, length, and mass of the elongating portion of the twiner's stem determine the maximum usable support diameter" (F. E. Putz, 1984). Rough surfaces are more suited for trellises because the stability of twiners depends heavily on the friction between the stem and the support structure.

The trellis diameter of leaf climbers can be even larger than for stem twiners. The maximum diameter for the support structure of these plants is 16 cm, or 6.3 inches. However, most of the leaf climber species are not capable of winding around a support larger than 15 cm, or 5.9 inches (F. E. Putz, 1984; F. E. Putz & Mooney, 1991).

There are no restrictions for the support structure diameter of clinging climbers because their adhesive disks and rootlets allow the plants to utilize any surface. Hook climbers depend more on "dense arrangement of supports than on supports of a restricted diameter." (F. E. Putz, 1984; F. E. Putz & Mooney, 1991).

The trellis distribution distance of lianas and vines vary; it mostly depends on the length of the search shoot when the plant has reached the top of the support structure. This span can vary from 0.3 m (1 foot) to 3 m (9.8 feet). An average maximum of 1 m for 43 species has been observed (F. E. Putz, 1984; F. E. Putz & Mooney, 1991).

The success of a climbing plant is directly related to its host. To insure their survival, climbing plants have developed techniques to find the needed support structures. For example, root climbers increase their chance of finding a support structure by growing along the forest floor toward the darkest areas of the horizon. The mechanics of this behavior is still under investigation. One possible explanation is that the plant can detect minor variations in the concentration of ethylene, which is produced by other plants nearby (F. Putz, 2014).

4.3. Indirect Green Walls Design Considerations

Variables impacting the performance of a green wall are numerous. The environmental variables, plant biophysical traits, and support structure requirements are reviewed. Note that soil composition, irrigation, and nutrient regimes are other important factors. They directly influence the performance of a green wall.

The following section provides an overview of some of the current indirect green wall systems and possible planter locations.

4.3.1. 2D Indirect Green Walls

The support surface configuration can generally be categorized into 2D and 3D surfaces. A two-dimensional system is the most conventional solution for indirect green wall systems. It utilizes vertical cables, horizontal cables, rods, grids, or nets fixed on a frame or rigid structure. These structural frames hold the plant supports in tension.

Consequently, the connectors and the attachment points between the building and the structural frame are critical factors of the 2D systems. A combination of a 2D structural system and a vegetative mass impose a significant weight load on the building structure, which needs to be considered as a design factor (Green Screen, 2012).

Material selection for a 2D system is dependent on a plant's ecological needs and the structural requirements of the green wall system. The most common materials are wood and steel. The cavity of the 2D system can be adjusted for different design requirements. It can be either optimized for thermal performance of the building or designed as an occupiable/programmable space.

4.3.2. 3D Indirect Green Walls

The main difference between 3D and 2D indirect green walls is that 3D systems are self-supporting structures. Three-dimensional systems address scenarios that cannot be implemented by 2D walls, mostly due to structural limitations. Simply stated, 3D systems are panels that occupy a volume instead of just a surface used in two-dimensional systems.

Three-dimensional panels are normally prefabricated and standardized. The wire grid surface mesh is held apart "by intermittent wires and welded to a perimeter steel frame for strength in mounting" (Green Screen, 2012). The modular panels are rigid and can span openings either horizontally or vertically. The main limitation of this system is that it cannot be customized to address the performance needs of specific plant ecologies and architectures.

4.3.3. Planter Locations

Three-dimensional green wall systems are standardized so that in most cases the planting location of the vegetation is prescribed. However, 2D systems allow for different design options and planting locations.

Climbing plants can be planted in different heights of a building facade. This strategy will create a cascading effect and has a great visual impact. When the planting is repeated at each floor it creates a green screen for the entire building facade at a much faster rate. The downside of this strategy is the associated high maintenance and construction cost. For example, irrigation systems must be emplaced for each floor; in cold climates the planters must be highly insulated to avoid frosting the roots of the plants; the increased weight load negatively impacts the cost of the building construction; and the limited planting space can produce stress for matured plants.

Almost all indirect green wall designs can be broken down into 2D and 3D green wall systems. However, the configuration of the systems can vary according to each project. Numerous design solutions have been developed. These design approaches, although inspiring, are very specific and unique to a project and rarely can be replicated.

5. Cooling from Indirect Green Walls

The cooling effect of green walls is largely attributed to cooling from transpiration and solar radiation interception of the canopy (Cameron et al., 2014; Hoelscher et al., 2016; Koyama et al., 2015; Šuklje et al., 2016). In this chapter, the variables impacting each cooling component are introduced. The corresponding theoretical models are reviewed and modified to represent the cooling performance of various green wall designs during the summer months in six distinct climates.

5.1. Cooling from Canopy Transpiration

The objectives of this chapter are to (1) evaluate the transpiration cooling production from various green wall designs in six distinct climates, (2) establish performance trends accounting for canopy geometry, and (3) provide guidelines for maximum cooling power from the transpiration of green walls.

To do so, the theoretical background impacting the transpiration of a canopy is reviewed. Each variable has been considered, and if needed, modified to reflect the green wall design characteristics. The possible range of values for each variable has been investigated and reported. The gathered data is then used to conduct a sensitivity analysis and a series of scenario studies. These studies identify designs corresponding with the maximum cooling power production from the transpiration of green walls in various climate conditions.

The result shows that:

- For maximum cooling power design, a canopy with stomatal resistance less than 100 m/s, a height between 3 and 6 m, and a Leaf Area Index of 3 or larger is recommended.
- The largest cooling power corresponds with hot climates, followed by warm climates and cool climates.
- With the exception of the cool and dry climate, the transpiration cooling power produced from dry climates is larger than their humid counterparts. This deviation of the cool and dry climate is due to high water efficiency of the associated vine for this climate.

5.1.1. Introduction

The Penman-Monteith (P-M) model is widely used to estimate the transpiration rate of a vegetative canopy. The model has been adopted by the Food and Agriculture Organization of the United Nations (the FAO 56 model) to estimate the transpiration rates of various crop fields. The P-M model, Eq. (6), is robust enough to account for environment variables, plant biophysical traits, and various time scales.

$$TR = \frac{\Delta \, . R_n + K_{time} \, . \frac{\rho . C_p . VPD}{r_a}}{\lambda[\Delta + \gamma(1 + {}^{r_c}/_{r_a})]} \tag{6}$$

Where

TR canopy transpiration rate [mm/h, mm/d]

Δ the slope of saturation vapor pressure vs. temperature [kPa/°C]

R_n the net radiation absorbed by the canopy [MJ/m^2.h, MJ/m^2.d]

ρ the density of dry air [kg/m^3]

C_p the specific heat of dry air at constant pressure [MJ/kg°C]

VPD the vapor pressure deficit of air [kPa]

r_a the canopy aerodynamic resistance [s/m]

r_c the canopy resistance [s/m]

λ the latent heat of vaporization of water [MJ/kg]

γ the Psychrometric constant [kPa/°C]

K_{time} a unit time conversion, equals to 86,400 s/day for mm/day and 3,600 s/h for mm/h

The P-M model treats the canopy as a large, continuous, horizontal leaf with no water limitation. Therefore, it is rather successful when applied to large crop fields that mimic these conditions. In contrast to crops, the irrigation regime of urban green infrastructure is normally not as rigorous—which can drastically reduce the transpiration rate of the canopy. Therefore, it is important to note that for this study well-watered canopy conditions have been considered.

Furthermore, studies on isolated plants such as vineyard, orchards, and isolated trees report that the P-M model lacks precision since isolated plants are more coupled with their surrounding environments (Dragoni, Lakso, Piccioni, & Tarara, 2006; Lu, Yunusa, Walker, & Müller, 2003; Thom & Oliver, 1977; Yunusa, Walker, Loveys, & Blackmore, 2000). For example, P. Lu et al. (2003) reported that the FAO 56 model underestimated the transpiration rate by 55%.

In this research, the P-M model has been used to estimate the transpiration rate—and ultimately the cooling power—of green walls. Similar to vineyards, green walls are isolated plants that are more coupled with their surrounding environments. Therefore, the P-M model must be adjusted to account for these variations. The following sections will describe each variable in the P-M model and highlight the adaptation of the model to account for the particular conditions of green walls.

The model parameters are comprised of variables accounting for environmental conditions (e.g., net radiation and the thermal properties of air), plant characteristics (e.g., aerodynamic and canopy resistances), and the time step in which the transpiration rate is evaluated. Similarly, the variables discussed in the next chapters are broken down into three general categories: (a) Time Scale, (b) Environmental, and (c) Biophysical.

5.1.2. Model Development

5.1.2.1. Time Scale

The FAO 56 guideline offers detailed instructions for calculations of both daily and hourly time steps. However, the goal of this research is to estimate the average monthly cooling power produced from the transpiration rate of a canopy. For an early-design phase of a project, the monthly time interval provides an appropriate scale of resolution.

Furthermore, the monthly estimation is particularly advantageous when using the P-M model, as some studies have reported that the model can predict the water use of canopies within an accuracy of 1%. The accuracy of the model is reduced as the time steps become smaller, such as daily or hourly (Dragoni et al., 2006).

Because the nighttime transpiration of vines is negligible due to stomatal closure (Yunusa et al., 2000), only transpiration during daylight hours was considered. The daylight hours of the 15th of each month were calculated and converted to the number of seconds in a month (R. G. Allen, Pereira, Raes, & Smith, 1998; R. Allen & Walter, 2003).

According to FAO 56 guidelines the obtained environmental values (e.g., solar radiation) from this method "deviate from values that are averaged over each day of the month by less than 1% for all latitudes during non-frozen periods and are included for simplicity of calculation" (R. G. Allen et al., 1998).

$$K = N_h \,.3600 \tag{7}$$

Where

K amount of daylight time in a month [s]

N_h daylight hours in the 15th day of a month

The Daylight Hours, N_h, as a function of Sunset Hour Angle, ω_s, is given by:

$$N_h = \frac{24}{\pi . \omega_s} \tag{8}$$

Where

N_h number of daylight hours in the 15th day of a month

ω_s sunset hour angle [rad] (Eq. (16))

Note that all environmental variables have been adjusted to the monthly time scale. Each change is described in the following sections.

5.1.2.2. Environmental Variables

5.1.2.2.1. *Absorbed Net Radiation, R_n*

Solar radiation has a large impact on the transpiration rate of plants. It is essential to adjust the P-M model to reflect the appropriate net radiation that is absorbed by a vertical surface against a building facade. The P-M model assumes the canopy as a large uniform horizontal leaf. Accordingly, the absorbed net radiation (R_n) is evaluated by Eq. (9):

$$R_n = R_{ns} - R_{nl} \tag{9}$$

Where

R_{ns} net short wave radiation [MJ/m^2.h, MJ/m^2.d]

R_{nl} net outgoing long wave radiation [MJ/m^2.h, MJ/m^2.d]

The net shortwave radiation is calculated as a fraction of the total received shortwave radiation, R_s, where α represents the albedo (dimensionless) of the canopy. The albedo of vegetative surfaces varies between 0.2 and 0.25 (R. G. Allen et al., 1998). The FAO 56 model considers the albedo value of a grass field to be 0.23. This value has been used throughout this investigation.

$$R_{ns} = (1-\propto)R_s \tag{10}$$

A vertical surface only collects a fraction of the total radiation received by a horizontal surface. This fraction is equivalent to $\cos\theta_v$, where θ_v is the angle of incidence on the vertical surface. The angle of incidence, θ_v, is a function of both the wall's solar azimuth angle (the angle between a hypothetical vector normal to the wall and the projection of the sun's rays onto a horizontal plane) and the solar altitude angle. This means that the received shortwave radiation on a vertical surface depends not only on the geographical location and the time of the day, but also on the orientation of the wall.

For this research, the R_s values were estimated using the solar simulation software Diva for Rhino. This program "is a highly optimized daylighting and energy modeling plug-in for the Rhinoceros - NURBS modeler" that can be used for radiation mapping simulations (www.diva4rhino.com).

The monthly R_s values of south and west facing vertical unit surfaces were simulated for each climate condition using 30-year Typical Meteorological Year (TMY3) weather files for each location. The detailed description of each scenario and obtained *Rs* values are reported in the model verification section (Table 5).

5.1.2.2.2. ***Net Long Outgoing Wave Radiation, R_{nl}***

The net outgoing long wave radiation, R_{nl}, was calculated following the FAO 56 equations. Accordingly, R_{nl} is proportional to the absolute temperature of the surface raised to the fourth power. This relationship is expressed by the Stefan-Boltzmann constant. The FAO 56 model further refines the equation by considering humidity and cloudiness factors (Eq. (11)).

$$R_{nl} = \sigma \,. \left[\frac{T_{max-k}^4 + T_{min-k}^4}{2}\right] . \left(0.34 - 0.14\sqrt{e_a}\right) . (1.35 \, \frac{R_s}{R_{so}} - 0.35) \qquad (11)$$

Where

R_{nl} net outgoing long wave radiation [MJ/m^2. day]

σ Stefan-Boltzmann constant [4.903 x 10^-9 MJ/K^4.m^2.day)

T_{max} maximum absolute air temperature during the 24 hour period [K]

T_{min} minimum absolute air temperature during the 24 hour period [K]

e_a actual vapor pressure [kPa]

R_s/R_{so} relative shortwave radiation

R_s shortwave radiation [MJ/m^2.day] (for this study the values were simulated using Diva for Rhino software)

R_{so} clear-sky radiation [MJ/m^2. day]

The first term of Equation (11) accounts for the long wave radiation leaving the surface of the canopy. The second term, $\left(0.34 - 0.14\sqrt{e_a}\right)$, describes the correction for air humidity. Its value decreases as humidity increases. The third term,$(1.35\,\frac{R_s}{R_{so}} - 0.35)$, accounts for the cloudiness. Its value decreases as there are more overcast days. The clear-sky radiation, R_{so}, can be calculated by Equation (12) as a function of the daily extraterrestrial radiation.

$$R_{so} = (0.75 + 2\,\times\,10^{-5}z)R_a \tag{12}$$

Where

R_a extraterrestrial radiation [MJ/m^2.day]

Z elevation above the sea level [m]

The daily extraterrestrial radiation, R_a, can be estimated for each day of the year and various latitudes from the solar constant, solar declination, and time of year (Eq. (13)).

$$R_a = \frac{24\,(60)}{\pi} G_{sc} d_r [\omega_s \sin\varphi \sin\delta + \cos\varphi \cos\delta \sin\omega_s] \tag{13}$$

Where

R_a extraterrestrial radiation [MJ/m^2.day]

G_{sc} solar constant, 0.0820 [MJ/m^2.min]

d_r inverse relationship distance Earth-Sun (Eq. (14))

ω_s sunset hour angle [rad] (Eq. (16))

ϕ latitude [rad]

δ solar declination [rad] (Eq. (15))

The inverse relative distance Earth-Sun, d_r, and solar declination, δ, are both a function of the number of days in a year, J, and are given by:

$$d_r = 1 + 0.033\cos(\frac{2\pi}{365}.J) \quad (14)$$

$$\delta = 0.409\sin(\frac{2\pi}{365}.J - 1.39) \quad (15)$$

The sunset hour angle, ω_s, is defined by:

$$\omega_s = \arccos[-\tan(J).\tan(d)] \quad (16)$$

The *Ra* values for the 15th day of each month can be used as a good approximation (< 1% error) for each day of the month. Therefore, for this investigation, the 15th of each summer month was used (R. G. Allen et al., 1998). Note that for this research only the cooling effect (transpiration and solar radiation interception) of the canopy during the summer is investigated.

The sky view of a vertical surface is half of its counterpart (Nellis, 2009). Therefore, to adjust for the sky view of a vertical green wall, a factor of 0.5 was considered. The final R_{nl} values were multiplied by the number of days in the month to provide the monthly net outgoing long wave radiation (Eq. (17)) (R. G. Allen et al., 1998).

$$R_{nl} = d_m \left[\frac{1}{2}.\sigma.\left[\frac{T^4_{max-k} + T^4_{min-k}}{2}\right].\left(0.34 - 0.14\sqrt{e_a}\right).\left(1.35\frac{R_s}{R_{so}} - 0.35\right)\right] \quad (17)$$

Where

d_m *number of days in a month*

R_{nl} net outgoing long wave radiation [MJ/m^2. day]

σ Stefan-Boltzmann constant [4.903 x 10^-9 $MJ/K^4.m^2$.day)

T_{max} maximum monthly air temperature [K]

T_{min} minimum monthly air temperature [K]

e_a actual vapor pressure [kPa]

R_s/R_{so} relative shortwave radiation

R_s shortwave radiation [MJ/m^2.day] (for this study the values were simulated using *Diva for Rhino* software)

R_{so} clear-sky radiation [MJ/m^2. day]

5.1.2.2.3. Atmospheric Pressure, P

The atmospheric pressure, P, is the pressure exerted by the weight of the atmosphere. According to the FAO 56 model, the average value of P of a location is a good approximation. The relationship is given by Equation (18) which assumes 20 °C for a standard atmosphere (R. G. Allen et al., 1998).

$$P = 101.3\,(\frac{293 - 0.0065.z}{293})^{5.26} \qquad (18)$$

Where

P atmospheric pressure [kPa]

Z elevation above sea level[m]

5.1.2.2.4. Latent Heat of Vaporization, λ

The latent heat of vaporization describes the required energy to change a unit of mass of water from liquid to vapor state at a constant pressure and temperature. For this investigation, a single value of 2.45 MJ/kg is used, which represents the latent heat for a temperature of 20 °C at standard sea-level pressure (R. G. Allen et al., 1998).

5.1.2.2.5. Psychrometric Constant, γ

The psychrometric constant, γ, "relates the partial pressure of the air to the air temperature so that vapor pressure can be estimated using paired dry and wet thermometer blub temperature." The FAO 56 model recommends the average atmospheric conditions (C_p = 1.013x10^{-3} MJ/kg.°C). Accordingly, the psychrometric constant, γ, is given by:

$$\gamma = \frac{C_p . P}{\varepsilon\lambda} = 0.00065P \quad (19)$$

Where

γ the psychrometric constant [kPa / ℃]

P atmospheric pressure [kPa] Eq. (18)

λ latent heat of vaporization, 2.45 [MJ / kg]

C_p specific heat at constant pressure, 1.013×10^{-3} [MJ / kg.°C]

ε ratio molecular weight of water vapor/dry air, 0.622

5.1.2.2.6. Air Temperature, T

To obtain the daily transpiration rate, the FAO 56 model recommends using the maximum and minimum temperatures measured at 2 m above the canopy. These values are used to estimate the mean daily temperature, mean saturation vapor pressure, e_s, and slope of saturation vapor pressure, Δ. Because the goal of this investigation is to estimate the monthly transpiration rate of a canopy, the monthly maximum and minimum temperatures were considered. (Please refer to section 5.1.2.1 for a detailed discussion.)

$$T_{mean} = \frac{T_{max} + T_{min}}{2} \quad (20)$$

Where

T_{mean} mean monthly air temperature [°C]

T_{max} maximum monthly air temperature [°C]

T_{min} minimum monthly air temperature [°C]

5.1.2.2.7. Mean Saturation Vapor Pressure, e_s

The saturation vapor pressure is a function of air temperature and is given by:

$$e_{(T)} = 0.6108 \exp\left[\frac{17.27T}{T + 237.3}\right] \tag{21}$$

Where

$e_{(T)}$ saturation vapor pressure at the air temperature T [kPa]

T air temperature [°C]

To calculate the mean saturation vapor pressure, e_s, (Eq. (24)), the maximum (Eq. (22)) and minimum (Eq. (23)) must be calculated (R. G. Allen et al., 1998). Note that for this research, the monthly maximum and minimum temperatures were used.

$$e_{(T_{max})} = 0.6108 \exp\left[\frac{17.27T_{max}}{T_{max} + 237.3}\right] \tag{22}$$

$$e_{(T_{min})} = 0.6108 \exp\left[\frac{17.27T_{min}}{T_{min} + 237.3}\right] \tag{23}$$

$$e_s = \frac{e_{(T_{max})} + e_{(T_{\min})}}{2} \tag{24}$$

Where

T_{max} maximum monthly air temperature [°C]

T_{min} minimum monthly air temperature [°C]

5.1.2.2.8. *Actual Vapor Pressure, e_a*

The dewpoint temperature is the temperature to which the air would have to cool to be fully (100%) saturated. The actual vapor pressure, e_a, is "the saturation vapor pressure at the dewpoint temperature" (R. G. Allen et al., 1998). The value of e_a can be calculated from relative humidity and is given by Equation

(25). Note that to obtain monthly e_a values, the average monthly maximum and minimum relative humidity values, *RH*, were used. Relative Humidity, *RH*, is the amount of water vapor present in air expressed as a percentage of the amount needed for saturation at the same temperature.

$$e_a = \frac{e_{T_{min}}\left[\frac{RH_{max}}{100}\right] + e_{T_{max}}\left[\frac{RH_{min}}{100}\right]}{2} \tag{25}$$

Where

e_a actual vapor pressure [kPa]

e_{Tmin} saturation vapor pressure at monthly minimum temperature [kPa]

e_{Tmax} saturation vapor pressure at monthly maximum temperature [kPa]

RH_{max} monthly maximum relative humidity [%]

RH_{min} monthly minimum relative humidity [%]

5.1.2.3. Biophysical Variables

5.1.2.3.1. Aerodynamic Resistance r_a

Aerodynamic resistance, r_a, defines the water vapor and heat transfer from the plant into the air above the canopy. A high r_a value of 250 s/m corresponds with dense crops, which are poorly connected to their surrounding environment. An r_a value of 5 m/s corresponds with well-coupled conditions such as forests. According to the FAO 56 model, r_a, can be calculated by:

$$r_a = \frac{In\left[\frac{z_m - d}{z_{om}}\right].In[\frac{z_h - d}{z_{oh}}]}{k_{von}^2.u_z} \quad (26)$$

Where

r_a aerodynamic resistance [s/m]

Z_m height of wind measurements [m]

Z_h height of humidity measurement [m]

d zero plane displacement height [m]

Z_{0m} roughness length governing momentum transfer [m]

Z_{0h} roughness length governing transfer of heat and vapor [m]

k_{von} Von Kaman's constant, 0.41 [-]

u_z wind speed at height Z [m/s]

Although Equation (26) has proven useful for short dense crops, many studies on grapevines have reported poor correlation for tall isolated plants, which are highly coupled to their surrounding environments. In a study done on Sultana grapevines in Victoria, Australia, P. Lu et al. (2003) found that the r_a suggested by the FAO 56 model underestimated the transpiration rate by 55%. To address this problem, several studies have used the aerodynamic calculation, Equation (27), developed by Thom and Oliver (Thom & Oliver, 1977) for tall, isolated plants.

$$r_a = \frac{4.72[In\left(\frac{Z_w}{Z_0}\right)]^2}{(1 + 0.54U)} \tag{27}$$

Where

Z_w height of measurement of wind speed, 2 m

Z_0 roughness height taken as 0.13 of the canopy height, *h* [m], which was used for grapevines by van den Hurket al. (1995), i.e., $Z_0 = 0.13$h

U wind speed (m/s)

Various studies showed reasonable agreement with the data from field measurements in both hot and dry climates, and cool and humid climates (Dragoni et al., 2006; Lu et al., 2003; Yunusa et al., 2000). It stands to reason that Equation (27) provides a better estimate for the aerodynamic conductances of green walls. Therefore, for this investigation, Equation (27) was used to estimate r_a values.

5.1.2.3.2. ***Bulk/Surface/Canopy Resistance r_c***

"The 'bulk' surface resistance [canopy resistance] describes the resistance of vapour flow through the transpiring crop and evaporating soil surface" (R. G. Allen et al., 1998). In reality the surface resistance, r_c, continuously changes because the stomata rapidly respond to environmental conditions (Lu et al., 2003). Variables impacting stomatal resistance, r_l, are solar radiation, temperature, humidity, and leaf water status (Jones, 1992). Although lab experiments have separated and studied the impact of each variable independent of the others, predicting the stomatal behavior in the field conditions is complicated (Jones, 1992).

Furthermore, r_c is highly correlated with water availability and canopy geometry (Jones, 1992). The FAO 56 model requires a fixed canopy resistance to calculate plant transpiration:

$$r_c = \frac{r_l}{LAI_{Sunlit}} \tag{28}$$

Where

r_c canopy surface resistance [s/m]

r_l bulk stomatal resistance of the well-illuminated leaf [s/m]

LAI_{Sunlit} sunlit Leaf Area Index (LAI) [-]

The leaf area index (*LAI*) is a dimensionless value describing the ratio of one-sided leaf area to unit ground area, and in the case of green walls, the ratio of leaf area [m^2] to unit wall area [m^2]. The sunlit LAI, LAI_{Sunlit}, uses as the numerator the amount of leaf area that receives sunlight and contributes to the transpiration rates of green walls. LAI_{Sunlit} can be calculated by (R. G. Allen et al., 1998; Jones, 1992):

$$L_{sunlit} = \frac{(1 - e^{-k\,LAI})}{k} \tag{29}$$

Where

L_{sunlit} sunlit Leaf area index [-]

k extinction coefficient [-]

LAI leaf area index

Although the FAO 56 model's method for estimating surface resistance (Eq. (28)) is simple, bulk stomatal resistance values, r_l, can be challenging to obtain because there are limited studies on urban vine species. A few studies have faced the problem of accounting for the canopy transpiration rates of green walls, but have used a generic value derived from woody plants for bulk stomatal resistance.

To address this problem, the author consulted published literature that has recorded the stomatal resistances of various vine species in six different climates. The goal of this literature review was to (a) define a range of acceptable values of r_l of vines, (b) assess the variation of r_l for different vine species (agricultural and non-agricultural), and (c) evaluate the impact of particular climatic conditions on r_l.

5.1.3. Stomatal Resistance Library

To evaluate r_l, an extensive library on the stomatal resistances of vines for six climates was developed. The climates are categorized according to typical summer conditions. Table 1 describes each category.

Table 1. Considered six climate scenarios

Climate type	***Monthly Average Maximum Temperature Range (°C)***	***Monthly Precipitation Range (mm)***
Cool & Humid	20 to 26	> 50
Cool & Dry	20 to 26	< 50
Warm & Humid	27 to 32	> 50
Warm & Dry	27 to 32	< 50
Hot & Humid	32 to 40	> 50
Hot & Dry	32 to 40	< 50

A total of 27 studies and 89 vines were considered (Barker & Pérez-Salicrup, 2000; Bell et al., 1988; BOTA, Flexas, & Medrano, 2001; Carter & Teramura, 1988; Chaves, Harley, Tenhunen, & Lange, 1987; Correia, Pereira, Chaves, Rodrigues, & Pacheco, 1995; Cuevas, Baeza, & Lissarrague, 2006; Downton, Grant, & Loveys, 1987; Edwards & Warwick, 1984; Escalona, Flexas, & Medrano, 2000; Fichtner & Schulze, 1990; Leuzinger, Hartmann, & Körner, 2011; Liu, Pool, Wenkert, & Kriedemann, 1978; Liu, Wenkert, Allen Jr, & Lemon, 1978; Padgett-Johnson, Williams, & Walker, 2003a; Quick et al., 1992; Rogiers, Greer, Hutton, & Clarke, 2011; Sanches & Válio, 2008; Schultz, 1995; R. Smart, 1974; Winkel & Rambal, 1990). The vine species include grapevines, urban vines, and tropical vines. The library includes 11 countries in order to assure well-mixed sampling conditions. Figure 7 shows the number of recorded vines per climate type and Table 2 shows the geographical distribution of the library. As expected, a majority of studies found was on grapevines and were mostly concentrated in warm and dry climates.

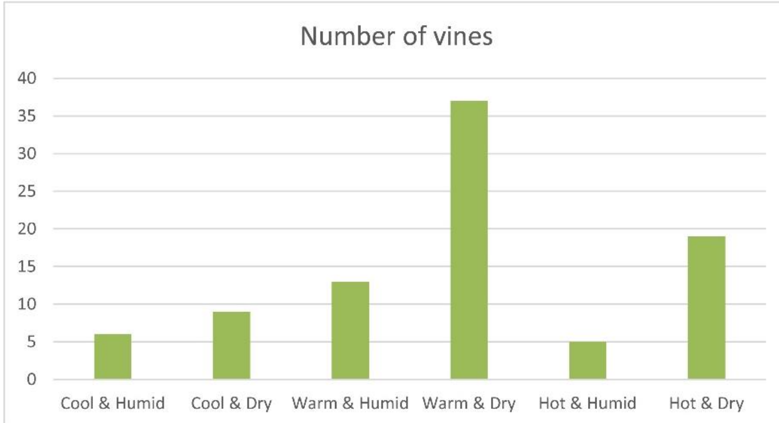

Figure 7. Number of considered vines per climate

Table 2. Geographical distribution of the recoded vines

	Cool & Humid	*Cool & Dry*	*Warm & Humid*	*Warm & Dry*	*Hot & Humid*	*Hot & Dry*
Australia			1	3		2
Bolivia		3				
Brazil					2	
France				6		
Germany	1					
Mexico					3	
New Zealand	2					
Portugal		6		3		
Spain				25		
Switzerland	1					
USA	2		12			17

The average, highest, and lowest limits of r_l for each climate category were compiled. Special attention was given to whether experiments were irrigated, partially irrigated, or non-irrigated. Figure 8 shows that, in general, irrigation increases in climates with higher summer temperatures. Any values of r_l corresponding to vines suffering from high water stress were not included in the final calculations.

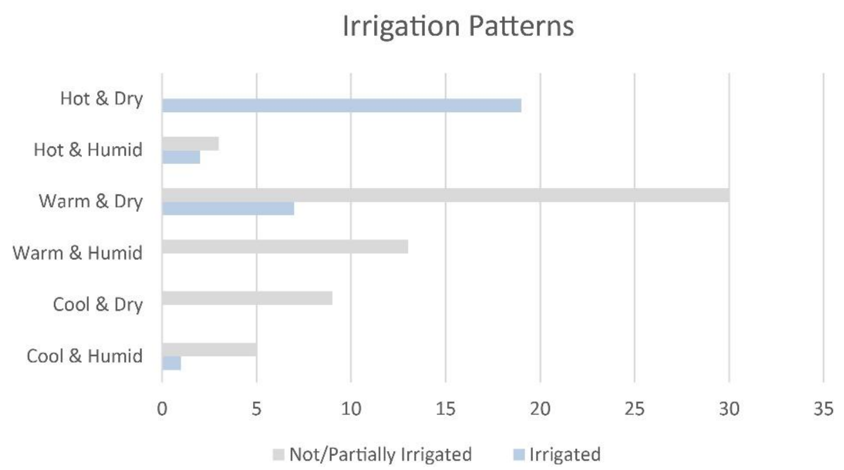

Figure 8. Number of occurrences of irrigation patterns for each climate condition

5.1.3.1. Results

Figure 9 shows the average, high, and low r_l values of grapevines and urban vines (non-agricultural vines). Two distinct patterns can be observed. First, the r_l range is larger in dry climates compared to its humid counterpart. In other words, the difference between the highest and lowest r_l values increases in dry climates.

Second, in general, urban vines are more water efficient, meaning that they are more sensitive to humidity and water availability. As a result, their average r_l values are larger than those of grapevines in the same climate.

This pattern was also observed by Bell et al. (1988). They measured the leaf resistances of three urban vines: Japanese honeysuckle (*Lonicera japonica*), Virginia creeper (*Parthenocissus quinquefolia*), and Forest grape (*Vitis vulpine*) in Maryland, USA, for two summers. Their investigation showed that the forest grape, a relative of grapevines, consistently had the highest transpiration rate and the lowest stomatal resistance (Bell et al., 1988).

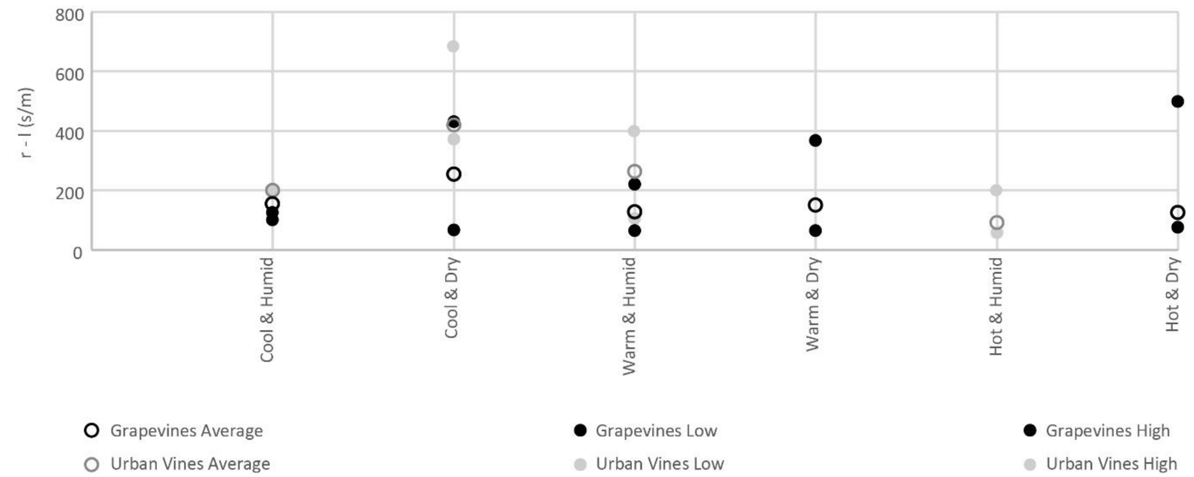

Figure 9. Stomatal resistance, r_l, averages and ranges per climate conditions for grapevine and urban vines (non-agricultural vines)

Table 3 shows the average, high, and low values of r_l for each climate condition. For this investigation (with the exception of the hot and humid climate), the average grapevine values of stomatal resistance obtained in this section will be used for scenario and simulation studies. For the hot and humid climate, the average value of stomatal resistance of urban vine is used because no information was found on the Vitis species.

Table 3. Average, high and low values of the stomatal resistances of grapevines and urban vibes for various climates

	Grapevines r-l [s/m]			Urban Vines r-l [s/m]		
	Average	Low	High	Average	Low	High
Cool & Humid	115	100	125	199	198	200
Cool & Dry	255.71	66.41	431.13	419.93	372.35	682.64
Warm & Humid	128.45	65.39	221.05	263.74	106.57	397.72
Warm & Dry	151.62	64.02	367.1			
Hot & Humid				91.55	57.06	199.7
Hot & Dry	125.09	76.8	500			

5.1.4. Model Sensitivity Analysis

The developed P-M model for vertical green walls was written in Engineering Equation Software (EES). This software was selected because it is a robust tool for parametric studies. The model was analyzed and verified in two stages. First, the general trends of the model were compared to the sensitivity analysis conducted by (Jones, 1992). Second, a series of scenario studies for six various climates were conducted (see the methodology section under Bulk/Surface Resistance). The predicted transpiration (TR) values were compared to the reported TR values of grapevines in similar climates.

5.1.4.1. The Influence of Environmental and Biophysical Variables on Transpiration Rate

To investigate the influence of environmental and biophysical variables, a parametric investigation was conducted. Figure 10 to Figure 13 illustrate the results. Assumed values for each variable are reported in Table 4. These values are adopted from Jones (1992) for comparative studies. They have been used throughout all studies unless otherwise indicated. Aerodynamic resistance was calculated using Equation (27). Plant height and roughness height were assumed to be 1.5 m and 0.13 m, respectively (Thom & Oliver, 1977).

Table 4. Considered values of variables for P-M model sensitivity analysis

Radiation (W/m^2)	Temperature (°C)	Relative Humidity (%)	Wind Speed (m/s)	Bulk Stomatal Resistance (s/m)	Aerodynamic Resistance (s/m)
100	20	50	1	200	12.3

5.1.4.2. Transpiration as a Function of Vapor Pressure Deficit and Radiation

Figure 10 shows *TR* as a function of *VPD* and R_n. As expected, *TR* increases linearly with both *VPD* and R_n. This is apparent from Equation (1) where the two variables have a direct relationship with *TR*. This trend can also be observed in Figure 11 and Figure 12.

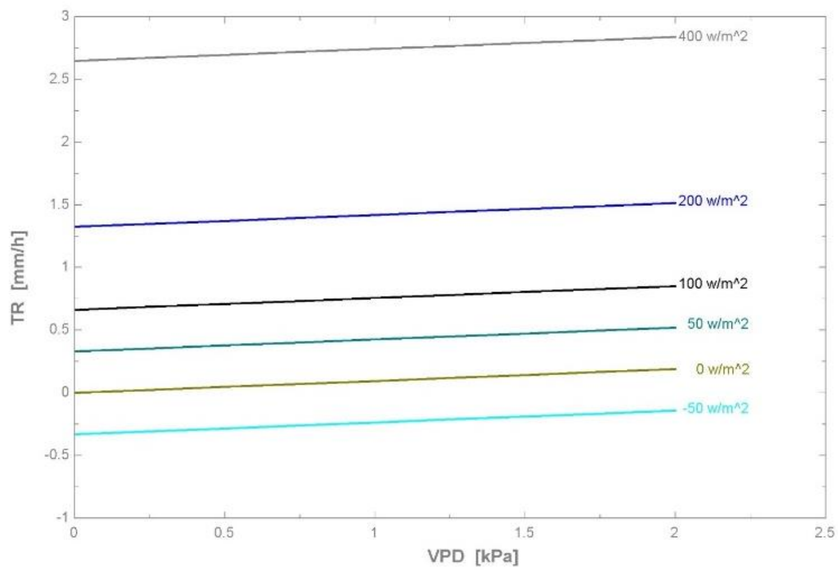

Figure 10. Transpiration as a function of Vapor Pressure Deficit and Radiation (see Table 4 for considered variables). Considered variables unless otherwise indicated; u = 0.8 m /s, Rn = 100 W/m², Air temperature = 20 °C, Relative humidity = 50%, Stomatal conductance = 4 mm /s

5.1.4.3. Transpiration as a Function of Radiation and Wind Speed

Figure 11 shows *TR* as a function of radiation and wind speed. Similar to Figure 10, *TR* increases linearly with R_n. Less intuitively, *TR* decreases as wind speed increases. This trend arises since aerodynamic resistance, r_a, appears both in the numerator and denominator of the P-M model (Eq. (1)). The crossover point defines the condition where the leaf surface temperature has reached the ambient temperature (Jones, 1992).

As the wind speed increases, the boundary layer thickness over the leaf surface is reduced, causing the boundary layer conductance to increase. This condition induces sensible heat transfer. However, it does not promote the best conditions for latent heat transfer, and by extension, an increase in *TR*. On the other hand, low wind speeds cause high boundary layer thicknesses, and in turn, low boundary layer conductances. Under these conditions, *TR* increases and sensible heat transfer decreases.

The negative *TR* values correspond to negative radiation values where the leaf is losing heat through radiative heat transfer. In this circumstance, dew forms on the leaf. As expected, as wind speed increases, dewfall decreases.

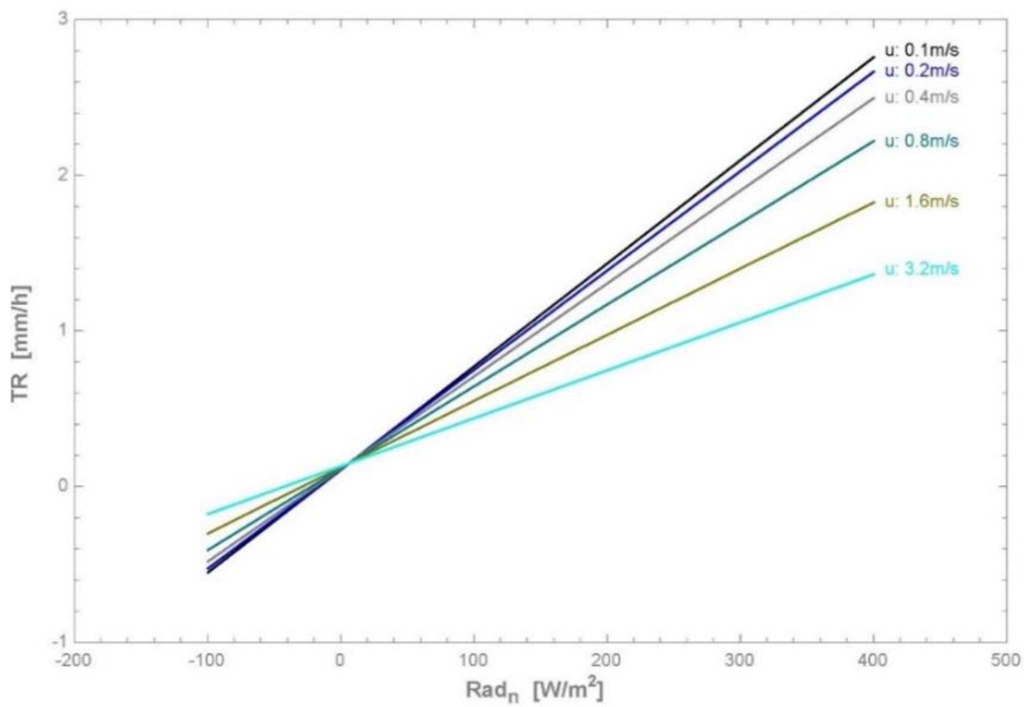

Figure 11. Transpiration as a function of Radiation and Wind Velocity (see Table 4 for considered variables), Considered variables unless otherwise indicated; u = 0.8 m /s, Rn = 100 W/m², Air temperature = 20 °C, Relative humidity = 50%, Stomatal conductance = 4 mm /s

5.1.4.4. Transpiration as a Function of Wind and Radiation

Figure 12 shows *TR* as a function of wind speed, *u*, and R_n. Where $R_n = 0$, the leaf surface temperature is at the ambient temperature. Similar to previous graph, positive values of R_n increase *TR* and negative values promote dewfall conditions. As the wind speed increases, *TR* decreases. This is best shown at high R_n values (i.e., 400 W/m^2), where the graph shows the fastest decaying trend. This indicates that in high wind speeds, sensible heat transfer is dominant, whereas in low wind speeds, latent heat transfer is promoted.

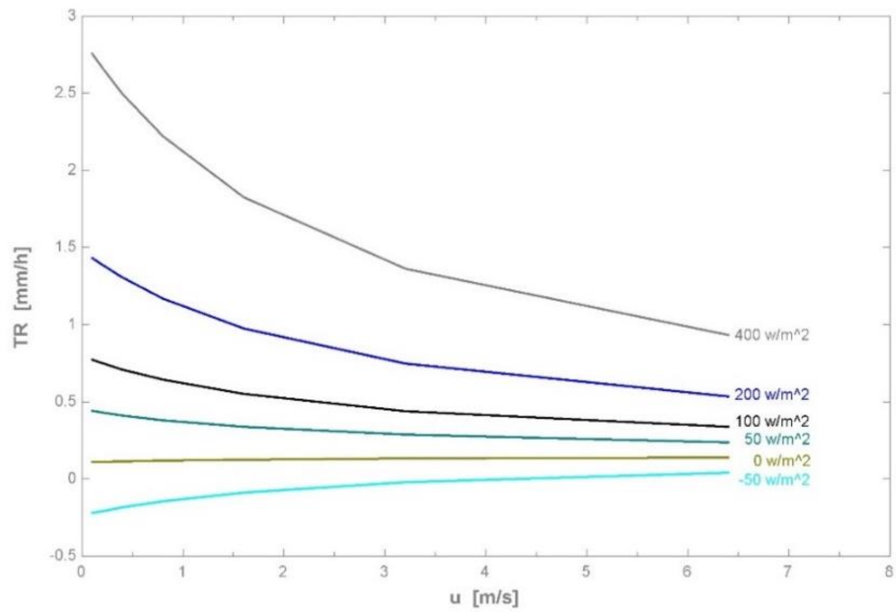

Figure 12. Transpiration as a function of Wind Speed and Radiation (see Table 4 for considered variables), Considered variables unless otherwise indicated; u = 0.8 m /s, Rn = 100 W/m², Air temperature = 20 °C, Relative humidity = 50%, Stomatal conductance = 4 mm /s

5.1.4.5. Transpiration as a Function of Surface Resistance and Wind Speed

The dependence of *TR* on canopy/surface resistance, r_c, for various wind speeds is illustrated in Figure 13. This figure best demonstrates the relationship between r_c (biophysical resistance) and r_a (boundary layer resistance). The largest *TR* values correspond with the lowest r_c values where stomata exert the least control (associated with well-watered or wet leaves) on water vapor loss. Not surprisingly, in this condition, the largest boundary layer conductance from the highest wind speed produces the greatest *TR* value.

On the other hand, when r_c is large, canopy transpiration is reduced because it is being limited by the stomatal apertures (i.e., water-stressed plants). In this condition, the lowest wind velocity, which promotes low boundary conductance, corresponds with the greatest *TR* value.

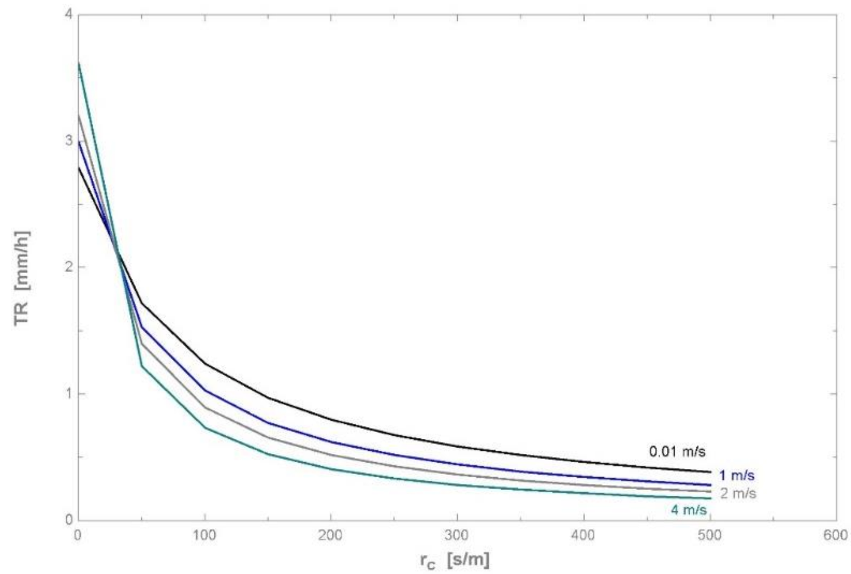

Figure 13. Transpiration as a function of Canopy/Surface Resistance and Wind Speed (see Table 4 for considered variables), Considered variables unless otherwise indicated; u = 0.8 m /s, Rn = 100 W/m^2, Air temperature = 20 °C, Relative humidity = 50%, Stomatal conductance = 4 mm /s

The above investigation focused on the impact of environmental conditions on the transpiration rates of canopies. The results were comparable to studies conducted by Jones, 1992 showing that the model follows the correct trends. Note that this is purely a numerical investigation and does not reflect the interdependency of the considered variables in field conditions. However imperfect, the sensitivity analysis provides a useful overall understanding of the model's expected behavior.

The study illustrates that to achieve the maximum transpiration rate (and in turn cooling power) both aerodynamic and canopy/surface resistances must be optimized in relation to the climate in which the plant is located.

Aerodynamic resistance, r_a, is a function of plant height, h, and wind speed, u (Eq. (27)). Canopy resistance, r_c, is a function of leaf surface resistance, r_l, and the sunlit leaf area index, LAI_{sunlit} (Eq. (28)). Accordingly, the h, r_l (species selection), and LAI_{sunlit} can be designed and optimized so that a green wall can produce the maximum possible cooling power within a climate.

5.1.5. Model Verification-Climatic Scenario Studies

The objectives of this study are to (a) verify the developed P-M model for green walls in various climates, (b) provide a sensitivity analysis of r_a and r_c per climate type, (c) define the optimal canopy biophysical and architecture traits for maximum transpiration rates, and (d) investigate the thermodynamic limits of green walls as a passive cooling system.

5.1.5.1. Method

To further verify the proposed P-M model for green walls, six various climatic scenarios were considered. Table 1 shows detailed descriptions of each climate type. A U.S. city was selected that corresponded to one of the six climates of interest. These cities were selected based on their maximum and minimum monthly temperatures and average precipitation during the summer months. The geographical and climatic conditions of each city were used as the environmental variables of the scenario studies (Table 5).

Table 5. Six climatic scenarios and the considered corresponding U.S cities

JUNE

Climate	Selected cities	Latitude [dg]	Altitude [m]	Monthly Average Precipitation [mm]	Average T-Max [C]	Average T-Min [C]	RH-Max [%]	RH-Min [%]
Cool & Humid	Bemidji Muni, MN	47.4810	1358	111	22.7	11.3	70	45
Cool & Dry	Cut Bank, MN	48.6033	1169	65	21.4	7.2	69	35
Warm & Humid	New York, NY	40.7128	3	89	26.3	17.7	81	59
Warm & Dry	Denver, CO	39.7392	1609	50	28.0	11.0	65	23
Hot & Humid	Miami, FL	25.7617	2	246	31.9	24.4	90	65
Hot & Dry	Phoenix, AZ	33.4484	304	1	39.9	25.4	35	15

JULY

Climate	Selected cities	Latitude [dg]	Altitude [m]	Monthly Average Precipitation [mm]	Average T-Max [C]	Average T-Min [C]	RH-Max [%]	RH-Min [%]
Cool & Humid	Bemidji Muni, MN	47.4810	1358	100	25.2	13.9	90	55
Cool & Dry	Cut Bank, MN	48.6033	1169	33	26.3	9.8	79	32
Warm & Humid	New York, NY	40.7128	3	115	29.3	21.0	90	61
Warm & Dry	Denver, CO	39.7392	1609	55	32.0	15.0	73	30
Hot & Humid	Miami, FL	25.7617	2	165	32.7	25.2	85	60
Hot & Dry	Phoenix, AZ	33.4484	304	27	41.2	28.6	56	21

AUGUST

Climate	Selected cities	Latitude [dg]	Altitude [m]	Monthly Average Precipitation [mm]	Average T-Max [C]	Average T-Min [C]	RH-Max [%]	RH-Min [%]
Cool & Humid	Bemidji Muni, MN	47.4810	1358	82	24.0	12.3	85	52
Cool & Dry	Cut Bank, MN	48.6033	1169	29	26.1	9.0	70	30
Warm & Humid	New York, NY	40.7128	3	105	28.4	20.3	80	50
Warm & Dry	Denver, CO	39.7392	1609	43	31.0	14.0	60	28
Hot & Humid	Miami, FL	25.7617	2	226	32.8	25.2	83	68
Hot & Dry	Phoenix, AZ	33.4484	304	25	40.2	25.0	50	22

The monthly average solar radiation on vertical surfaces (north, south, east, and west orientations) and horizontal surfaces was simulated using Diva for Rhino (see the Absorbed Net Radiation section for a detailed description). The biophysical and geometry traits were based on those of a typical grapevine canopy during the summer months (Table 6). Note that the r_a value was calculated using Equation (27) assuming a canopy height of 1.5 m and a 2 m/s wind speed. The canopy geometry values (height and LAI) were selected based on the typical conditions of a grapevine in a vineyard (Cox, 2015). The monthly and daily canopy transpiration rates and cooling power of each climatic scenario were calculated and compared to the existing literature.

Table 6. Considered biophysical variables for climatic scenario studies

LAI	Canopy Height [m]	Wind speed [m/s]	r_c [s/m]	r_a [s/m]
5	1.5	2	150	12.3

5.1.5.2. Results

Except in the case of the cool and dry climate, the summer average daily canopy transpiration values estimated by the P-M modified model show good agreement with the published field experiment values in Figure 14 (Braun & Schmid, 1999; Bucks, Erie, NAKAVAMA, & French, 1974; Dragoni et al., 2006; Eastham & Gray, 1998; Erie, French, & Harris, 1965; Evans, Spayd, Wample, Kroeger, & Mahan, 1993; I. Forseth & Teramura, 1987; Intrigliolo, Lakso, & Piccioni, 2009; Lascano, Baumhardt, & Lipe, 1992; Moutinho-Pereira, Correia, Gonçalves, Bacelar, & Torres-Pereira, 2004; Padgett-Johnson, Williams, & Walker, 2003b; Patakas, Noitsakis, & Chouzouri, 2005; Poblete-Echeverría & Ortega-Farias, 2013; Yunusa et al., 2000). Note that because grapevines do not thrive in humid climates, the TR_c value of a Kudzu vine was used for the warm and humid climate. I was not able to find a comparable vine for the hot and humid climate.

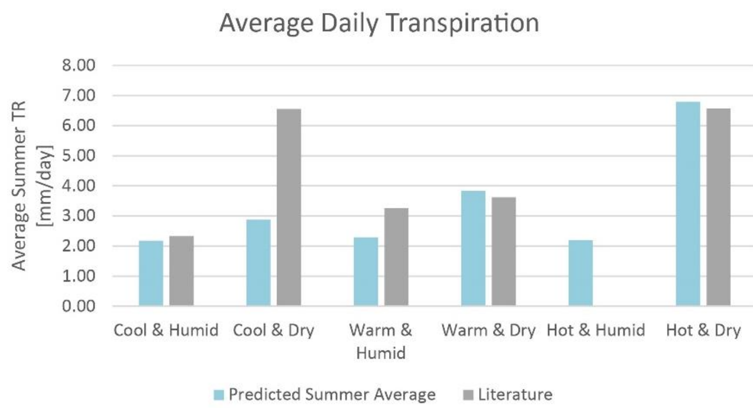

Figure 14. Summer daily average canopy transpiration rates from the developed model and published field experiments

Figure 15 illustrates the estimated cooling power values for each climate for the summer months. As expected, the climates with warmer summer temperatures promote higher canopy transpiration rates. The TR rate increases drastically in the hot and dry climate due to advection, where the hot ambient temperature provides an extra source of energy "so that the latent heat loss can significantly exceed any net radiation gain" (Jones, 1992).

As illustrated, the oasis effect is adequately considered in the P-M model. In hot and dry climates, it is possible for the air to be significantly hotter and drier than the canopy. This provides an extra source of energy so that the "latent heat loss can significantly exceed any net radiative gain" (Jones, 1992). This phenomenon is called the Oasis effect.

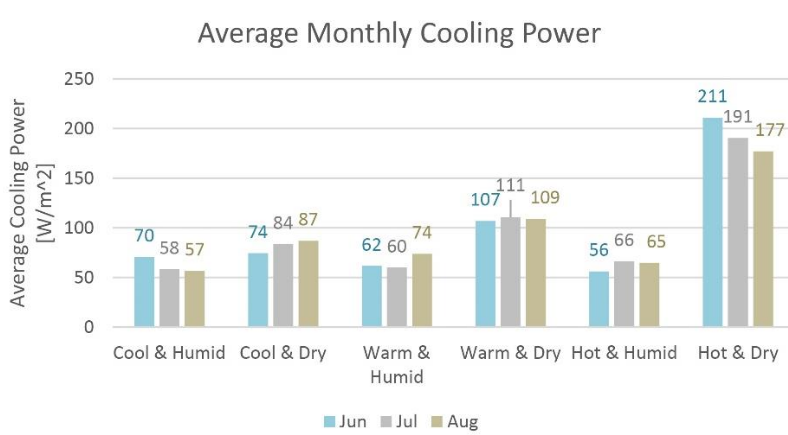

Figure 15. Summer average monthly cooling power values per climatic condition

Figure 15 illustrates the direct relationship between *VPD* and the transpiration rate of canopies. Dry climates are associated with high *VPD* because the air temperature rises during the summer with a minimal increase in humidity. In contrast, humid climates are associated with low *VPD* where the temperature and the water vapor content of the air increase during the summer.

Consequently, the drying power of air is larger in dry climates than in their humid counterparts. Therefore, as shown in Figure 15, the cooling power produced in humid climates is less than that produced in dry climates.

5.1.6. Design Optimization - Aerodynamic and Canopy Resistances Sensitivity Analysis

The goal of this section is to (a) investigate the dependence of canopy transpiration on surface/bulk resistance, r_c, and aerodynamic resistance, r_a, within different climate conditions, and (b) define the optimal biophysical and geometry characteristics of a green wall for maximum transpiration within the mentioned climates.

5.1.6.1. Method

Climatic scenario case studies are particularly advantageous to provide realistic environmental conditions. That is because the variables impacting transpiration rate are interdependent, and consequently, dynamic.

Therefore, climatic data representing typical environmental conditions provides an effective comparative study to evaluate canopy cooling power and best design options.

To evaluate the optimal r_c values, a series of parametric studies were conducted for six distinctive climate conditions. The corresponding environmental values that were used for each climatic scenario are listed in Table 5. The green walls are assumed to be facing south.

5.1.6.2. Results

The cooling power range of a green wall as a function of r_c and r_a in various climates is shown in Figure 16. The dotted lines represent the average, high, and low values of the canopy surface resistances. These lines define the possible range of r_c values for the grapevine and urban vine species. The various aerodynamic resistances, r_a, have been plotted per climate condition. The largest value (250 s/m) and the smallest value (5 s/m) correspond with short grass and forest, respectively. The r_a of 10 s/m represents a typical canopy aerodynamic resistance value for a grapevine in a vineyard (h = 1.5 m, z = 0.13 h, and u = 2).

The greatest transpiration rate occurs in the hot and dry climate followed by the warm and dry climates and the cool and dry climates. Humid regions with hot, warm, or cool summers correspond with the lowest ranges of canopy cooling power.

Two patterns were observed for the canopy surface resistance values corresponding with the crossover points, r_{cp}, where the canopy temperature reaches the ambient temperature. First, the r_{cp} values were reduced for both the dry and humid climates as summer temperatures decrease. This indicates that the influence of the boundary layer resistance on cooling power becomes greater as ambient temperatures decrease. In other words, sensible cooling becomes the prevalent cooling method of a canopy in cooler climates.

Second, in both the dry and humid climates with similar summer temperatures (i.e., hot and dry vs. hot and humid) the r_{cp} values of the dry climates are consistently larger than their counterparts. This indicates that in dry climates, the biophysical resistance has more impact on the cooling of a canopy. In this condition, latent cooling is the dominant cooling force.

For all the climate scenarios, the transpiration rate of a canopy increases as r_a decreases. The large r_a values (from 250 s/m to 50 s/m) correspond with dense, uniform field conditions such as grass and crop fields, where plants are poorly connected to their surrounding environments. On the other hand, the small r_a values (10 s/m and 5 s/m) represent conditions where the canopy is highly coupled with its surroundings; i.e., grapevines and forests. Theoretically, transpiration rates increase when the height of the canopy increases and wind speed decreases. In reality, transpiration is restricted by the biophysical resistance of canopies, r_l. For example, forest transpiration is often less than field transpiration because most forest species (especially in coniferous forests) have relatively high r_l values (Jones, 1992). The dotted reference lines on each climate scenario represent the biophysical restrictions imposed by the vine species on the transpiration rates of the canopies.

Because r_c has a direct relationship with the leaf surface resistance, r_l, (Eq. (28)) and an inverse relationship with *LAI* (Eq. (29)), canopies with low r_l and high *LAI* values should produce the largest transpiration rates. Figure 17 illustrates r_c as a function of r_l and *LAI*. The dotted lines represent the r_c values corresponding with a cooling power of 100 W/m^2, and average r_c values of grapevines and urban vines.

Of the six climate conditions, only three vine canopies have the potential to produce 100 W/m^2 or more of cooling power. As expected, the hot and dry climate provides the most robust conditions (designated by the pink box). In this scenario, r_c and r_l can reach values as large as 400 s/m and 370 s/m, respectively. Within this boundary, most sun-loving vine species can produce significant cooling power.

The warm and dry climate provides the second largest boundary. In this environment, vines' r_c and r_l values of 200 s/m and less can produce 100 W/m^2 or more of cooling power. Most Vitis (grapevine) species can meet this requirement easily. Finally, r_c and r_l values of approximately 100 s/m can produce 100 W/m^2 or more of cooling power in hot and humid climates. In these environments, most urban vines thrive.

The 100 W/m^2 cutoff point eliminated warm and humid, cool and dry, and cool and humid scenarios. However, a green wall canopy still produces cooling power in those climatic conditions. The average cooling power values during the summer months are approximately 80 W/m^2 for the cool and dry climate followed by 60 W/m^2 for the warm and humid climate and the cool and humid climate.

Figure 17 illustrates the identical relationship between r_c, r_l, and *LAI* for all climates. For low values of *LAI*, the impact of leaf surface resistance, r_l, on canopy resistance, r_c, is significant. As *LAI* increases to 3, 4, and 5, the influence of r_l on r_c diminishes because there are more leaves within the canopy to transpire. The influence of *LAI* on cooling power for each climate is illustrated in Figure 18. As expected, the impact of *LAI* on canopy cooling power becomes minimal as its value reaches 3. This is because LAI_{sunlit} and *LAI* have an exponential relationship (Eq. (29)). Note that during the summer months, *LAI* values of 3, 4, and 5 are fairly common for green walls.

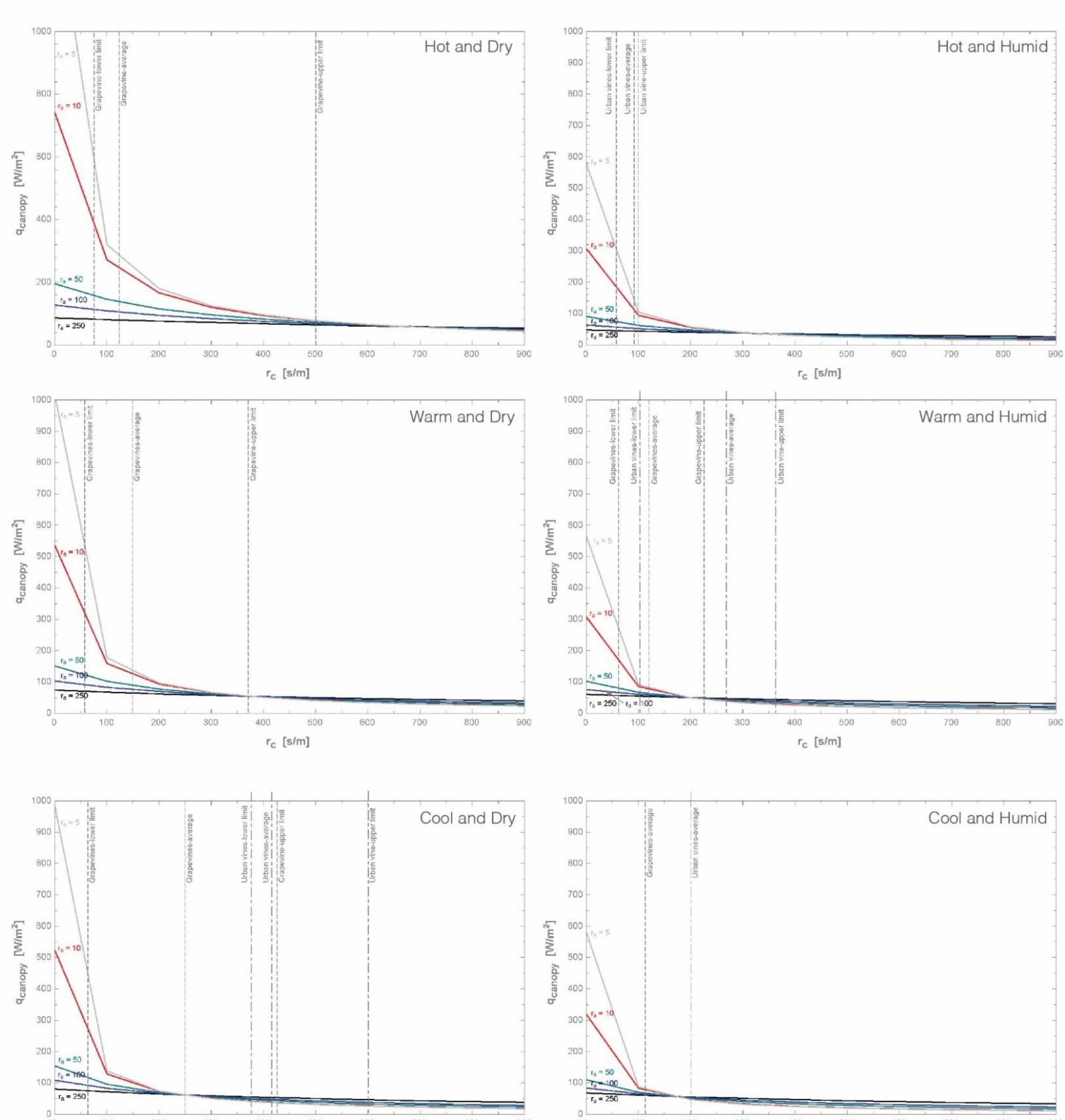

Figure 16. Cooling power as a function of canopy surface resistance (r_c, s/m) and aerodynamic resistance (r_a, s/m) for the month of July. Dashed lines indicate the average, low, and high r_c values of grapevines and urban vines. See Table 5 for environmental variable values.

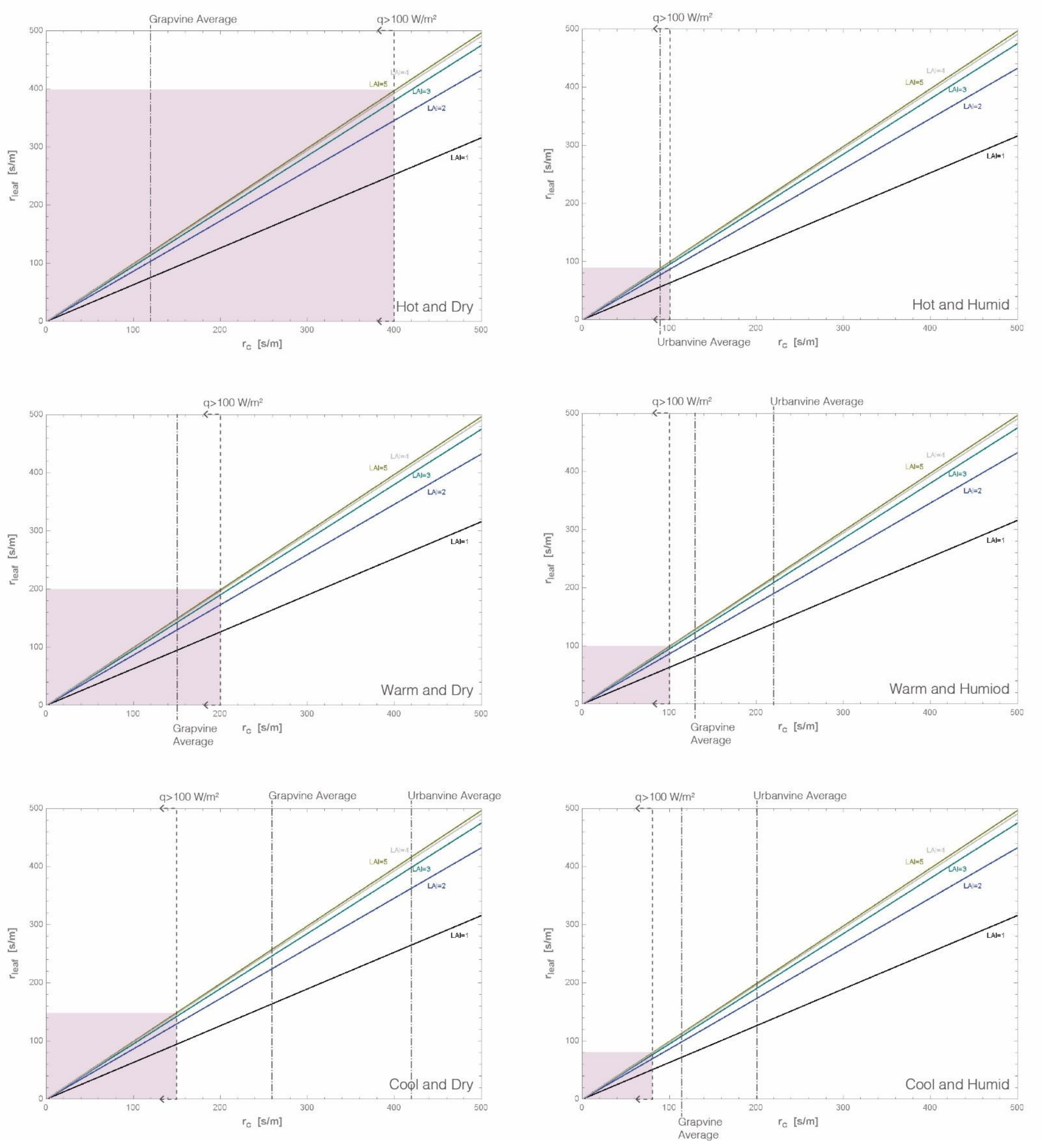

Figure 17. r_c (s/m) as a function of r_l (s/m) and LAI per climate scenario

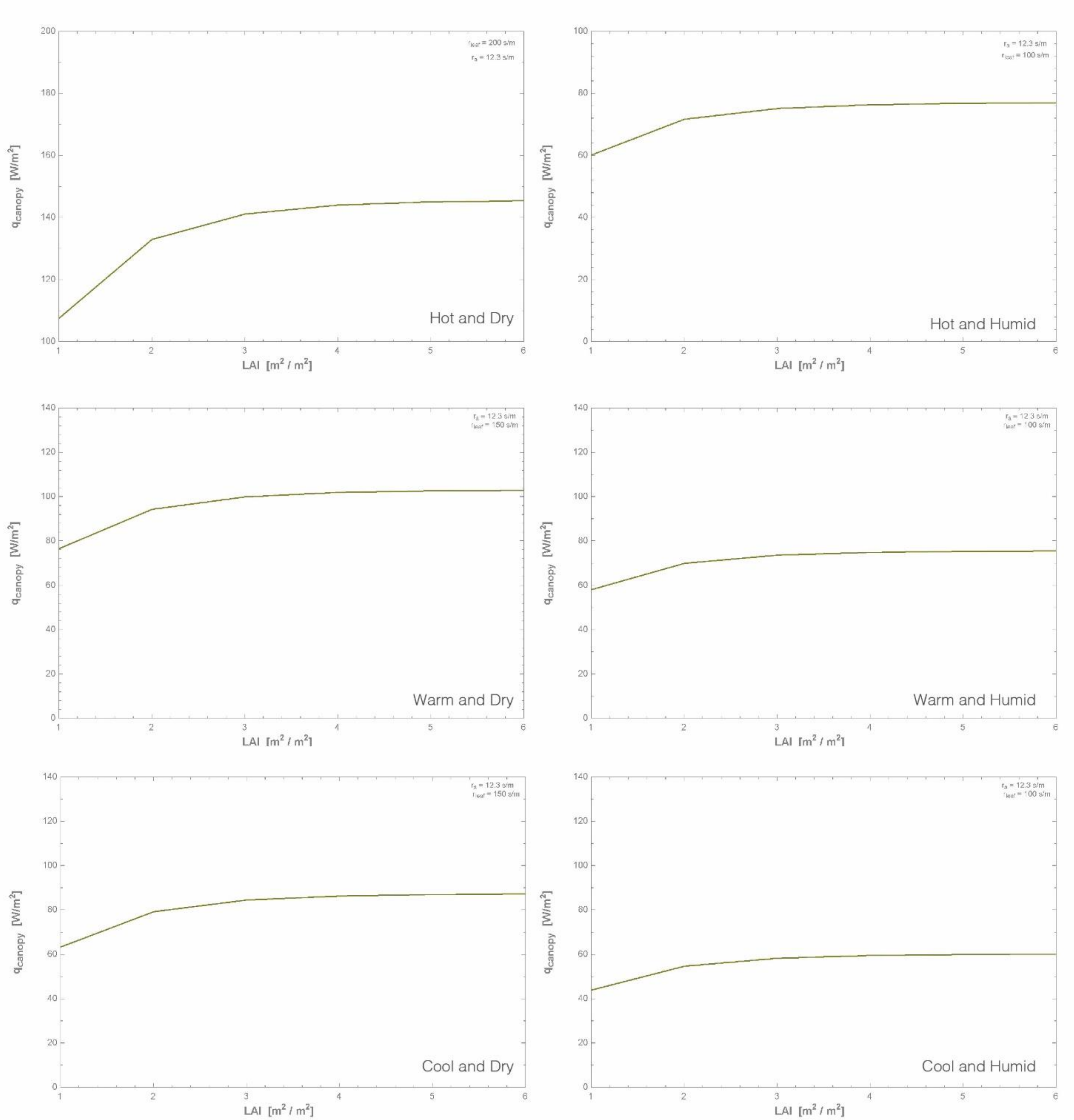

Figure 18. Cooling power as a function of LAI for month of July, r_a =12.3 s/m. See Table 5 for environmental variable values.

Most vines, such as leaf bearers, tendril climbers, and stem twiners, can climb up to 20 m if provided with a strong support structure. Figure 19 illustrates r_a as a function of wind speed and canopy height up to 20

m. Although in most cases wind speed cannot be controlled, the height of the canopy can be adjusted to reduce the canopy's aerodynamic resistance.

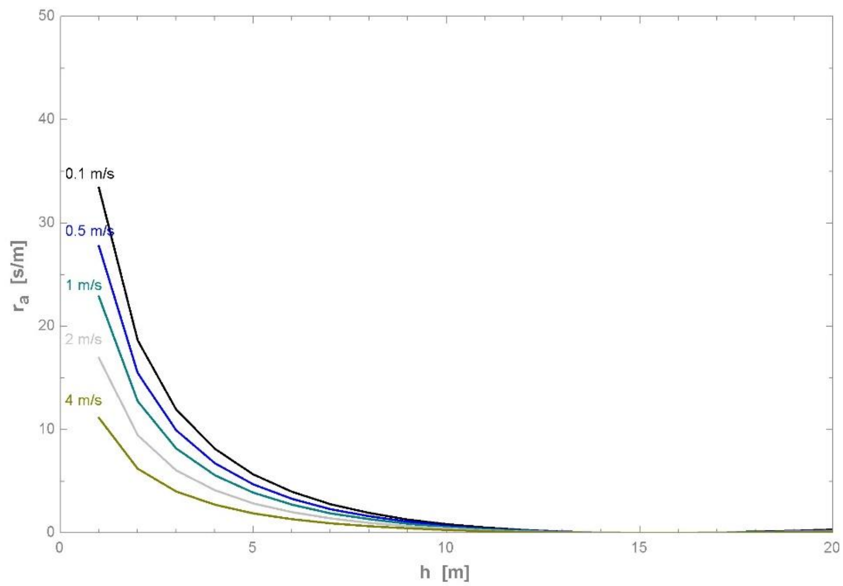

Figure 19. Aerodynamic resistance (r_a) as a function of canopy height (h) and wind speed (u)

As canopy height *h* increases, r_a decreases. However, the impact of *h* on r_a becomes negligible as its height reaches 10 m. As expected, an increase in wind speed reduces canopy aerodynamic resistance. However, as was illustrated, greater wind speeds can reduce canopy transpiration if stomata exert strong control on water vapor loss.

Figure 20 to Figure 25 illustrate the best design options for maximizing the cooling power of south and west facing green walls in the month of June, July, and August per climate conditions. The average r_c values (accounting for the possibility of 10% variability), and the corresponding maximum cooling power values, are highlighted with a pink bar and text, respectively. The cooling power values of three green walls with different heights (3 m, 6 m, and 9 m) for no wind (0.1 m/s) and a wind speed of 2 m/s are considered. Below are the summary of the trends between various climates and green wall orientations.

The difference in cooling power produced from green walls facing south and west is negligible. For all climates, the performances of the canopies are very similar throughout the summer months. Note: The study assumes that the canopies have reached an *LAI* larger than 3.

The largest cooling power is produced in the hot and dry climate with q between 200 W/m^2 and 300 W/m^2. The canopies in hot and humid climates and in warm and dry climates perform similarly with q mostly equal or slightly larger than 100 W/m^2. The canopies in warm and humid climates and in cold and humid climates have similar performances with q between 80 W/m^2 and 100 W/m^2.

The least cooling power is produced in the cold and dry climate, where the cooling is mostly provided through convection and not transpiration. This is due to high average r_c values (256 s/m). Values of r_c 100 s/m or smaller can significantly improve the cooling power of the canopy.

The tallest canopy (9 m) with a wind speed of 2 m/s produces the largest cooling power. However, for all climates, the positive impact of the wind on cooling power decreases as the height of the canopy increases. The largest impact of wind on cooling power is when the canopy is 3 m tall. This study suggests that in all climates, wind only slightly improves the cooling power of canopies taller than 6 m.

In all climates, r_c values of 100 s/m or less greatly improve canopy cooling power. However, the influence of canopy height must be further investigated because some studies on forests suggest that stomatal resistance increases as height increases. This would result in lower transpiration rates and cooling power rates at higher canopy elevations.

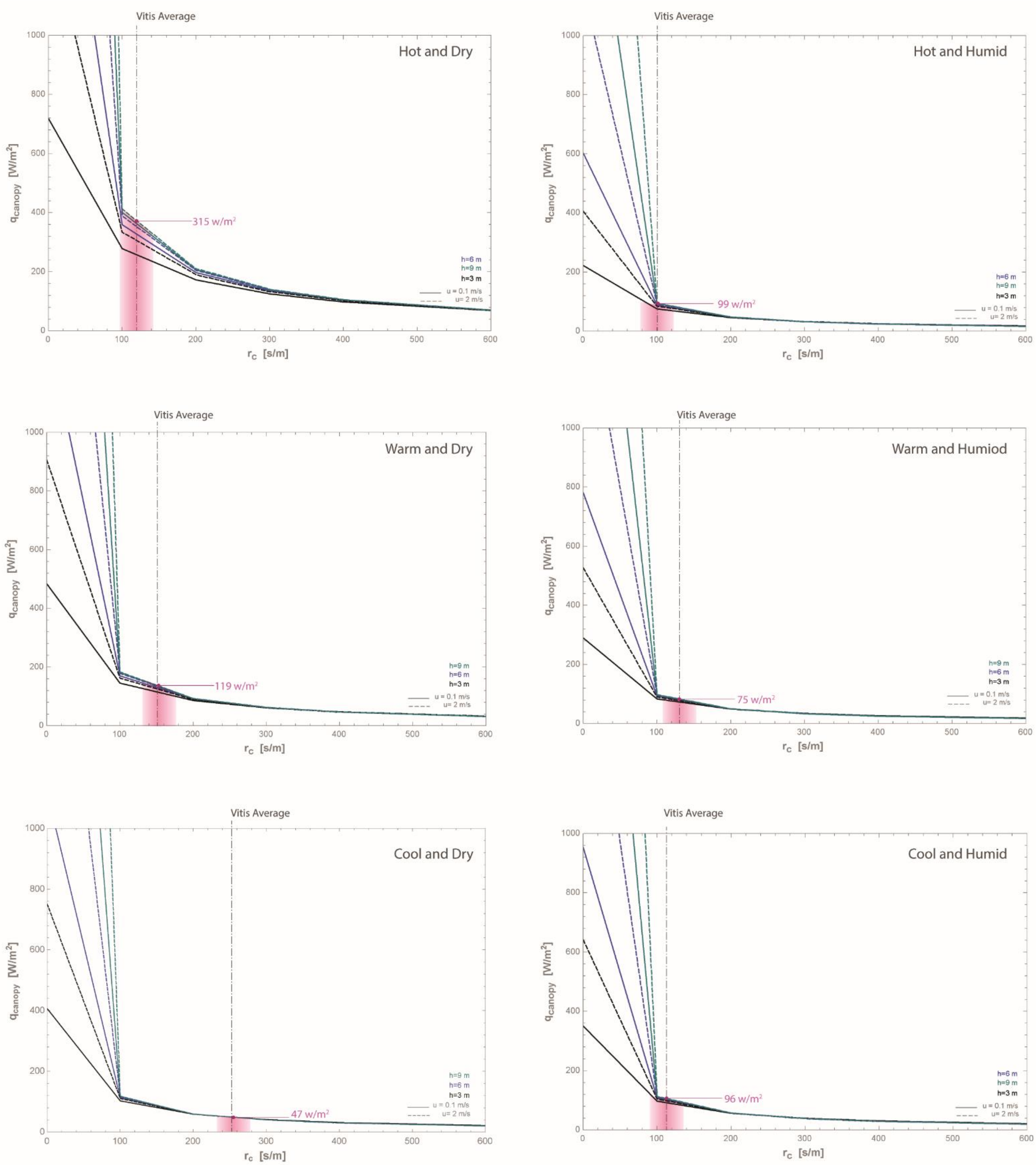

Figure 20. Month of June cooling power of south facing canopy in various climates as a function of canopy resistance (r_c) and aerodynamic resistance (r_a) for various canopy heights (3 m, 6 m, and 9 m) and wind speeds (0.1m/s and 2 m/s). The pink bar represents the average r_c values per climate with 10% possible changes. The highlighted cooling power values correspond with 6 m canopy height.

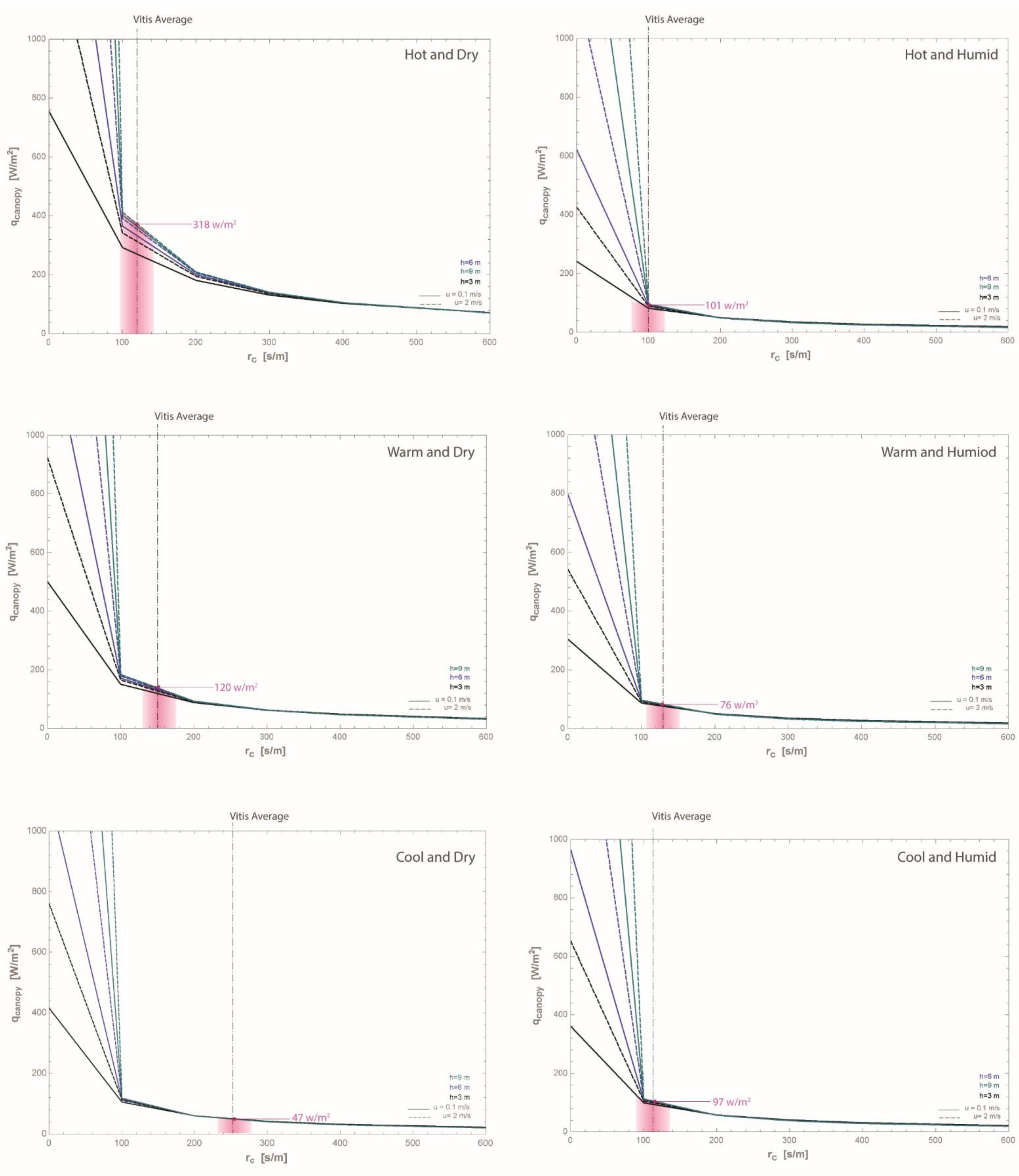

Figure 21. Month of June cooling power of west facing canopy in various climates as a function of canopy resistance (r_c) and aerodynamic resistance (r_a) for various canopy heights (3 m, 6 m, and 9 m) and wind speeds (0.1 m/s and 2 m/s). The pink bar represents the average r_c values per climate with 10% possible changes. The highlighted cooling power values correspond with 6 m canopy height.

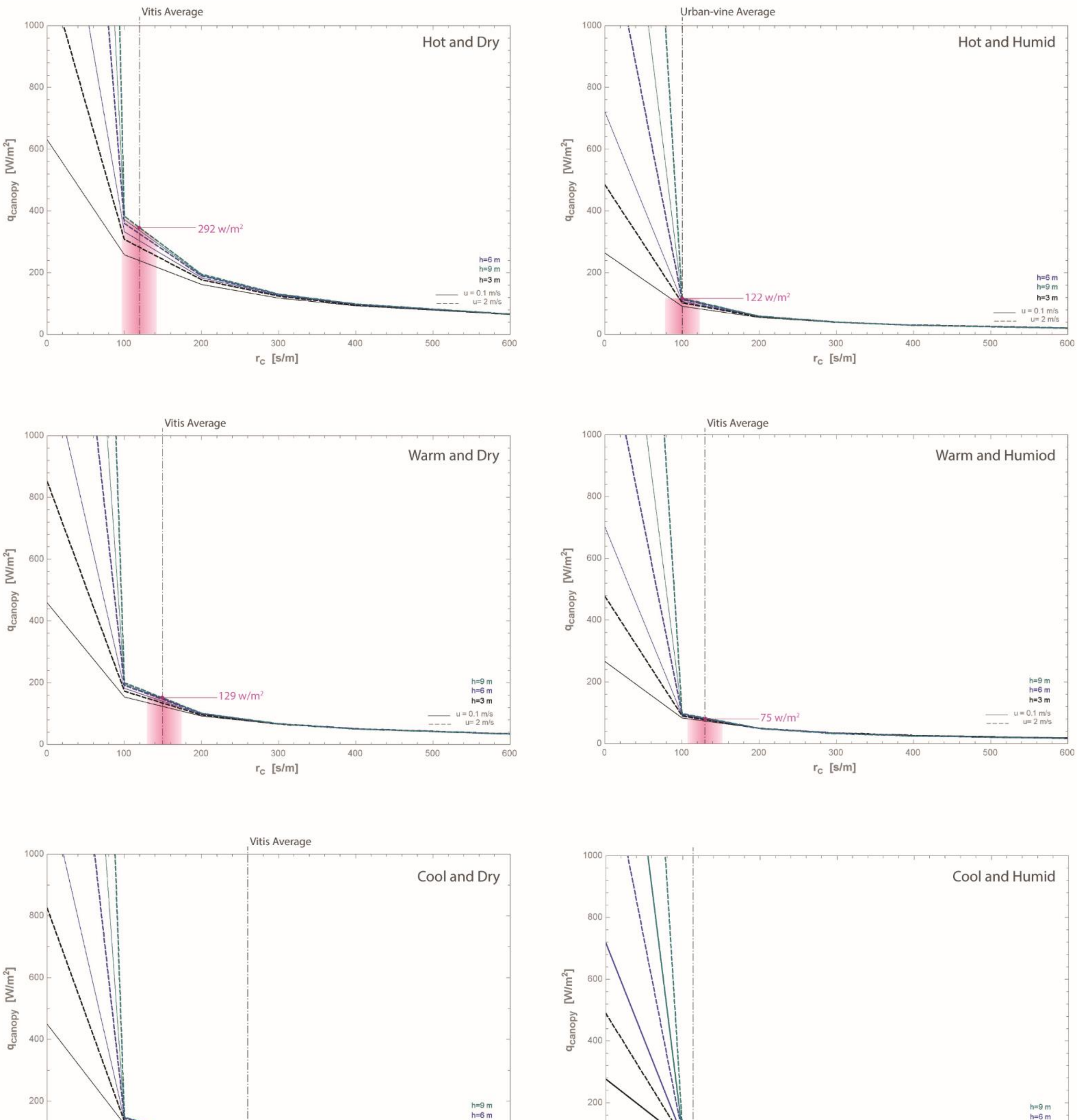

Figure 22. Month of July cooling power of south facing canopy in various climates as a function of canopy resistance (r_c) and aerodynamic resistance (r_a) for various canopy heights (3 m, 6 m, and 9 m) and wind speeds (0.1 m/s and 2 m/s). The pink bar represents the average per climate with 10% possible changes. The highlighted cooling power values correspond with a 6 m canopy height.

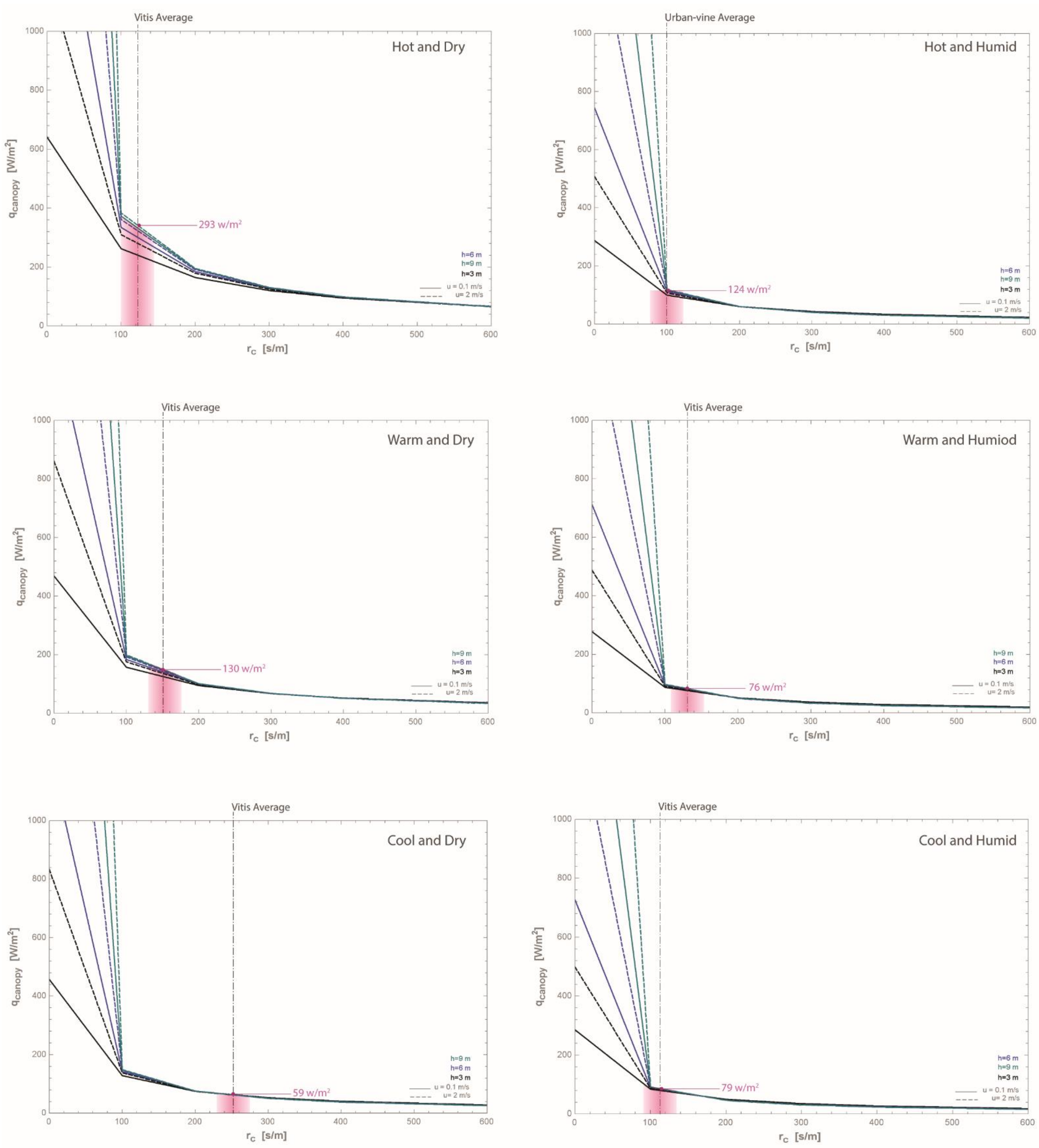

Figure 23. Month of July cooling power of west facing canopy in various climates as a function of canopy resistance (r_c) and aerodynamic resistance (r_a) for various canopy heights (3 m, 6 m, and 9 m) and wind speeds (0.1m/s and 2 m/s). The pink bar represents the average r_c values per climate with 10% possible changes. The highlighted cooling power values correspond with a 6 m canopy height.

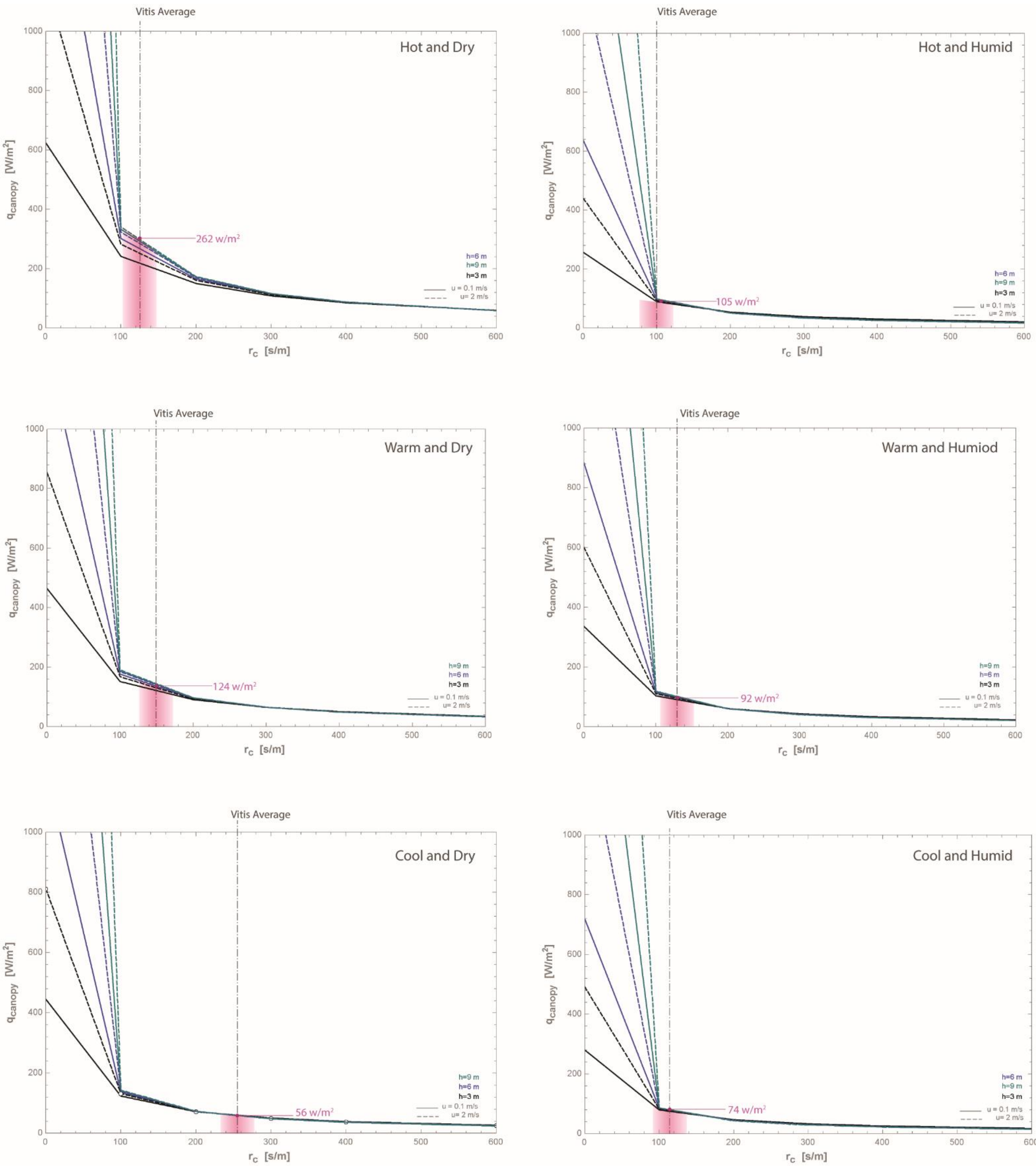

Figure 24. Month of Aug cooling power of south facing canopy in various climates as a function of canopy resistance (r_c) and aerodynamic resistance ($_{ra}$) for various canopy heights (3 m, 6 m, and 9 m) and wind speeds (0.1 m/s and 2 m/s). The pink bar represents the average r_c values per climate with 10% possible changes. The highlighted cooling power values correspond with 6 m canopy height.

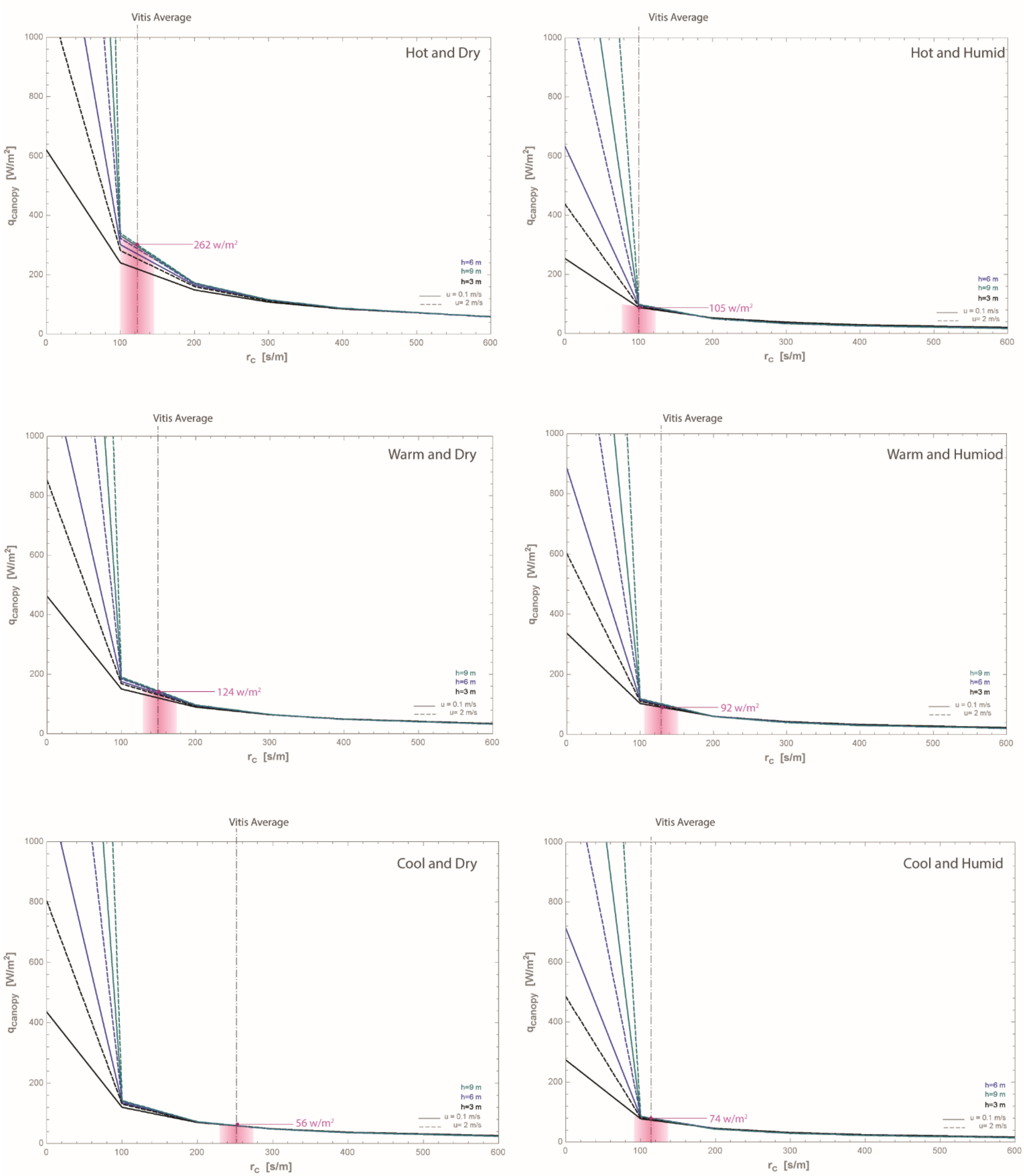

Figure 25. Month of Aug cooling power of west facing canopy in various climates as a function of canopy resistance (r_c) and aerodynamic resistance (r_a) for various canopy heights (3 m, 6 m, and 9 m) and wind speeds (0.1m/s and 2 m/s). The pink bar represents the average r_c values per climate with 10% possible changes. The highlighted cooling power values correspond with 6 m canopy height.

5.2. Cooling from Canopy Solar Interception

The objectives of this chapter are to (1) evaluate solar gain reductions from various green wall designs in six distinct climates, (2) establish performance trends that are sensitive to green wall design variables, and (3) provide guidelines for the design of high-performing green walls for each climatic condition.

To begin, the theoretical background on variables impacting solar transmittance of a canopy is reviewed. Each variable was considered and the possible range of values for each variable was investigated. Available data was then used to conduct a sensitivity analysis. Several scenarios were studied to identify the best performing design option for green walls in each climatic condition.

The results show that:

- For a fixed vertical declination and random leaf azimuth angles, the largest cooling from shading of south-facing green walls occurs in high latitude angles, followed by mid latitude angles and low latitude angles.
- For a fixed vertical declination and random leaf azimuth angles, the shading effect of a canopy increases at a decreasing rate with increasing *LAI*. Excepting sites at low latitudes, *LAI* values of 3, 4, and 5 approximately correspond with 70%, 80%, and 90% solar radiation reductions, respectively.
- Values of the extinction coefficient, *k*, obtained from the statistical model can overestimate the solar radiation reduction of green walls. However, a *k* value of 0.5, obtained from empirical studies, can serve as a conservative estimate for calculating the solar transmittance of green walls.

5.2.1. Introduction

The shading effect contributes the most to the cooling impact of green walls on buildings. The magnitude of this cooling depends on the geometry and orientation of the green wall canopy. Of the total net solar radiation received by green walls, some is transmitted through the leaves and canopy, some is reflected, and a small portion is absorbed for photosynthesis processes. The exact distribution of radiation within a canopy is difficult to evaluate because the geometry and orientation of canopies, as well as the spectral properties of leaves, are variant and complex (Jones, 1992).

To simplify this problem, plant ecologists model canopies as uniform horizontal sections consisting of randomly arranged leaves with specific *LAI* values. As the depth of a green wall increases, the amount of transmittance—the amount of irradiance reaching a surface behind the canopy—is reduced. For opaque leaves, the amount of irradiance transmitted through a canopy is a function of the *LAI* and the extinction coefficient, *k*, Eq. (30) (Jones, 1992).

$$I = I_0 e^{-K\,LAI} \tag{30}$$

Where

I Irradiance passing through a canopy [W/m²]

I_o Irradiance at the top of the canopy [W/m²]

k Extinction coefficient [-]

LAI Leaf area index [-]

The extinction coefficient, *k*, defines the ratio of the shadow area to the actual leaf area (Jones, 1992). For vertically oriented canopies, *k* is related to cot β, where β is the solar elevation. Depending on the leaf angle distribution, the extinction coefficient can be calculated as a function of solar altitude (Table 7) (Jones, 1992; J. L. Monteith, 2008).

In practice, these simple geometric approximations cannot easily be translated to describe real canopy behavior. "Therefore it is convenient for many purposes to replace geometric [sic] derived values of the extinction coefficient, *k*, by an empirically determined value" (Jones, 1992). Empirically derived values for the extinction coefficient vary between 0.3 and 1.5, depending on the species of vine considered. In general, values less than 1.0 are observed for non-horizontal and irregularly distributed leaves. Values equal or greater than 1.0 occur with horizontal or more evenly distributed leaves (Jones, 1992).

Table 7. Extinction coefficient, k, as function of solar altitude, β, for various leaf angle distributions. (a: where x is the ratio of the horizontal to the vertical axis of the elliptical and A≈ (x + 1.774 (x + 1.182) - 0.733)/x, (Jones 1992)).

Leaf Angle Distribution	**Leaf Arrangement Assumption**	**Extinction Coefficient (*k*)**
Horizontal	Fix horizontal leaf	k = 1
Vertical	Fix vertical leaf	$k = (2 \cot \beta)/\pi$
Spherical	Fix leaf angle, and variable azimuth angle	$k = 1/(2 \sin \beta)$
Ellipsoidal[a]	Variable leaf angle, and variable azimuth angle	$k = (x^2 + \cot^2 \beta)^{1/2}/(Ax)$

5.2.2. Methodology

A literature review of each variable impacting canopy performance was conducted to define a range of expected green wall performance. Defining a range of performance for an early design phase of a project is highly valuable because it allows for a fast method of decision making with an appropriate scale of resolution.

5.2.3. Leaf Area Index

The *LAI* values for different plant species vary widely. In practice, *LAI* is empirically obtained through various direct or indirect methods (Jones, 1992). The Food and Agriculture Organization of the United Nations suggests an *LAI* value of 3 to 5 for most mature crops. This assumption seems consistent with *LAI* values observed for mature green walls (R. G. Allen et al., 1998; Schumann, 2007). Note that larger *LAI* values can also be achieved within growing seasons, depending on plant traits and growing conditions. However, as will be discussed later in the chapter, green wall performance will only slightly improve with a larger *LAI*. It is expected that thicker green walls with high *LAI* values have lower transmittance. Therefore, the design of the support structure of a green wall directly affects the *LAI* of a canopy. In practice, to evaluate the exact value of the *LAI* of a green wall, each design typology must be considered and measured separately.

5.2.4. Extinction Coefficient

It was described in Section 5.2.1 that the values for the extinction coefficient, *k*, can be obtained from empirical and statistical methods. The following sections investigate the best range of *k* considering both methods.

5.2.4.1. Empirical Method for Defining the Extinction Coefficient (k)

The field measured values of *k* for trained grapevine canopies can serve as a good estimate for green walls because the geometries of the two canopies are similar. There are many variations of grapevine trellis training systems, and so a comprehensive study on trellis designs was conducted to select only those ones that produced canopy geometries similar to green walls. The goal was to identify the training systems, and the corresponding *k* values, which best mimic green wall designs.

Trellis systems for grapevines are designed to increase productivity by making harvesting and maintenance easier and, most importantly, by maximizing solar exposure (A. Reynolds et al. 2009). Grapevine training systems are developed to minimize the depth of a canopy while increasing the surface area. This ensures that the maximum leaf area is exposed to sunlight which, in turn, will increase the productivity of a grapevine. Note that in contrast to grapevines, an increase in the depth of a canopy will increase the performance of a green wall via increased shading. Therefore, the *k* values obtained from grapevine canopies are conservative values. Ideally, each green wall training system should be evaluated separately.

Most grapevine studies describe training system designs as they relate to the vine structure. Therefore, to evaluate the designs of grapevine training systems, it is essential to understand the structure of a grapevine. Below is an overview of grapevine structure terminology. Vine structure can be generally described by the following elements (Cox, 2015):

1. *Trunk*, which is permanent and supports the vine above the ground. The height of the trunk varies and depends on the training systems. The top of the trunk is called the *head*.

2. *Arms*, which are older branches extending from the trunk. Horizontally-trained arms are called *cordons*.

3. *Cane*, which is a young branch (one year old) that is raised from an arm/cordon. Cranes have smooth dark surfaces. When canes are pruned to have only one to four buds (described below), they are referred to as *spurs* (also described below).

4. *Shoots*, which define the unit of growth of a vine. They are green stems that rise from primary *buds* (described below). As shoots get older they become canes, which in turn become arms.

5. *Buds*, which are highly compressed shoots that are developed in nodes (leaf axils).

Note that the above list has been limited to the structural parts pertaining to training system designs. There are various methods for categorizing training systems. For this investigation, the category used by A. Reynolds and J. Heuvel (2009) is used. The grapevine training systems are broken down into four major categories:

- *Head/spur*, which is basically a short trunk with a few two-node bearing units (e.g., bush vine)
- *Head/cane*, which consists of a short trunk with one or more longer bearing units (e.g., Guyot)
- *Cordon/spur*, which involves horizontal training of the arm(s) with several two-node spurs (e.g., midwire cordon)
- *Cordon/cane*, which is similar to head/spur but has longer bearing units (e.g., Sylvoz)

Except for the head/spur training system, all other systems can produce canopy geometries similar to those of a vining green wall. Therefore, the major defining design factors to consider are the methods of management (the position of the shoots) and the division of canopies.

There are two major types of shoot arrangements: (a) vertical shoot positioning (VSP), where the shoots are positioned upright to increase solar exposure, and (b) non-VSP, where the shoots are allowed to grow and cascade to their natural directions (e.g., top wire cordon) (Reynolds & Heuvel, 2009). The pictures below show both systems during growing and dormant seasons. It is evident that VSP shoot systems closely mimic green wall geometry, whereas non-VSP systems create wide and unruly canopies which are dissimilar to conventional green wall designs (Figure 26 and Figure 27).

Figure 26. High cordon system using a non-VSP shoot arrangement (Erwin Elsner, 2014)

Figure 27. Guyot training system using a VSP shoot arrangement (Erwin Elsner, 2014)

Canopy division is another factor impacting the geometry of a green wall (discussed in more detail below). Many training systems such as Midwire Cordon, Hudson River Umbrella, and Guyot, do not require canopy division..The Four-Arm Kniffin Training, Hudson River Training, and Umbrella Kniffin Training are some examples of such systems. The shoots can be positioned either VSP or non-VSP. For this study, only VSP canopy arrangements are considered because they most closely resemble the geometry of green walls.

"Canopy division involves a modification to the configuration of the trellis so that two or more canopies are created from the initial single canopy curtain" (Reynolds & Heuvel, 2009). A canopy can be divided horizontally or vertically. In either case the goal is to improve the solar exposure of the canopy and, by extension, its growth rate. For grape cultivars grown for wine production, horizontally divided training systems are exclusively used. Typically, a pair of canes is trained on parallel wires about 1 m tall and 1 m apart from each other (Reynolds & Heuvel, 2009). The Geneva Double Curtain and Lyre training systems are examples of horizontally divided canopies. Horizontally divided training systems are not similar to green walls and therefore are excluded from this investigation.

Vertically divided training systems are comprised of a bilateral cordon positioned about 1 m from the ground with spurs facing upward and downward (Reynolds & Heuvel, 2009). Some popular examples of such training systems are Smart Dyson and Smart Henry. Both systems produce canopies resembling green wall geometries.

Undivided and vertically divided canopies with VSP shoot positioning (both upward and downward shoot positioning) can closely mimic green wall geometries. Therefore, the field measured extinction coefficient values from such training systems can be used as a conservative estimate of *k* values for green walls.

M. Bindi et. al. (1997) introduced a model to simulate the growth and development of grapevines. The model was verified through a field study on Sangiovese cultivars that were cordon trained (vertical trellises). They found a *k* value of 0.5.

B. Wermelinger and J. Baumgartner (1991) developed and tested a mathematical model to account for the carbon assimilation of grapevines. Although the study did not specify the training system used, it states that the vines were double cane pruned. This pruning method is analogous to the double Guyot system, which most likely requires a VSP canopy arrangement (Wermelinger & Koblet, 1990). The model was successful in predicting carbon assimilation values using a *k* value of 0.6. This *k* value was adapted from Jackson's and Palmer's (1979) empirical study of apple orchards.

Jackson and Palmer (1979) found that a *k* value of 0.6 gave the best fit for both daily direct and diffused light penetration into mature canopies in mid-August. They noted that

> although k will vary with solar altitude and the relative contribution of leaves, fruits and ranches to the total shading area of the trees, its empirically determined average over period of time is relevant to the estimation of daily or weekly interception and allows for effects of variety, pruning etc on transmission. (Jackson & Palmer, 1979)

P.Cavallo et al. (2001) measured the daily extinction coefficients of three different types of grapevine training systems: Bilateral Guyot (BG), Bilateral Spur-Pruned Cordon (BSPC), and Bilateral Free Cordon (BFC). They reported the average daily *k* values for matured canopies. They observed *k* values of 0.63 for the BG system and 0.62 for the BSPC system. These values are similar to the *k* value used by B. Wermelinger and J. Baumgartner (1991). However, for the BFC system, they observed an increased *k* value of 0.85. They concluded that the high value of *k* for the BFC training system was due to "close-to horizontal orientated leaves" and "canopy widening" (Cavallo et al., 2001). This experiment demonstrates the influence of training system design on canopy geometry, density, and light distribution. As previously highlighted, the BFC system does not resemble green wall design. However, its corresponding *k* value serves as a good indicator of a theoretical upper limit on the extinction coefficient of a green wall.

S. Fuentes et al. (2008) proposed a computational method to estimate the *LAI* of grapevine canopies. Their model showed good agreement with two field measured studies conducted on Merlot (Chile) and Chardonnay (Australia) vineyards from November to January. Both sites used VSP canopy arrangements and three and two wire training systems. For their model, S. Fuentes et al. (2008) considered a *k* value of

0.7. This value was previously obtained through parametric studies of eight sites in Australia using an image analysis tool written in MATLAB (Fuentes et al., 2008).

Based on the above field study measurements, an extinction coefficient value of between 0.5 and 0.7 can be used for green wall designs. The next section reviews the range of possible k values using statistical methods.

5.2.4.2. Statistical Method Defining Extinction Coefficient (k)

R. Lumeur and B. Blad (1974) provided a comprehensive and critical overview of various statistical methods modeling light distribution within plant canopies. They defined four model categories: regular leaf dispersion, clumped leaf dispersion, random leaf dispersion, and variable leaf dispersion.

The regular leaf dispersion method assumes that leaves are systematically arranged in a canopy. This arrangement creates a regular, dense, and self-shading canopy.

Clumped leaf dispersion assumes the mutual shading of leaves with frequent large gaps within a canopy. This type of leaf arrangement will allow for more light penetration into a canopy compared to regular leaf dispersion.

As the name implies, random leaf dispersion assumes no clear relationship in the way leaves are dispersed within a canopy. More technically, each leaf has the same probability of being found at any position within a canopy. This method is the most popular modeling technique and is considered “as some type of balance” between the regular and clumped leaf approaches (Lemeur & Blad, 1974).

Finally, variable leaf dispersion uses a Markov chain model where “the probability of an interception in a deeper sublayer is determined by the status (i.e., one interception or no interception) of the preceding sublayer” (Lemeur & Blad, 1974). Although this model can be an effective method for predicting light distribution within a canopy, it is too complex to be easily used in most studies.

The particular arrangement of leaves within a green wall canopy is highly dependent on its support structure design and the selected vine species. For this study, the random leaf dispersion model was selected because it is the most robust method for addressing possible design variations.

The methods for calculating the extinction coefficient, *k*, for a random leaf dispersion model of various leaf arrangements are listed in Table 7. The extinction coefficient is a function of solar elevation, *β*, and leaf orientation. Leaf orientation is described by (a) the angle between the zenith and the projection normal to the leaf surface, α, and (b) the difference between leaf and sun azimuth angles, *θ* (Figure 28) (Lemeur & Blad, 1974).

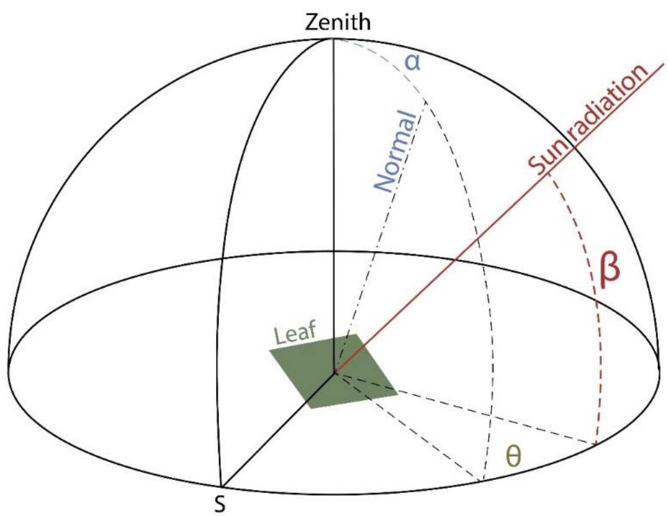

Figure 28. A leaf orientation defined in a spherical system coordinate. β: Solar altitude angle, α: the angle between a projection normal to the leaf surface and the zenith, which is equal to the angle between the leaf and the horizon, θ: the azimuth difference between the leaf and the sun's azimuth (redrawn from R. Lumeur and B. Blad, 1974)

The horizontal and vertical leaf distributions (Table 7) assume fixed leaf and azimuth angles. The spherical distribution assumes a fixed inclination angle and a random azimuth angle of the leaves. The ellipsoidal arrangement assumes both random inclination and azimuth angles in a canopy (Jones, 1992).

Many plant species respond to solar radiation by adjusting their leaf angles. Darwin (1888) observed two rapid and reversible leaf movements for vines: diaheliotropic, where a leaf's movements track the sun such that the leaf is perpendicular to the sun's rays so as to maximize solar exposure, and paraheliotropic, where a leaf's movement tracks the sun so that the leaf is parallel to the sun's rays so as to minimize solar exposure.

I. Forseth and A. Teramura (1986) observed rapid leaf movements in exposed leaves of *Puernaria lobate*, or Kudzu vine, in central Maryland, United States. Kudzu was first planted in the southeastern United States in the 1930s to be used as cattle fodder, for erosion control, and for land reclamation. It is a vigorous vine that produces dense canopies with *LAI* values of up to 7, and can grow up to 20 m tall. Currently it is considered an invasive species because it is a difficult plant to control due to "its lack of natural predators, rapid growth rate, and resistance to conventional herbicides and burning" (I. N. Forseth & Teramura, 1986).

Forseth and Teramura reported two different behaviors for the exposed and shaded leaves. The exposed leaves had random azimuth orientations while maintaining a diurnal orientation away from the sun. In July, when the canopy was mature, they observed a maximum mean angle of 75 degrees (midday) and a minimum mean angle of 30 degrees (sunset) from the horizontal.

Forseth and Teramura hypothesized that this large range of leaf movement allows the vine to maintain lower leaf surface temperatures, minimize solar damage, increase water use efficiency, and increase light penetration into the rest of the canopy, thereby increasing the productivity of the plant. In contrast, the shaded leaves exhibited minimal movement. They oriented themselves predominantly northward toward diffuse light throughout the day with fixed azimuth angles.

R. Smart (1985) reported mean leaf angles of 45°, 60° to 75°, and 75° for Concord, Cabernet Sauvignon, and Gewurztraminer, respectively. Similar to Forseth and Teramura (1986), he observed that the angles of grapevine leaves change depending on the solar radiation conditions.

To find the best canopy density for maximum solar exposure, he used the average values of leaf orientations in a canopy. This method is effective because the average values provide reliable results with relatively small errors—11% error of the canopy productivity term. (R. Smart & Lang, 1973).

H. Mabrouk et al. (1997) studied the light distribution in three different training systems for fifteen-year-old Merlot vines in France. They measured the inclination and azimuth angles of leaves in mid-July. The times of the measurements were not included in the study. They reported leaf inclination angles of 57.78° for a low vigor canopy and 53.30° and 54.34° for moderate vigor canopies. They also observed that the leaves exhibited random azimuth angle distributions for the Open Lyre training system. For the Open Lyre training system and the Geneva Double Curtain training system, the leaves were mostly oriented perpendicular to the row direction.

Iandolino et al. (2013) measured the leaf inclination and azimuth angles of an eighteen-year-old Cabernet Sauvignon in a vineyard located near Oakville, California. The vines were trained using a VSP system. The measurements were conducted in mid-August. The times of the measurements were not reported. They reported leaf inclination angles of 58.1° for an irrigated and non-fertilized vine, and 63.2° for an irrigated and fertilized vine. They also observed random azimuth angle distributions for both of the irrigated vines.

O. Grant et al. (2007) measured both inclination and azimuth angles of leaves for two grapevines (Castelao and Aragones) in south-east Chile during August. All the vines were trained on bilateral Royal Cordon systems. The measurements were taken during the morning and afternoon for four different vine treatments: (a) not irrigated (rain-fed), (b) partial root zone drying (only half of the root was irrigated), (c) deficit irrigated (half irrigation provided), and (d) full irrigated. They report leaf inclination angles of 40° to 80° and an azimuth angle of 180° where leaves were oriented perpendicular to the row direction.

O. Grant et al. (2007) reported the widest range of leaf inclination angles because they did not separate the inclination angles according to irrigation regimes. This differentiation is important because leaves under water stress have smaller leaf elevation angles (Iandolino et al., 2013).

Table 8. Leaf inclination angles for various vines

Vine type	Mean leaf angle from horizontal	Azimuth angle	Reference
Kudzu	30° to 75°	Random	I. Forest and A. Teramura (1986)
Concord	45°	-	R. Smart (1985)
Cabernet Sauvignon	60° to 75°	-	R. Smart (1985)
Gewurztraminer	75°	-	R. Smart (1985)
Merlot	54.34°	Random	H. Mabrouk et al. (1997)
Merlot	53.30°	Perpendicular to row	H. Mabrouk et al. (1997)
Merlot	57.78°	Perpendicular to row	H. Mabrouk et al. (1997)
Cabernet Sauvignon	58.1°	Random	A. Iandolino et al. (2013)
Cabernet Sauvignon	63.2°	Random	A. Iandolino et al. (2013)
Castelao and Aragones	40° to 80°	Perpendicular to row	O. Grant et al. (2006)

Table 8 summarizes the reviewed leaf inclination and azimuth angles for various vine types. It shows that the range of inclination angles varies between 30° and 80° from the horizon. It is important to note that the lowest angle of 30° belongs to the rain-fed Kudzu vine. For this study, I have assumed that both nutrients and water are limitless. Therefore, leaf inclination angles from 45° to 80° will be considered. Furthermore, four out of seven studies have observed random azimuth angles. This assumption is consistent with the findings of other researchers who have investigated theories of light distribution within canopies (Isobe, 1969).

Some literature such as Lumeur and Blad (1974) and Isobe (1969) have provided tables for extinction coefficient values for various leaf inclination and solar altitude angles. Table 9 shows the theoretical k values reported by Lumeur and Blad (1974).

Table 9. Extinction coefficients, k, for various leaf inclinations, α, and solar altitudes, β

α / ***β***	**0°**	**15°**	**30°**	**45°**	**60°**	**75°**	**90°**
15°	1.000	0.966	1.1313	1.740	2.082	2.300	2.376
30°	1.000	0.966	0.866	0.914	1.008	1.078	1.103
45°	1.000	0.966	0.866	0.707	0.646	0.637	0.637
60°	1.000	0.966	0.866	0.707	0.500	0.394	0.367
75°	1.000	0.966	0.866	0.707	0.500	0.259	0.170
90°	1.000	0.966	0.866	0.707	0.500	0.259	0.000

In contrast with this detailed approach, Table 9 provides a general equation for different leaf inclinations as a function of solar elevation, β. Because well irrigated grapevines are mostly vertical and exhibit random azimuth distributions, Equation (31), for spherical leaf distributions, is appropriate (Jones, 1992).

$$k = \frac{1}{2 \sin \beta} \quad (31)$$

Figure 29 shows k as a function of β. The graph shows that as the sun reaches an altitude of 90°, the solar radiation penetration through the canopy increases while k decreases.

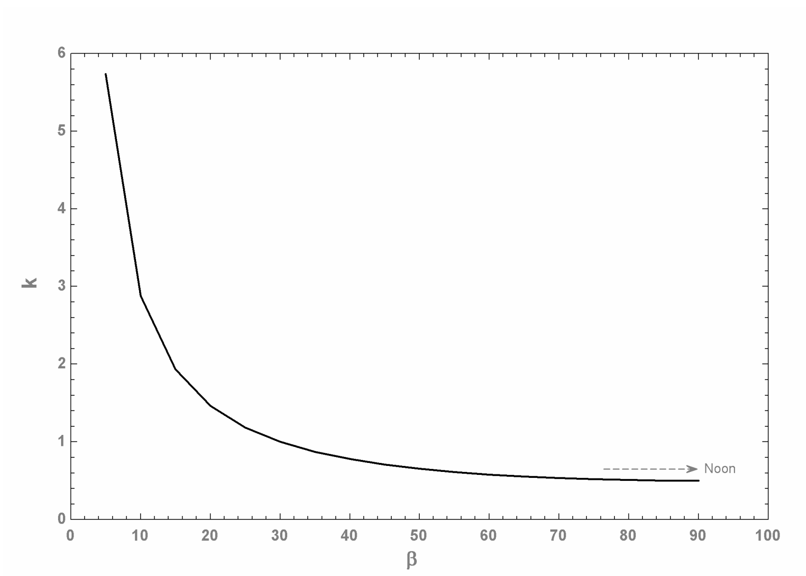

Figure 29. Extinction coefficient, k, as a function of solar elevation, β

A comparative study was conducted to examine the differences in the level of precision between the various approaches. Two cities (New York City and Miami) in different latitudes were selected. The average daily extinction coefficients for the 15th of each summer month were calculated using the detailed Lumeur and Blad (1974) approach, and the general Equation (31) approach. The results were then compared to determine the best method.

As Jackson and Palmer (1979) suggested, the average k over time can serve as a good estimate for the k value at each time within said time interval. The daily average extinction coefficient was calculated by averaging the *k* values obtained every two hours from 6 a.m. to 6 p.m. This twelve-hour time period roughly tracks sunrise to sunset for each location.

The solar attitudes for each city and time were obtained using the National Oceanic and Atmospheric Administration (NOAA) Solar Position Calculator (National Oceanic and Atmospheric Administration, 2017).

In Table 9, the values of the solar altitudes were rounded because Lumeur and Blad (1974) provided the *k* values for 15° intervals. Values of α of 45°, 60°, and 75° were considered. Exact latitude values were considered when using Equation (31).

Table 10. Comparative study of extinction coefficient, k. values using the detailed, Lumeur and Blad (1974), and general, Equation (29, methods for New York City and Miami from 6 a.m. to 6 p.m. of the 15th of each summer month.

Miami (25.7617° N, 80.1918° W)				H. Jones, 1992	Extinction Coefficient, *K*, per leaf angle [°], Lambur & Blad (1974)		
Month & Day	**Time**	**Altitute [°]**	**Rounded Altitutes for the Detailed Method**	**Sperical Model**	**45**	**60**	**75**
Jun 15th	6:00 AM	5.62	0	0.000	0.0000	0	0
	8:00 AM	31.18	30	0.966	0.914	1.008	1.078
	10:00 AM	57.87	60	0.590	0.707	0.5	0.394
	12:00 PM	84.57	90	0.502	0.707	0.5	0.259
	2:00 PM	67.47	75	0.541	0.707	0.5	0.259
	4:00 PM	40.59	45	0.768	0.707	0.646	0.637
	6:00 PM	14.49	15	1.998	1.740	2.082	2.3
Daily Average				**0.894**	**0.879**	**0.812**	**0.748**
July 15th	6:00 AM	3.72	0	0.000	0	0	0
	8:00 AM	29.41	30	1.018	0.914	1.008	1.078
	10:00 AM	56.21	60	0.602	0.707	0.5	0.394
	12:00 PM	82.48	90	0.504	0.707	0.5	0.259
	2:00 PM	68.23	75	0.538	0.707	0.5	0.259
	4:00 PM	41.28	45	0.758	0.707	0.646	0.637
	6:00 PM	14.9	15	1.945	1.740	2.082	2.3
Daily Average				**0.894**	**0.914**	**0.873**	**0.821**
Aug 15th	6:00 AM	0.91	0	0.000	0	0	0
	8:00 AM	27.14	30	1.096	0.914	1.008	1.078
	10:00 AM	53.99	60	0.618	0.707	0.5	0.394
	12:00 PM	76.69	75	0.514	0.707	0.5	0.259
	2:00 PM	64.75	60	0.553	0.707	0.5	0.394
	4:00 PM	38.41	45	0.805	0.707	0.646	0.637
	6:00 PM	11.54	15	2.499	1.740	2.082	2.3
Daily Average				**1.014**	**0.914**	**0.873**	**0.844**

NYC (40.7128 N, 74.0059 W)				H. Jones, 1992	Extinction Coefficient, *K*, per leaf angle [°], Lambur & Blad (1974)		
Month & Day	**Time**	**Altitute [°]**	**Rounded Altitutes for the Detailed Method**	**Sperical Model**	**45**	**60**	**75**
Jun 15th	6:00 AM	15.63	15	1.856	1.740	2.082	2.3
	8:00 AM	37.98	45	0.812	0.707	0.646	0.637
	10:00 AM	60.1	60	0.577	0.707	0.5	0.394
	12:00 PM	72.6	75	0.524	0.707	0.5	0.259
	2:00 PM	58.87	60	0.584	0.707	0.5	0.394
	4:00 PM	36.72	30	0.836	0.914	1.008	1.078
	6:00 PM	14.4	15	2.011	1.740	2.082	2.3
Daily Average				**1.029**	**1.032**	**1.045**	**1.052**
July 15th	6:00 AM	13.49	15	2.143	1.740	2.082	2.3
	8:00 AM	35.86	30	0.854	0.914	1.008	1.078
	10:00 AM	57.79	60	0.591	0.707	0.5	0.394
	12:00 PM	70.69	75	0.530	0.707	0.5	0.259
	2:00 PM	58.47	60	0.587	0.707	0.5	0.394
	4:00 PM	36.62	30	0.838	0.914	1.008	1.078
	6:00 PM	14.19	15	2.040	1.740	2.082	2.3
Daily Average				**1.083**	**1.061**	**1.097**	**1.115**
Aug 15th	6:00 AM	9.02	15	3.189	1.740	2.082	2.3
	8:00 AM	31.56	30	0.955	0.914	1.008	1.078
	10:00 AM	54.45	60	0.615	0.707	0.5	0.394
	12:00 PM	63.12	60	0.561	0.707	0.5	0.394
	2:00 PM	52.55	60	0.630	0.707	0.5	0.394
	4:00 PM	31.67	30	0.952	0.914	1.008	1.078
	6:00 PM	9.09	15	3.165	1.740	2.082	2.3
Daily Average				**1.438**	**1.061**	**1.097**	**1.134**

The daily average values were calculated from the sunlit hours of the day. In another words, if the solar altitude was 0°, the corresponding time period was not considered for the calculation of the average daily *k* value.

Table 10 shows the results of the comparative studies of New York City and Miami. The rounded solar altitude, β, was used for the detailed calculations whereas the exact altitude values were used for the general method. Three different solar inclination angles, α, were considered for the detailed method. The general model assumes vertical leaves. Both methods assume random azimuth angles for the leaves.

Except in the month of August, the differences between the *k* values using the detailed and the general methods were negligible. However, for the month of August, the detailed model underestimated *k* by approximately 13% for Miami and 20% for New York City. This discrepancy is most likely due to the large rounding of the solar altitude value for the sunrise and sunset times.

This comparative study shows that the general method, Equation (31), provides a good estimate of extinction coefficient values. For this study, both the empirical and statistical methods and their corresponding ranges of *k* values are considered and the resulting solar interception values are further discussed.

5.2.5. Sensitivity Analysis

Equation (30) estimates the solar radiation transmittance though a canopy as a function of *LAI* and *k.* Figure 30 shows the fraction of light transmitted (I/I_0) during the summer months (*LAI* = 3, 4, or 5). The dotted lines define the *k* values obtained from the literature review of the empirical field studies, as well as calculated daily average values using Equation (31).

5.2.5.1. Results

The results show that the influence of the extinction coefficient diminishes as *LAI* increases. Simply put, the possibility of light passing through a canopy decreases as the number of leaves in a canopy increases. The percentage of light passing through a canopy—solar transmittance—is highlighted for each extinction coefficient in Figure 30.

The largest solar transmittance is associated with a canopy with an *LAI* of 3 and *k* of 0.5. Even for this low performing scenario, approximately 80% of the solar radiation is intercepted by the canopy. This still represents a significant reduction in solar gains for a building.

The best scenario occurs when *k* has reached 1. In this condition, all canopies (*LAI* = 3, 4, or 5) perform similarly in that they allow negligible solar radiation to pass through the canopy.

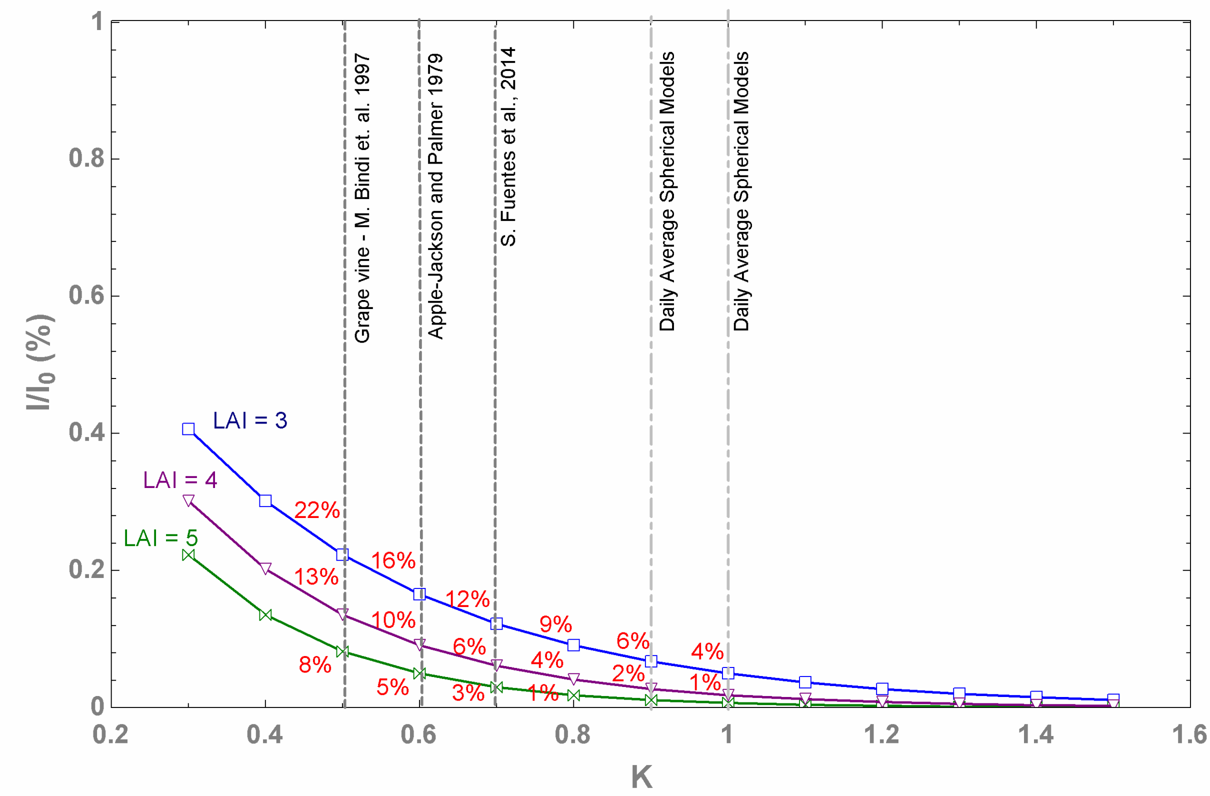

Figure 30. Fraction of light transmittance through a canopy as a function of the extinction coefficient, k, for various Leaf Area Indices (LAI values). The dotted lines are k values obtained from empirical and statistical methods. See Section 5.2.4 for a detailed discussion.

To evaluate the fraction of sunlight passing through a canopy, designers can use Figure 30 directly if the total solar radiation for the considered vertical surface is available. If radiation values are unavailable, the following scenario studies can serve as a general guideline for the early design phase of a project.

5.2.6. Scenario Study

To evaluate the possible cooling power from the solar interception of a canopy, a comparative study of six distinct climatic scenarios was conducted. A detailed discussion of each climatic condition can be found in Section 5.1.5.1. The method used for estimating solar radiation was described in Section 5.1.2.2.

Table 11 shows the simulated average monthly solar radiation values for each climatic condition for the months of June, July, and August. Both south- and west-facing orientations were simulated.

Table 11. Simulated solar radiation values for the six United States cities representative of each climatic condition.

JUNE

Climate	*Selected cities*	*Altitude [m]*	*Latitude [°]*	*Monthly Average Precipitation [mm]*	*Average T-Max [C]*	*Average T-Min [C]*	*RH-Max [%]*	*RH-Min [%]*	*Monthly averag global radiation [kWh/m^2]*	*South - Monthly average global radiation [kWh/m^2]*	*West - Monthly average global radiation [kWh/m^2]*
Cool & Humid	Bemidji, MN	1358	47.4875	111	22.7	11.3	70	45	175.12	68.47	87.84
Cool & Dry	Cut Bank, MT	1169	48.633	65	21.4	7.2	69	35	195.21	79.4	97.52
Warm & Humid	New York, NY	3	40.7128	89	26.3	17.7	81	59	177.5	58.72	82.48
Warm & Dry	Denver, CO	1609	39.7392	50.04	28	11	65	23	215.66	60.76	90.11
Hot & Humid	Miami, FL	2	25.7617	246.13	31.9	24.4	90	65	164.2	35.05	63.57
Hot & Dry	Phoenix, AZ	304	33.4484	1.02	39.9	25.4	35	15	248.23	46.99	108.41

JULY

Climate	*Selected cities*	*Altitude [m]*	*Latitude [°]*	*Monthly Average Precipitation [mm]*	*Average T-Max [C]*	*Average T-Min [C]*	*RH-Max [%]*	*RH-Min [%]*	*Monthly averag global radiation [kWh/m^2]*	*South - Monthly average global radiation [kWh/m^2]*	*West - Monthly average global radiation [kWh/m^2]*
Cool & Humid	Bemidji, MN	1358	47.4875	100	25.2	13.9	90	55	182.83	77.91	92.53
Cool & Dry	Cut Bank, MT	1169	48.633	33	26.3	9.8	79	32	209.89	90.52	106.17
Warm & Humid	New York, NY	3	40.7128	115	29.3	21	90	61	177.05	63.55	80.76
Warm & Dry	Denver, CO	1609	39.7392	55.12	32	15	73	30	205.54	67.17	83.06
Hot & Humid	Miami, FL	2	25.7617	165.1	32.7	25.2	85	60	184.2	40.58	74.87
Hot & Dry	Phoenix, AZ	304	33.4484	26.92	41.2	28.6	56	21	234.28	54.47	101.19

AUGUST

Climate	*Selected cities*	*Altitude [m]*	*Latitude [°]*	*Monthly Average Precipitation [mm]*	*Average T-Max [C]*	*Average T-Min [C]*	*RH-Max [%]*	*RH-Min [%]*	*Monthly averag global radiation [kWh/m^2]*	*South - Monthly average global radiation [kWh/m^2]*	*West - Monthly average global radiation [kWh/m^2]*
Cool & Humid	Bemidji Muni, MN	1358	47.4875	82	24	12.3	85	52	156.14	91.71	79.65
Cool & Dry	Cut Bank, MT	1169	48.633	29	26.1	9	70	30	174.73	109.26	91.25
Warm & Humid	New York, NY	3	40.7128	105	28.4	20.3	80	50	181.43	89.87	91.26
Warm & Dry	Denver, CO	1609	39.7392	42.92	31	14	60	28	167.7	86.49	82.11
Hot & Humid	Miami, FL	2	25.7617	226.06	32.8	25.2	83	68	184.2	53.81	75.69
Hot & Dry	Phoenix, AZ	304	33.4484	24.89	40.2	25	50	22	217.78	79.22	107.19

To obtain the monthly average extinction coefficient, k_{avg}, the elevations of the sun at the solar noon of the 15th of each summer month were calculated using the National Oceanic and Atmospheric Administration (NOAA) Solar Position Calculator (National Oceanic and Atmospheric Administration, 2017).

The solar noon corresponds with the maximum solar altitude, β_{max}, for each climate. Because in most site conditions the solar radiation at sunrise and sunset is blocked from reaching the façade of a building due to various obstacles such as surrounding buildings, the minimum solar altitudes were considered to be 10° for morning and evening conditions.

Table 12. Monthly average extinction coefficient, k_{avg}, for each summer month for six climatic scenario. B_{max}: solar noon elevation.

Climate & Site Coordinates	**June**		**July**		**August**	
	β_{max}	k_{avg}	β_{max}	k_{avg}	β_{max}	k_{avg}
Cool & Dry (48° 38' 5" N, 112° 19' 52" W)	64.7°	1.05	62.74°	1.07	55.16°	1.16
Cool & Humid (47° 28' 52" N, 94° 53' 18" W)	65.76°	1.04	63.89°	1.06	56.30°	1.14
Warm & Dry (39° 43' 59" N, 104° 58' 59" W)	73.60°	0.98	74.62°	0.99	64.06°	1.06
Warm & Humid (40° 43' 0" N, 74° 1' 0" W)	72.60°	0.99	70.69°	1.00	63.12°	1.07
Hot & Dry (33° 25' 59" N° , 112° 4' 1" W)	79.90°	0.94	77.92°	0.95	70.36°	1.01
Hot & Humid (25° 46' 1" N, 80° 10' 59" W)	86.86°	0.90	85.57°	0.91	78.00°	0.95

The k value for each solar altitude angle, starting from 10° to solar noon and then back to 10°, was calculated for each climatic condition. The k_{avg} values were calculated by averaging the k values for each solar altitude angle throughout each day. Table 12 provides a summary of the k_{avg} and β_{max} values for each climatic condition. The results demonstrated a few interesting trends:

- The value of k decreases as the latitude of the site decreases. Recall that the model assumes vertical leaves with random azimuth distributions. The solar radiation from the relatively low solar noon altitude angle in cool climates is mostly blocked from entering the canopy. In hot climates where the solar noon elevations are high, light can easily penetrate the canopy (Figure 31).

- In all climates, the k_{avg} for the month of August is the largest. That is due to the reduction in β_{max} compared to the months of June and July. Similarly, because the leaves are vertical, solar radiation is mostly blocked by the leaves, reducing the canopy transmittance (Figure 31).

- Field measured studies show that *k* values of 1 are associated with horizontal leaves (Jones, 1992). Therefore, it seems that the statistical model overestimates the capacity of the canopy to block sunlight.

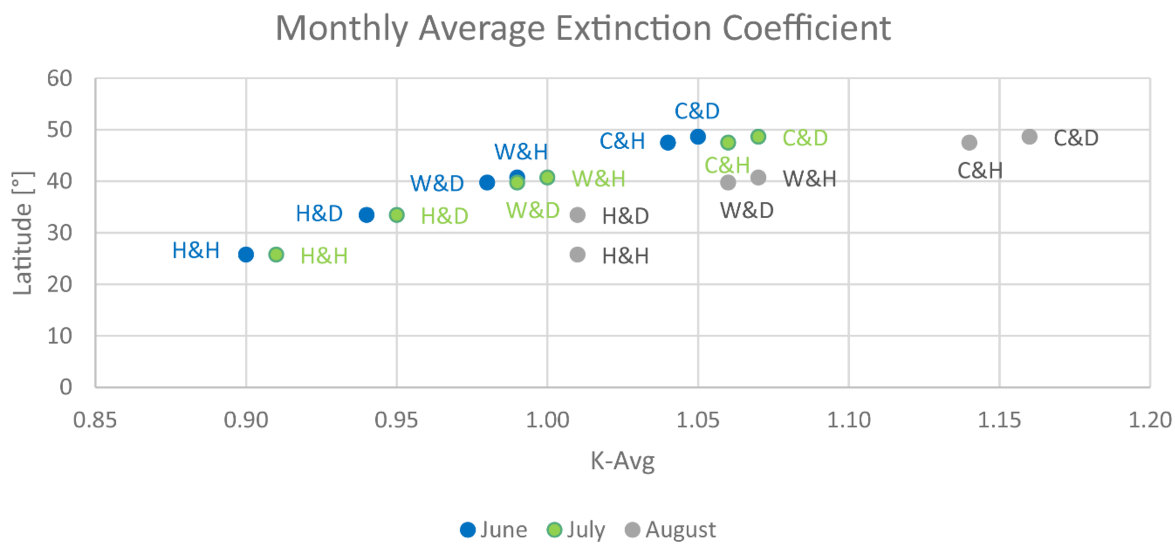

Figure 31. The monthly average extinction coefficients of summer months for various climates. (C&D: cool and dry, C&H: cool and humid, W&D: warm and dry, W&H: warm and humid, H&D: hot and dry, H&H: hot and humid)

5.2.6.1. Results

A series of parametric studies were conducted for various *k* and *LAI* values using Equation (30). EES software was used for the calculation of the parametric studies. Figure 32 though Figure 37 illustrate the results for both south- and west-facing green walls for each summer month for each climatic condition.

The range of radiation transmitted through the canopy, *I,* drastically varies depending on the considered *LAI* and *k* values. The dotted lines show the referenced *k* values from both the empirical and statistical methods. The pink text shows that the best performing green wall has an *LAI* of 5, and shows the associated statistical *k* value for each climate. The parametric studies show that:

- The south-facing green wall produces the largest cooling (solar gain reduction) in cool climates, followed by warm climates and hot climates. This is due to the lower solar elevation in higher latitudes as well as the considered vertical inclination angles of the leaves.

- As expected, a green wall has a greater cooling impact in dry climates compared to humid climates because the net solar gains are larger due to clearer sky conditions.
- A west-facing green wall provides the largest cooling for the hot and dry climate (with long sunset hours) followed by the warm and dry climate and the cool and dry climate.

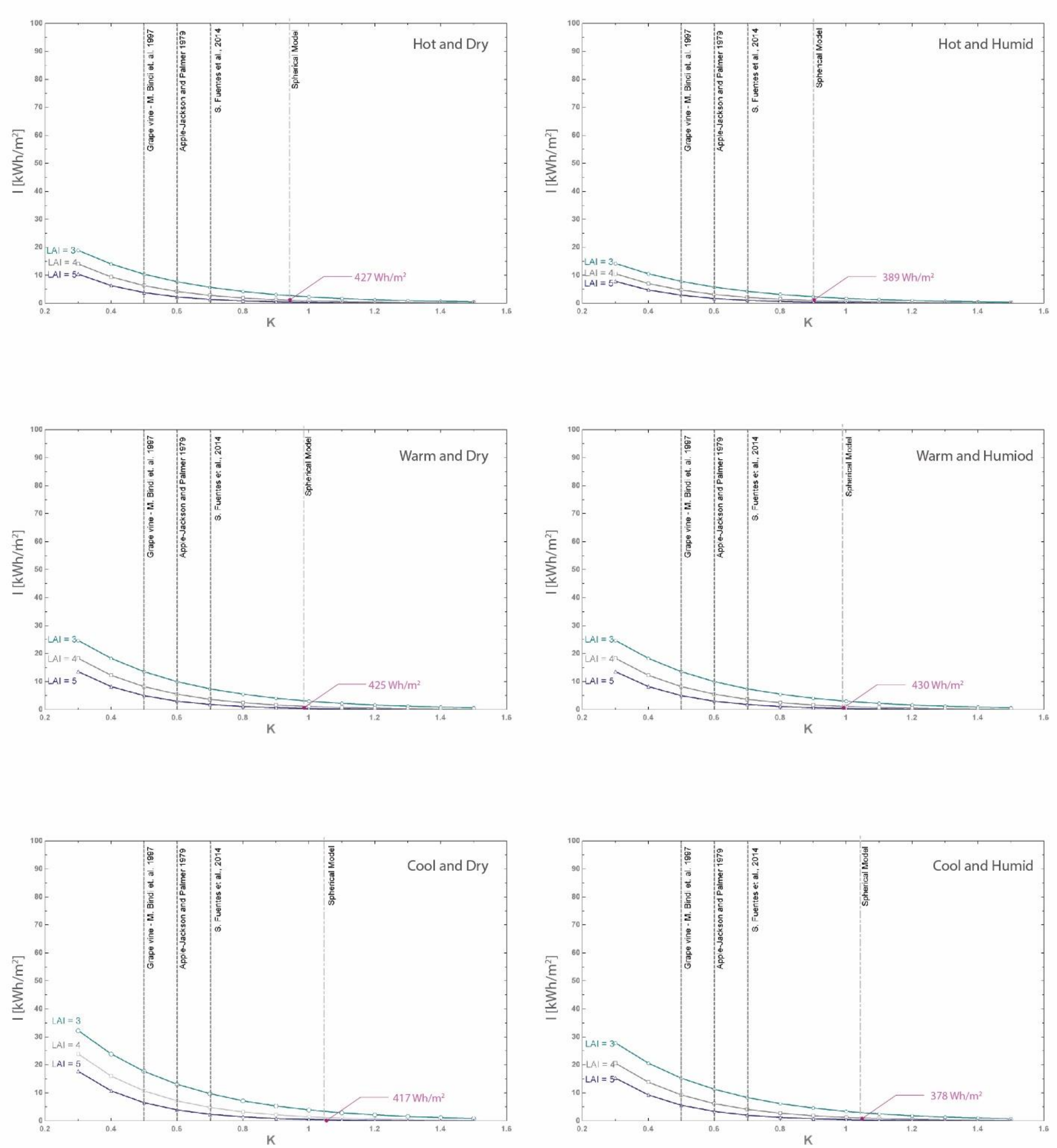

Figure 32. Solar radiation transmitted through the canopy, I, as a function of extinction coefficient, k, for various LAI values for a south-facing green wall in the month of June. The dotted lines are the referenced k values from the empirical and statistical methods (see Section 5.2.4 for details). The highlighted pink texts show the transmitted radiation for a green wall with an LAI of 5 and corresponding daily average extinction coefficient.

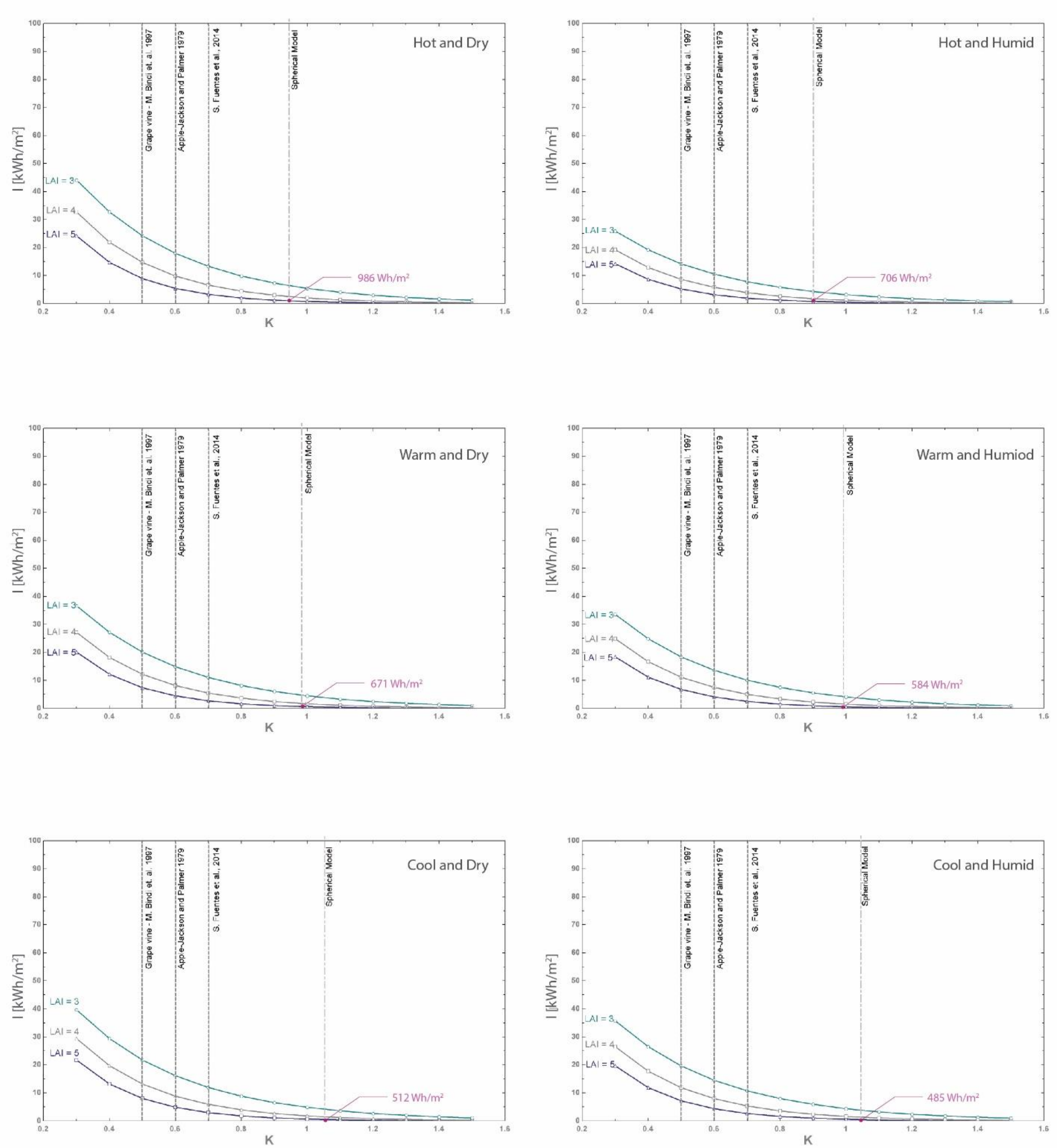

Figure 33. Solar radiation transmitted through the canopy, I, as a function of extinction coefficient, k, for various LAI values for a west-facing green wall in the month of June. The dotted lines are the referenced k values from the empirical and statistical methods (see Section 5.2.4 for details). The highlighted pink texts show the transmitted radiation for a green wall with an LAI of 5 and corresponding daily average extinction coefficient.

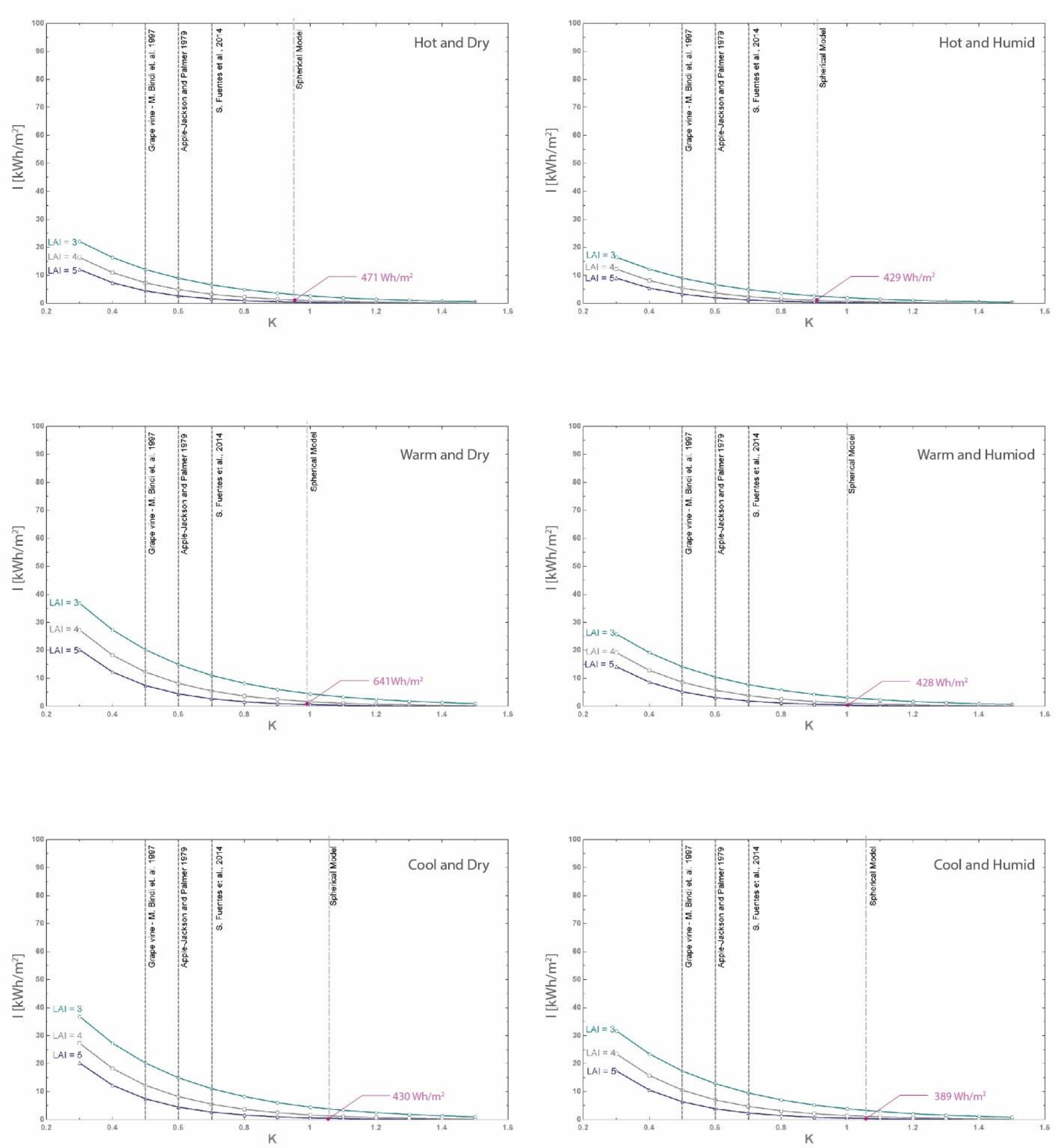

Figure 34. Solar radiation transmitted through the canopy, I, as a function of extinction coefficient, k, for various LAI values for a south-facing green wall in the month of July. The dotted lines are the referenced k values from the empirical and statistical methods (see Section 5.2.4 for details). The highlighted pink texts show the transmitted radiation for a green wall with an LAI of 5 and corresponding daily average extinction coefficient.

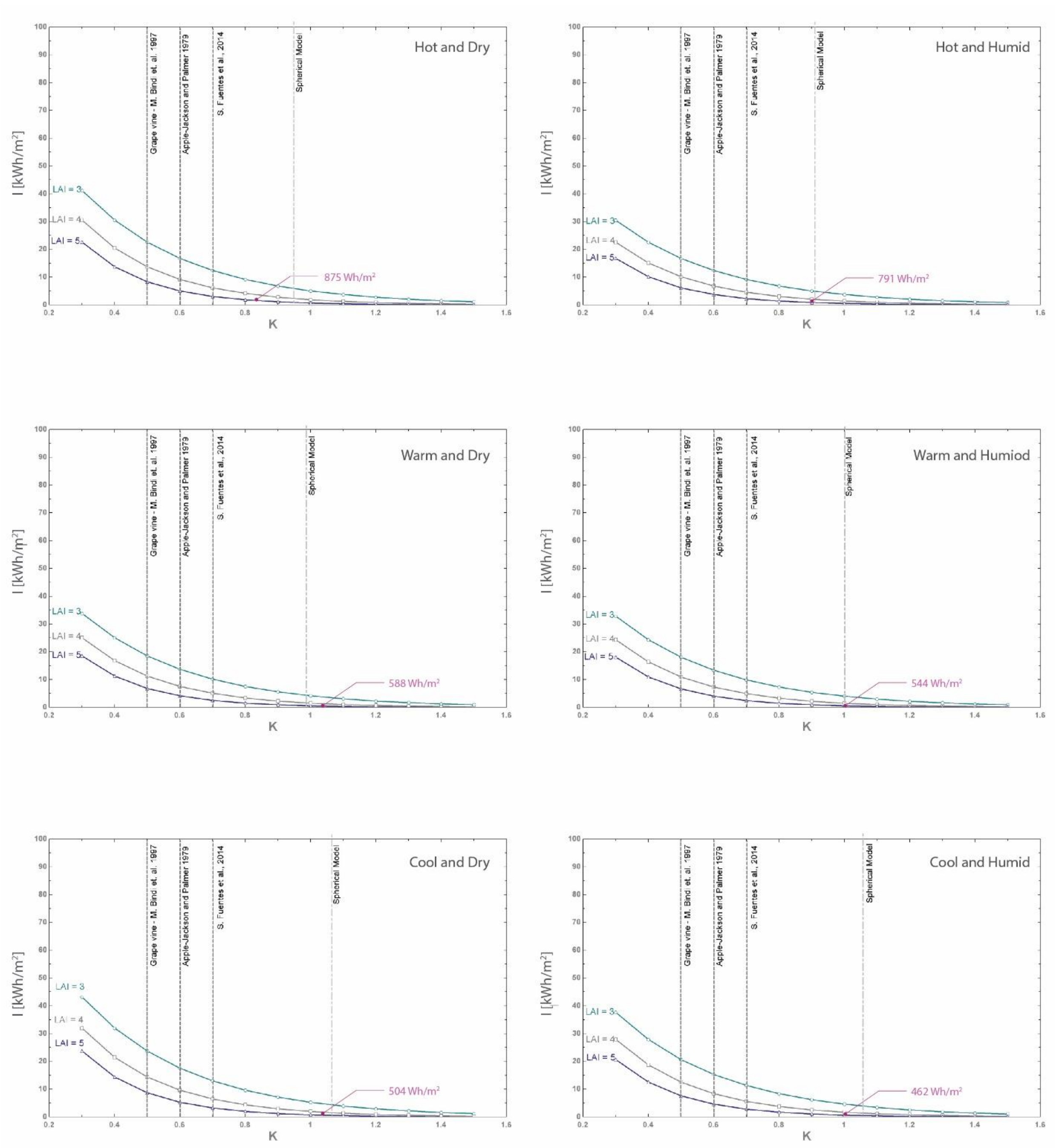

Figure 35. Solar radiation transmitted through the canopy, I, as a function of extinction coefficient, k, for various LAI values for a west-facing green wall in the month of July. The dotted lines are the referenced k values from the empirical and statistical methods (see Section 5.2.4 for details). The highlighted pink texts show the transmitted radiation for a green wall with an LAI of 5 and corresponding daily average extinction coefficient.

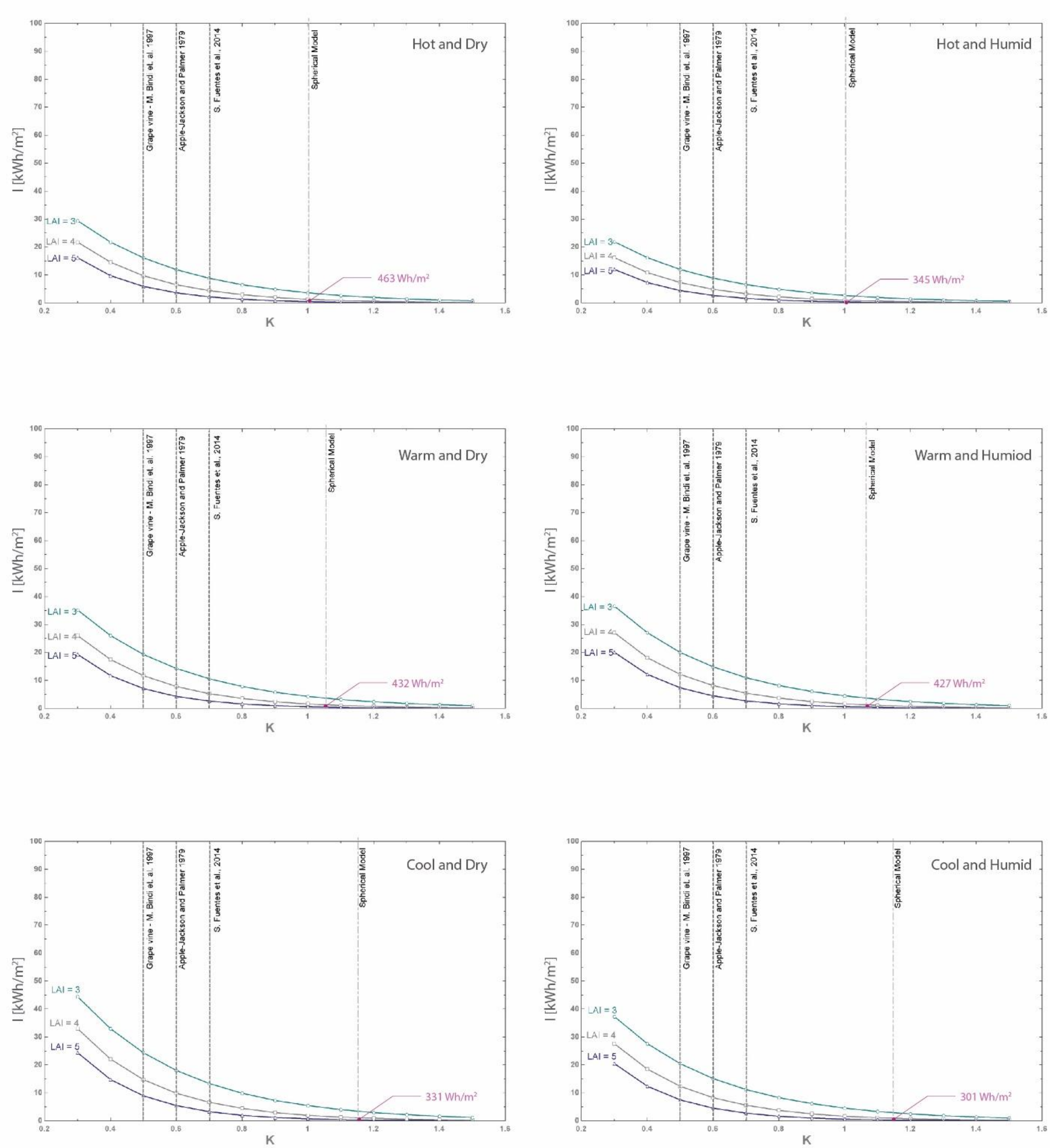

Figure 36. Solar radiation transmitted through the canopy, I, as a function of extinction coefficient, k, for various LAI values for a south-facing green wall in the month of August. The dotted lines are the referenced k values from the empirical and statistical methods (see Section 5.2.4 for details). The highlighted pink texts show the transmitted radiation for a green wall with an LAI of 5 and corresponding daily average extinction coefficient.

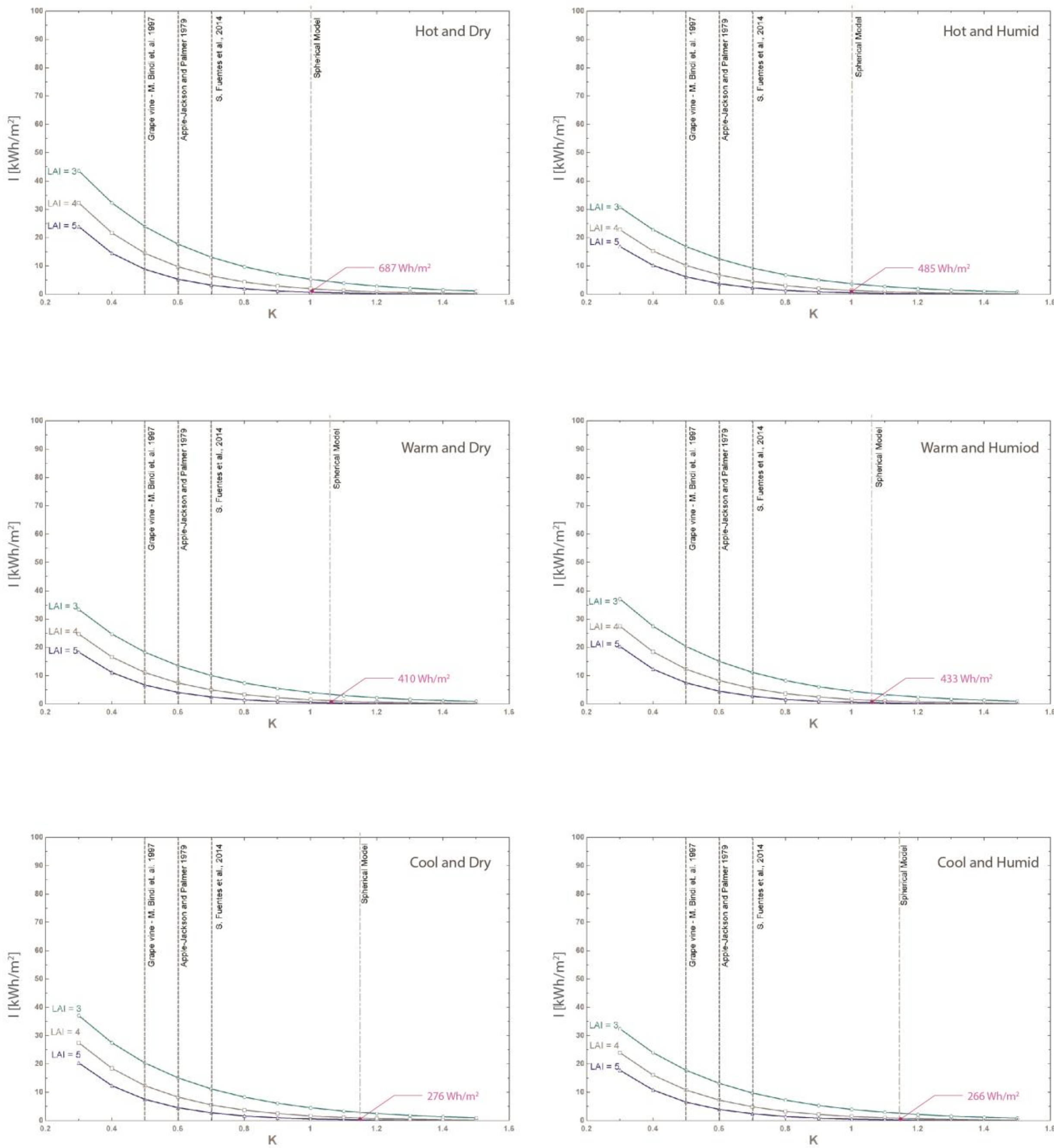

Figure 37. Solar radiation transmitted through the canopy, I, as a function of extinction coefficient, k, for various LAI values for a west-facing green wall in the month of August. The dotted lines are the referenced k values from the empirical and statistical methods (see Section 5.2.4 for details). The highlighted pink texts show the transmitted radiation for a green wall with an LAI of 5 and corresponding daily average extinction coefficient.

Figure 32 through Figure 37 provide a granular understanding of the solar energy [kW/m^2] passing through canopies for various *LAI* and *k* values. However, it is difficult to decipher the general trends of solar transmittance for the considered climatic conditions at various latitudes.

Accordingly, the percentages of solar transmittance for each climate for the summer months were calculated using *k* values obtained from the statistical method (Table 12). The results (Figure 38 through Figure 40) show that:

- In the months of June and July the performances of green walls in blocking solar radiation are very similar. In August, for all climates, this performance increases due to lower solar altitude angles.
- For all *LAI* values and summer months the smallest solar tranmittance (largest cooling from shading) occurs in cool climates, followed by warm climates and hot climates.
- For all summer months and latitude angles, the impact of the extinction coefficient, *k*, decreases as *LAI* increases. However, the positive impact of canopy performance increases at a diminishing rate as *LAI* increases past 3 (the point of diminishing return).
- The range of solar transmittance values for all summer months is reduced as *LAI* increases. For example, in the month of June the percentage of solar transmittance varies from 4.2% to 6.8% for an *LAI* of 3. In the same month, for an *LAI* of 5, the solar transmittance percentage ranges only from 0.5% to 1.2%. This trend continues to show a diminishing return as *LAI* values become larger. One can conclude that *LAI* values of 6 and 7 will provide roughly similar percentages of solar transmittance for all climatic conditions.

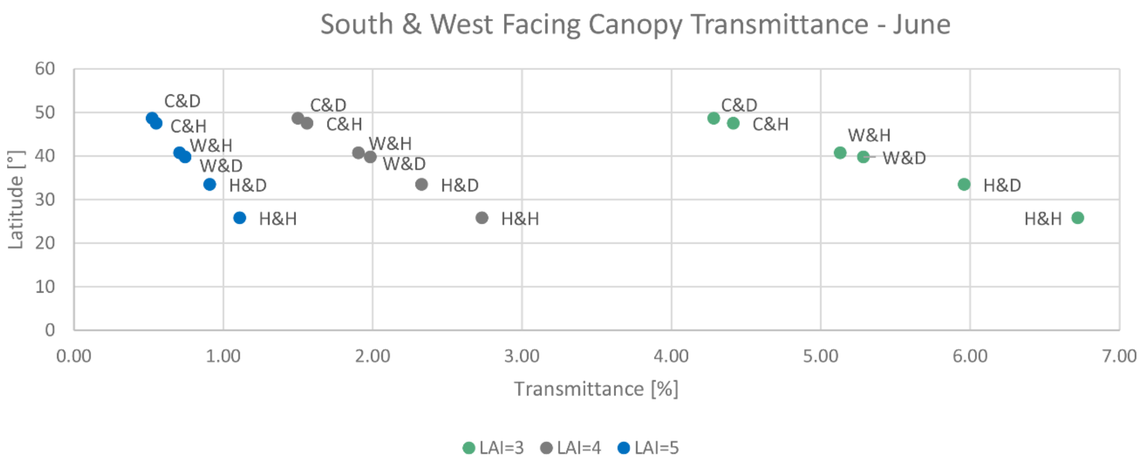

Figure 38. Percentage of solar transmittance as a function of various latitudes for south- and west-facing green walls in the month of June. The k values obtained from the statistical method (Table 12) were used for calculations.

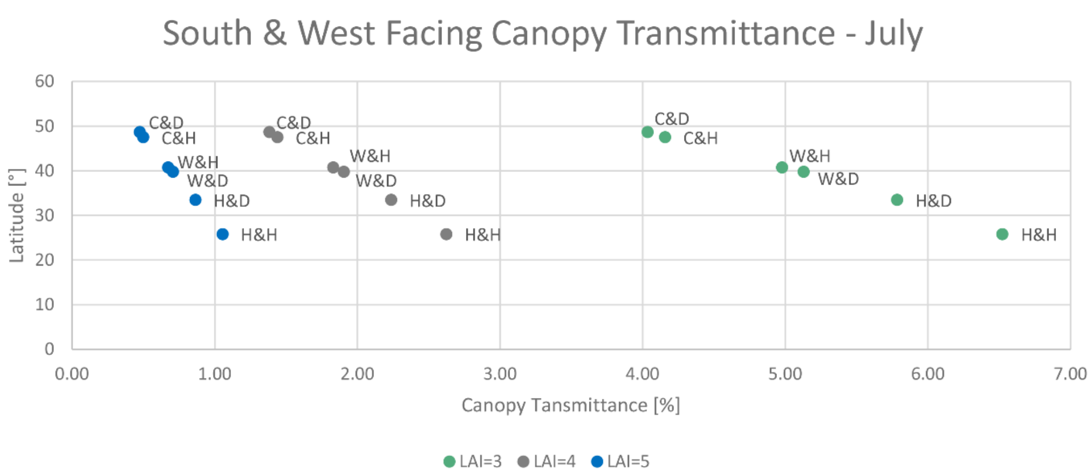

Figure 39. Percentage of solar transmittance as a function of various latitudes for south- and west-facing green walls in the month of July. The k values obtained from the statistical method (Table 12) were used for calculations.

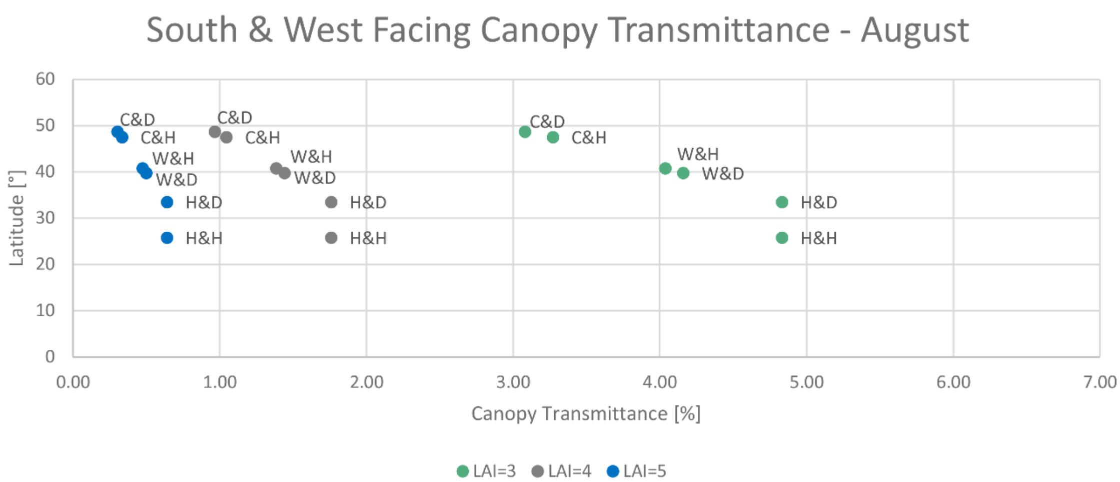

Figure 40. Percentage of solar transmittance as a function of various latitudes for south- and west- facing green walls in the month of August. The k values obtained from the statistical method (Table 12) were used for calculations.

5.2.7. Statistical vs. Empirical Extinction Coefficient Evaluation

Compared to the empirical method, the statistical method overestimated the *k* values, resulting in significant overestimation of the solar gain reduction of green walls. Therefore, it is prudent to compare these results with the field measured studies of green walls to establish the appropriate value for *k*.

K. Ip et al. (2010) measured the solar transmittances of two vining (Virginia creeper) green walls in Brighton, England (latitude of 50.8225° N). They reported average transmittances of 22% for mid-June and 12% for mid-July. By the end of July, the solar transmittance of the canopies was so small (less than 5%) that the researchers' instruments were unable to measure solar radiation behind the green wall.

These reported transmittances correspond with *k* values of 0.4, assuming *LAI* ranged between 3 (transmittance of 27%) and 5 (transmittance of 12%). Note that Ip et al. calculated the solar transmittance of the canopies from the number of leaf layers instead of *LAI*. Although their method of calculation is different from this research, the final transmittance results can be used as good indicator of the shading performance of green walls.

L. Schumann (2007) measured the transmittances of two green walls against a southeast-facing barn in Southern Maryland, United States (latitude of 39.0458° N). She observed 40% transmittance for an *LAI* of

1 and 6% for an *LAI* of 5. These measured transmittances correspond with a *k* value of 0.58 (Price, 2010; Schumann, 2007).

D. Holm (1989) measured the solar transmittance of English ivy and Boston ivy green walls. He assumed that all leaves were "at an angle of 15° to the incident light rays and parallel to each other." He reported a solar transmittance of 12.8% for one layer of leaf and a 5% transmittance for two layers of leaves. These transmittance values are significantly smaller than other reported field measured values. Even the large *k* values from the statistical method do not explain Holm's reported transmittance values.

T. Šuklje et al. (2016) measured the *LAI* and transmittance values of two south-facing green walls comprised of *Phaseolus Vulgaris L* in Ljubljana, Slovenia (latitude of 46° N). They observed solar transmittances of 17% for canopies with an *LAI* value of 6.1, and 9% for canopies with an *LAI* value of 7.2. Their reported values correspond with *k* values of 0.34 for an *LAI* value of 6.1, and 0.3 for an *LAI* value of 7.2. In other words, although the canopies were denser than those observed in most other studies, Šuklje et al. reported the largest amount of solar radiation passing through the canopies. Because *k* is a function of leaf inclination, azimuth angle, and solar altitude, and assuming that the reported values were correct, the azimuth and inclination leaf angles might have been the cause of the large solar transmittance.

M. Hoelscher et al. (2016) measured the *LAI* and solar transmittances of a west-facing indirect vining (*F. baldschuanica*) green wall in Berlin, Germany (latitude of 52°N). They observed an *LAI* of 3 with a transmittance of 0.25. The corresponding *k* value was 0.54 for their study.

Perez et al. (2017) conducted a thorough investigation to establish a relationship between the *LAI* and transmittance of an indirect vining (Boston ivy) green wall in Lleida, Spain (42° N). The green wall was affixed around a building, covering the south-, east-, and west-facing façades to various extents. They observed average *LAI* values of 3.5, 3, and 2.4 for the east-, south-, and west-facing orientations, respectively. The low *LAI* values on the south- and west-facing façades were attributed to a shorter growth period compared to the east façade. They observed an average solar transmittance of 6% to 8% for the lower and middle sections of the south- and west-facing green walls. According to their findings, the associated *k* for their reported values was approximately 0.6.

Note that the above studies were specifically selected and reviewed because they not only evaluated indirect vining green walls, but also considered *LAI* and/or solar transmittance. Noting the differing findings of Šuklje et al. (2016) and Holm (1989), an average *k* value of 0.5 was most frequently observed. This value is similar to the empirical value obtained from the grapevine study by M. Bindi et al. (1997).

The extinction coefficient is highly dependent on the design of the support structure of a green wall, leaf angle, and leaf azimuth angle. Therefore, it is important to highlight that the studies mentioned above used various training systems and vine species. It is difficult to draw definite conclusions from them.

Furthermore, it was demonstrated in Section 5.2.6 that extinction coefficient values differ according to the latitude of a site and the month of observation. Although the statistical method proved to overestimate the specific values of the extinction coefficient, the relationships between the coefficients remain valid. This is because the ratios between the values of the extinction coefficients are established according to solar altitude and not canopy design specifications (Eq. (31)).

Accordingly, for this study, an extinction coefficient of 0.5 was used as a baseline for the month of August at a latitude of 40°, which best fit (in terms of percentage of error for predicted values) the above gathered data. From this baseline, all other extinction coefficient values for various latitudes and summer months were established. Table 13(a) shows the average daily *k* values calculated from the statistical model. To obtain the ratios, these values were divided by the *k* value for the month of August at a latitude of 40° as the baseline (Table 13(b)). The calculated ratios were then used to evaluate the extinction coefficients of each summer month for each of the considered latitudes (Table 13(c)).

Table 13. a) Calculated average daily extinction coefficients from the 15th of each summer month (see Section 5.2.6 for the method of calculation). b) Calculated ratios between k values according to the baseline; i.e., themonth of August at a latitude of 40°. c) The adjusted extinction coefficient values for the summer months of various latitudes according to the baseline of the month of August at a latitude of 40°.

a

Latitude [°]	*Month*		
	June	**July**	**Aug**
48	1.05	1.07	1.16
44	1.03	1.04	1.11
40	0.99	1.00	1.07
36	0.97	0.99	1.04
32	0.95	0.97	1.01
28	0.93	0.95	0.99
24	0.93	0.94	0.97

b

Latitude [°]	*Month*		
	June	**July**	**Aug**
48	0.98	1.00	1.08
44	0.96	0.97	1.04
40	0.93	0.93	1.00
36	0.91	0.93	0.97
32	0.89	0.91	0.94
28	0.87	0.89	0.93
24	0.87	0.88	0.91

c

Latitude [°]	*Recommended k-Values*		
	June	**July**	**Aug**
48	0.49	0.50	0.54
44	0.48	0.49	0.52
40	0.46	0.47	0.50
36	0.45	0.46	0.49
32	0.44	0.45	0.47
28	0.43	0.44	0.46
24	0.43	0.44	0.45

The calculated k values from Table 13(c) include latitudes from 24° to 48° at 4 degree intervals. It is recommended to consider the more detailed and site-specific k values (Table 13(c)) using Equation (31).

For a fast and easy evaluation of green walls, the next chapter provides designers with a series of simple matrices that provide the cooling power of green walls from canopy transpiration and solar interception. It also estimates the percentages of heat gain reduction for the summer months for the six climatic scenarios described herein.

6. Matrix for Designers

The cooling effect of a green wall can be chiefly attributed to solar radiation reduction (shading) and transpiration (Cameron et al., 2014; Hoelscher et al., 2016; Koyama et al., 2015; Šuklje et al., 2016). Therefore, evaluating these two components should serve as a sufficient performance indicator for the early design phase of a project.

The majority of studies on direct and indirect green walls highlight that the shading effect of a canopy contributes most significantly to the total cooling effect of a green wall during the summer months (Cameron et al., 2014; Susorova et al., 2013; Tilley et al., 2012; Wang, 1999). Regardless of climate, canopy design, and orientation, all studies report substantial surface temperature reductions of exterior façades due to shading.

In climates with cool summers, it has been shown that direct and indirect green walls reduce exterior wall surface temperatures by 15.5 °C, 13.9 °C, and 10.5 °C for south southwest-, east-, and west- facing facades, respectively (Hoelscher et al., 2016). In climates with dry and warm summers, it has been shown that east facing green walls reduce exterior wall surface temperature between 1.9 °C and 8.3 °C (Eumorfopoulou & Kontoleon, 2009). Similarly, in warm and humid climates south facing green walls reduced wall surface temperature between 3.7 °C and 11.3 °C (Koyama et al., 2013). In climates with hot summers, it has been reported that indirect green walls reduce exterior wall surface temperatures by 4.36 °C (N. H. Wong et al., 2010).

The significance of transpiration in reducing ambient air temperatures and negating the Urban Heat Island Effect has been long established (Alexandri & Jones, 2008; Huang et al., 1987). According to the U.S. Environmental Protection Agency, peak air temperatures in tree groves are 5° C cooler than over open terrain, and suburban areas with mature trees are 3° C cooler than similar suburbs without trees (E. Wong, Akbari, Bell, & Cole, 2011).

Although well regarded, only a few building scale studies on green walls have quantified and differentiated between total cooling and the cooling contributed specifically by transpiration (Cameron et al., 2014; Coma et al., 2017; Koyama et al., 2015; Tilley et al., 2012).

One of the first studies on this topic was by T. Cameron et al. (2014). They evaluated the cooling performance of six potted plants comprised of different vine and shrub species in a controlled, indoor environment. The performance of each plant was compared to a similar but non-transpiring (sealed leaves) plant. Normalized for *LAI*, they found that cooling performance varied significantly between species. For example, Fuchsia provided more cooling through transpiration (5.5 °C mean wall temperature reduction) than shading (3 °C mean wall temperature reduction). Jasminum provided cooling more through shading (4 °C mean wall temperature reduction) than transpiration (1.5 °C mean wall temperature reduction).

Although this study was ground breaking, the results can only serve as a proof of concept because the experiments were conducted on potted plants in a controlled space and only over a short period of time. More importantly, the reported results were expressed only in terms of temperature reductions and thus limits the usefulness of the data. Similarly, most studies report cooling power from transpiration solely in terms of ambient air temperature reductions (Cameron et al., 2014; Hoyano, 1988; Pérez et al., 2011; Perini et al., 2011).

Although informative, reported values of temperature reductions of ambient air and wall surfaces are not useful during the early design phase of a project. This is because these temperature values are highly dependent on the experimental conditions of the study. Canopy design—*LAI*, leaf angle, cavity dimension, training system design, plant biophysical traits, etc.—façade thermal and spectral properties, and site-specific microclimatic conditions during short experimental periods cannot be generalized (Hunter et al., 2014).

A few studies have developed numerical models to evaluate the impact of green walls on heat and mass transfer through building facades (Holm, 1989; Kontoleon & Eumorfopoulou, 2010; Stec et al., 2005;

Šuklje et al., 2016; Susorova et al., 2013; Tilley et al., 2012). K. Kontoleon et al. (2010) developed a heat transfer model to estimate cooling from the proportion of leaf coverage. Their model, however, did not consider latent heat flux, i.e., the cooling from transpiration.

Both Tilley et al. (2012) and Susorova et al. (2013) have developed empirical models that account for latent heat transfer. Both show good agreement with field study measurements. T. Šuklje et al. (2016) introduced a sophisticated theoretical model that uses the finite difference method. Their model showed high accuracy when compared to experimental data from a south-facing indirect vining green wall in Ljubljana, Slovenia.

These energy models can provide a high level of detail on the impact of green walls on the energy performance of a building. To be useful to designers, however, these models need to be re-written in a suitable platform/software. They also require advanced knowledge of thermodynamics, heat transfer, and theories of plant biophysics. Therefore, as an early-design decision-making tool, they are too time and labor intensive to be practical. Additionally, the scale of resolution obtained is far greater than is necessary during the beginning phases of a project.

Similarly, studies on the energy savings of green walls can hardly be informative in evaluating their efficacy for a specific project because these studies are not sufficiently generalizable (Hunter et al., 2014). This problem is especially acute relative to the early design phase of a project, where the construction type of a building is undetermined and design features impacting building loads are still evolving.

Therefore, it is crucial to have a means of estimating green wall performance independent of the particularities of a project. In a parametric study, Šuklje et al. (2016) found that regardless of exterior wall type, a green wall reduced the peak heat flux of a façade by 77%. The magnitude of this heat flux reduction depended on the thermal resistance of the wall. For example, the average heat flux reduction of a highly insulated wall ($R = 5\ m^2\ K/W$) was only $1.5\ W/m^2$, while for a minimally insulated wall ($R = 0.6\ m^2\ K/W$) it was $11.2\ W/m^2$.

Accordingly, an evaluation of the performance of a green wall can be decoupled from the exterior walls. This seemingly simple concept is crucial, especially during the early phases of a design project where the construction type of a building has not yet been established.

Furthermore, Šuklje et al. (2016) proved that the presence of an exterior façade of a building has negligible impact on the transpiration rate of a green wall. This is an important finding because it shows that a canopy can be understood as an independent heat sink for urban and building scale studies.

The cooling effects from the shading and transpiration of green walls can be described as a heat gain reduction and a cooling power production, respectively. Both are expressed in W/m^2. To the best of my knowledge, only a few studies have evaluated each cooling component separately (Cameron et al., 2014; Hoelscher et al., 2016; Koyama et al., 2015; Tilley et al., 2012; Wang, 1999). Only Wang (1999), Tilley et al. (2012), and M. Hoelscher et al. (2016) reported each value in terms of W/m^2.

The goal of this chapter is to introduce a series of matrices that allow designers to easily evaluate the cooling effects of various green wall designs for six climatic scenarios in terms of W/m^2 of heat gain reduction and cooling power production.

6.1. Transpiration Matrix—Cooling Power Production for Six Climatic Scenarios

The predicted average cooling power values from the transpiration of south- and west-facing green walls for each summer month are shown for six climates in Table 14 through Table 16. These values represent well-watered canopies with *LAI* values of 3, heights of 3 m, average canopy resistances corresponding to each climate, and no wind. These assumptions reduce the performance of green walls by approximately 20% to 30% compared to the optimal canopy designs discussed in Section 5.1.6. As was demonstrated, an increase in *LAI* above 3 improves canopy performance only marginally. This was also observed in the field by Šuklje et al. (2016), where they saw only a 10% transpiration rate increase between two canopies with *LAI* values of 6.1 and 7.2.

Additionally, the average monthly solar radiation (W/m^2) and the percentage of cooling power converted from the solar energy are reported.

Table 14. Estimated average transpiration cooling power for cool climatic scenarios for well-watered, south- and west-facing canopies for each June, July, and August. Assumed design variables: LAI of 3, height of 3 m, no wind condition (0.1 m/s), and average leaf resistances (r_l s/m) obtained for each climate. (For a detailed discussion of the assumed vine biophysical traits and climate scenario selections, see the section on Cooling from Canopy Transpiration.)

Cool & Humid Climate, r_l = 115 s/m																	
Jun						**July**						**August**					
South			*West*			*South*			*West*			*South*			*West*		
Average Cooling Power [W/m^2]	Monthly Average Solar Radition [W/m^2]	Average Cooling power [%]	Average Cooling Power [W/m^2]	Monthly Average Solar Radition [W/m^2]	Average Cooling power [%]	Average Cooling Power [W/m^2]	Monthly Average Solar Radition [W/m^2]	Average Cooling power [%]	Average Cooling Power [W/m^2]	Monthly Average Solar Radition [W/m^2]	Average Cooling power [%]	Average Cooling Power [W/m^2]	Monthly Average Solar Radition [W/m^2]	Average Cooling power [%]	Average Cooling Power [W/m^2]	Monthly Average Solar Radition [W/m^2]	Average Cooling power [%]
69.18	144.97	47.72	69.18	185.98	37.20	57.15	169.15	33.79	58.94	200.89	29.34	55.42	218.31	25.39	54.14	189.60	28.55

Cool & Dry Climate, r_l = 255.71 s/m																	
Jun						**July**						**August**					
South			*West*			*South*			*West*			*South*			*West*		
Average Cooling Power [W/m^2]	Monthly Average Solar Radition [W/m^2]	Average Cooling power [%]	Average Cooling Power [W/m^2]	Monthly Average Solar Radition [W/m^2]	Average Cooling power [%]	Average Cooling Power [W/m^2]	Monthly Average Solar Radition [W/m^2]	Average Cooling power [%]	Average Cooling Power [W/m^2]	Monthly Average Solar Radition [W/m^2]	Average Cooling power [%]	Average Cooling Power [W/m^2]	Monthly Average Solar Radition [W/m^2]	Average Cooling power [%]	Average Cooling Power [W/m^2]	Monthly Average Solar Radition [W/m^2]	Average Cooling power [%]
36.38	166.35	21.87	37.21	204.32	18.21	45.47	194.67	23.36	46.33	228.39	20.28	44.31	258.70	17.13	43.41	215.98	20.10

Table 15. Estimated average transpiration cooling power for warm climatic scenarios for well-watered, south- and west-facing canopies for June, July, and August. Assumed design variables: LAI of 3, height of 3 m, no wind condition (0.1 m/s), and average leaf resistances (r_l s/m) obtained for each climate. (For a detailed discussion of the assumed vine biophysical traits and climate scenario selections, see chapter on Cooling from Canopy Transpiration.)

Warm & Dry Climate, r_l = 151.62 s/m																	
Jun						**July**						**August**					
South			*West*			*South*			*West*			*South*			*West*		
Average Cooling Power [W/m^2]	Monthly Average Solar Radition [W/m^2]	Average Cooling power [%]	Average Cooling Power [W/m^2]	Monthly Average Solar Radition [W/m^2]	Average Cooling power [%]	Average Cooling Power [W/m^2]	Monthly Average Solar Radition [W/m^2]	Average Cooling power [%]	Average Cooling Power [W/m^2]	Monthly Average Solar Radition [W/m^2]	Average Cooling power [%]	Average Cooling Power [W/m^2]	Monthly Average Solar Radition [W/m^2]	Average Cooling power [%]	Average Cooling Power [W/m^2]	Monthly Average Solar Radition [W/m^2]	Average Cooling power [%]
82.16	136.82	60.05	84.96	202.90	41.87	88.08	144.96	60.76	90.00	184.22	48.86	86.64	220.70	39.26	86.16	224.12	38.44

Warm & Humid Climate, r_l = 128.45 s/m																	
Jun						**July**						**August**					
South			*West*			*South*			*West*			*South*			*West*		
Average Cooling Power [W/m^2]	Monthly Average Solar Radition [W/m^2]	Average Cooling power [%]	Average Cooling Power [W/m^2]	Monthly Average Solar Radition [W/m^2]	Average Cooling power [%]	Average Cooling Power [W/m^2]	Monthly Average Solar Radition [W/m^2]	Average Cooling power [%]	Average Cooling Power [W/m^2]	Monthly Average Solar Radition [W/m^2]	Average Cooling power [%]	Average Cooling Power [W/m^2]	Monthly Average Solar Radition [W/m^2]	Average Cooling power [%]	Average Cooling Power [W/m^2]	Monthly Average Solar Radition [W/m^2]	Average Cooling power [%]
53.56	131.31	40.79	56.14	184.44	30.44	53.92	144.96	37.20	56.14	184.22	30.48	66.44	220.70	30.10	66.60	224.12	29.72

Table 16. Estimated average transpiration cooling power for hot climate scenarios for well-watered, south- and west-facing canopies for June, July, and August. Assumed design variables: LAI of 3, height of 3 m, no wind condition (0.1 m/s), and average leaf resistances (r_l s/m) obtained for each climate. (For detailed discussion of the assumed vine biophysical traits and climate scenario selections, see section on Cooling from Canopy Transpiration.)

Hot & Dry Climate, r_l = 125.09 s/m																	
Jun						**July**						**August**					
South			*West*			*South*			*West*			*South*			*West*		
Average Cooling Power [W/m^2]	Monthly Average Solar Radition [W/m^2]	Average Cooling power [%]	Average Cooling Power [W/m^2]	Monthly Average Solar Radition [W/m^2]	Average Cooling power [%]	Average Cooling Power [W/m^2]	Monthly Average Solar Radition [W/m^2]	Average Cooling power [%]	Average Cooling Power [W/m^2]	Monthly Average Solar Radition [W/m^2]	Average Cooling power [%]	Average Cooling Power [W/m^2]	Monthly Average Solar Radition [W/m^2]	Average Cooling power [%]	Average Cooling Power [W/m^2]	Monthly Average Solar Radition [W/m^2]	Average Cooling power [%]
185.76	110.23	168.52	195.20	254.30	76.76	171.52	129.78	132.16	179.92	241.10	74.62	160.56	200.00	80.28	164.96	270.61	60.96

Hot & Humid Climate, r_l = 91.55 s/m																	
Jun						**July**						**August**					
South			*West*			*South*			*West*			*South*			*West*		
Average Cooling Power [W/m^2]	Monthly Average Solar Radition [W/m^2]	Average Cooling power [%]	Average Cooling Power [W/m^2]	Monthly Average Solar Radition [W/m^2]	Average Cooling power [%]	Average Cooling Power [W/m^2]	Monthly Average Solar Radition [W/m^2]	Average Cooling power [%]	Average Cooling Power [W/m^2]	Monthly Average Solar Radition [W/m^2]	Average Cooling power [%]	Average Cooling Power [W/m^2]	Monthly Average Solar Radition [W/m^2]	Average Cooling power [%]	Average Cooling Power [W/m^2]	Monthly Average Solar Radition [W/m^2]	Average Cooling power [%]
61.71	85.89	71.85	67.19	155.77	43.14	74.84	100.59	74.40	81.52	185.60	43.92	66.47	139.30	47.72	70.80	195.94	36.13

The predicted values show good agreement with field study measurements from the corresponding climates. In Berlin, Germany (latitude of 52° N) during the months of August and September, M. Hoelscher et al. (2016) quantified and differentiated the cooling effects from shading and transpiration of direct and indirect green walls using the sap flow measurement method.

The west-facing indirect system was comprised of *F. baldschuanica* while the east-facing direct green wall was covered with *Hedera Helix* vine. Both systems had *LAI* values of 3. The maximum and mean measured transpiration cooling powers were 65.6 W/m^2, 39.3 W/m^2, 49.5 W/m^2, and 45.6 W/m^2 for the indirect and direct systems, respectively.

The predicted value of 54 W/m^2 (Table 14) is in good agreement with the average of the maximum values (57.55 W/m^2) and is slightly larger than the average of the mean values (42.45 W/m^2) reported by Hoelscher et al. (2016). However, it is important to note that the sap flow measurement technique tends to underestimate canopy transpiration, a fact that Hoelscher et al. (2016) highlighted.

In Beijing, China, which has warm and humid summers (latitude of 39° N), H. Wang (1999) reported a cooling power of 56.8 W/m^2 for a west-facing direct green wall during the month of July. This value is in good agreement with the predicted value of 56 W/m^2.

Tilley et al. (2012) conducted an expansive and comprehensive study on various indirect green wall systems comprised of nine vine species in Maryland, MA (latitude of 39° N). They evaluated the impact of *LAI*, percentage of plant coverage, and orientation on the thermal performance of indirect green walls. They reported average values of 37 W/m^2, 30 W/m^2, and 50 W/m^2 for a west-facing *Vitis* green wall for the months of June, July, and August, respectively. These values, although smaller than the predicted values (Table 15), show a similar trend: The transpiration rate increases from the months of June through August due to the reduction in solar altitude.

The lower reported values can be attributed to the low *LAI* of the canopy, which varied between 1.5 and 2 during the summer months. Adjusting for the lower *LAI*, the cooling powers are reduced to 44 W/m^2, 45 W/m^2, and 52 W/m^2 respectively, which are within the reported standard of error.

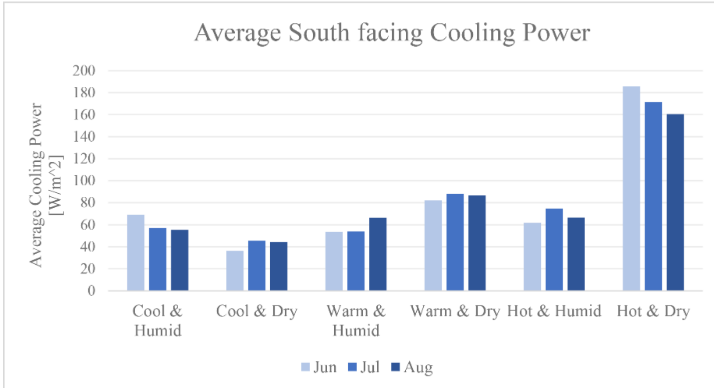

Figure 41. Average cooling power for south-facing green wall. Assumed variables: well-watered condition, LAI of 3, height of 3 m, average leaf resistance per climatic scenario, no wind condition.

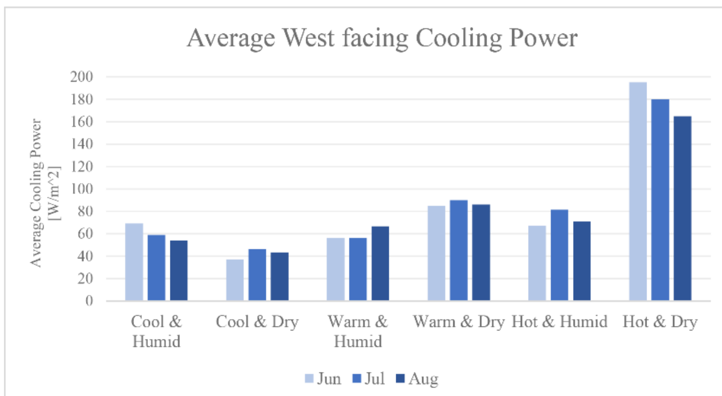

Figure 42. Average cooling power for west-facing green wall. Assumed variables: well-watered condition, LAI of 3, height of 3 m, average leaf resistance per climatic scenario, no wind condition.

Figure 41 and Figure 42 show bar graphs for the predicted average monthly cooling power values (W/m^2) for each climatic scenario for south- and west-facing green walls. As expected, the largest cooling power corresponds with the hot climate, followed by the warm climate and then the cold climate, controlling for humidity. For equivalent temperatures and except for cool climates, the cooling power produced in dry climates is larger than in humid climates. The reason for the deviation in the cool climates is the high average canopy resistance value of the associated vine.

As discussed in detail in Section 5.1, the transpiration rate is a function of plant biophysical traits as well as solar radiation and vapor pressure deficit (VPD), i.e., the drying power of the air. Therefore, it is not easy to decipher a one-to-one relationship between the transpiration rate and each variable.

For example, in cool and humid climates a south facing green wall receives the largest solar radiation during the month of August. However, the largest transpiration rate of the canopy corresponds with the month of June. That is because the daytime relative humidity in June is significantly lower (20%) than for the month of August.

The above conditions highlight the important role of the vapor pressure deficit of the air on the transpiration rate of a canopy. In hot and dry climates it is possible for the air to be significantly hotter and drier than the canopy. This provides an extra source of energy so that the "latent heat loss can significantly exceed any net radiative gain" (Jones, 1992). This phenomenon is called the Oasis Effect.

Therefore, in hot and dry climates, the influence of radiation is limited to its effect on air temperature and, consequently, on the VPD and the opening and closing of stomata (Yunusa et al., 2000). The Penman Monteith equation accounts for the Oasis Effect. This is most evident in the large predicted cooling power for the hot and dry climate (Table 16). To the best of my knowledge, no studies have quantified the cooling power or transpiration rate of green walls in these climates (latitudes 30° and below).

I. Yunusa et al. (2000) measured the transpiration rate of a 30-year old *Sultana* vine in Merbein, Australia at a latitude of 34° S during the summer months. Comparing field study measurements and the Penman Monteith equation, they found that the model perfectly predicted the transpiration rate trends but overestimated the values by 20%. It is important to note that the aerodynamic resistance term (accounting for the coupling of the canopy to its environment) used for my calculations is similar to that used by I. Yunusa et al. (2000).

The cooling power values reported for the hot and dry climate in Table 16 are not adjusted for the 20% overestimation of the Penman Monteith-based model. However, the final matrix in Section 6.3 provides adjusted estimated cooling power percentages.

Figure 41 and Figure 42 show that with the exception of the month of August in cool climates, the cooling power produced from the west-facing orientation is larger or equal to that produced from the south-facing orientation. This is because in these climates, the low-altitude August sun provides more solar radiation for the south-facing façade during the day. But the sun sets early, thus providing less sunlight for the west-facing façade.

Only one study has compared the transpiration cooling power produced from the south- and west-facing orientations. D. Tilley et al. (2012) found that at a latitude of 39° N, the average west-facing green wall transpired 10 W/m^2 (37%) more than did the south-facing green wall in the month of June.

For most climates, the most significant environmental variables impacting canopy transpiration are the incident solar radiation, VPD, and wind velocity (see Section 4.1). During an experimental period in July, Tilley et al. (2012) measured 65% more incident solar radiation on a west-facing green wall (174 W/m^2) than on a south-facing green wall (104 W/m^2).

For this study, simulated monthly average values were obtained from the 30-year weather files of New York City with a similar latitude of 40° N. Accordingly, the incident solar radiation at the west-facing façade is larger than south-facing facade by approximately 40%, 27%, and 1% for the months of June, July, and August, respectively. As a result, the west-facing green wall has a larger cooling power by 5%, 3%, and 0% for the months of June, July, and August, respectively.

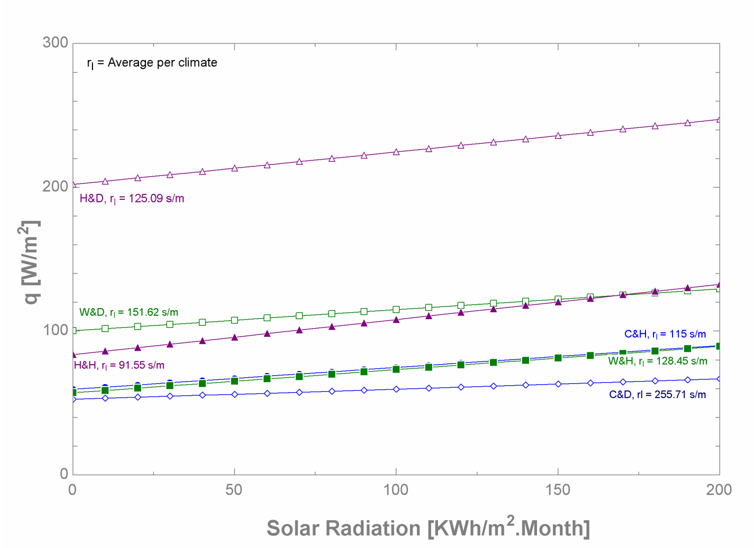

Figure 43. Transpiration cooling power of south-facing green walls as a function of average monthly solar radiation. Assumed variables: well-watered condition, LAI of 3, height of 3 m, average leaf resistance per climatic scenario (r_l m/s), no wind condition.

The linear relationship between transpiration cooling power and solar radiation is shown in Figure 43 for south-facing green walls for each climate. The slope of each line shows the rate of change of transpiration cooling power relative to that of the incident solar radiation. Accordingly, excepting the cool and dry climate, all climates with a latitude of 40° or above have rates of change between 12% and 15%. This explains the small variations between the values between the south- and west-facing orientations.

However, the slopes of the lines increase up to 25% in hot climates, at latitudes of 30° or below. In these climates, the cooling power produced from south-facing canopies is substantially lower than that produced from west-facing canopies.

Similar observations have been made in field studies investigating the impact of orientation on transpiration rates of vineyards. For latitudes of 40° or above, the transpiration rates of east-west oriented vineyards (analogous to south-facing green walls) are similar to those of north-south oriented ones (analogous to west-facing green walls), regardless of the maximum canopy height and inter-row spacing (Intrieri, Poni, Rebucci, & Magnanine, 1998; Lebon, Schultz, & Dumas, 1995; Magnanini & Intrieri, 1987). However, for latitudes close to and below 30°, it has been recommended to orient vineyards along the north-south axis (west-facing) to ensure a “higher seasonal light interception than east-west oriented rows” (Intrieri et al., 1998; R. E. Smart, 1973).

This trend is clearly shown in Table 16. For hot climates with latitudes of 32° and 25°, the difference in produced cooling power between the south- and west-facing orientations remains constant throughout the summer months. This is because the solar elevation continuously remains high throughout the summer. Therefore, “the diurnal’s sun’s path tends to be parallel to the canopy, losing much light directly to the ground especially during the midday hours” (Intrieri et al., 1998).

The cooling power values produced as a percentage of incident solar radiation, for each summer month, in each climate and for each orientation, are shown in Table 14 through Table 16. At a latitude of 50° N, Hoelscher et al. (2016) found the cooling power produced as a percentage of incident solar radiation ranged between 21.6% and 39.9%. These values are in good agreement with the predicted percentages for the corresponding cool and humid climates in Table 14.

At a latitude of 39° N, the cooling power values produced as a percentage of incident solar radiation were 30% and 42.5%, respectively (D. Tilley et al., 2012; H. Wang, 1999). These values are similar to those predicted by this research for the corresponding warm and humid climates (Table 15).

Finally, Figure 44 assumes a scenario where for all climates, the leaf resistance is 100 s/m. Compared to Figure 43, the graph shown in Figure 44 is more predictable and rationalized, so that the largest cooling power is associated with hot climates, followed by warm climates, and then cool climates.

Only a few studies have investigated the impact of plant biophysical traits on the cooling effect of green walls (Cameron et al., 2014; Koyama et al., 2015; Tilley et al., 2012). For this study, an average canopy resistance value was used for climate conditions as observed in field studies. However, it is important to note that plant selection may influence the expected cooling power. For example, T. Yoshinaga et al. (2015)

measured transpiration cooling power values ranging from 400 W/m^2 to 600 W/m^2 for a vigorous south-facing *Kudzu* vine, whereas D. Tilley et al. (2012) observed a value of 27 W/m^2 for a *Vitis* species.

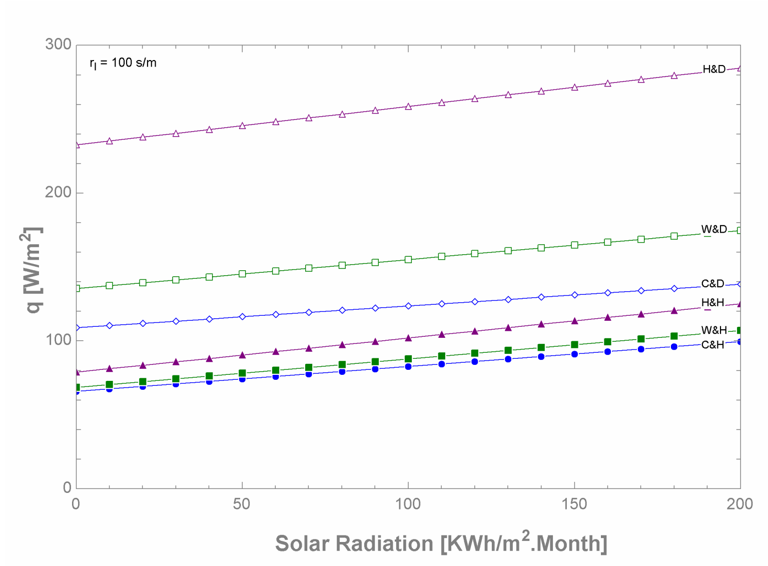

Figure 44. Transpiration cooling power of south-facing green walls as a function of average monthly solar radiation. Assumed variables: well-watered condition, LAI of 3, height of 3 m, leaf resistance of 100 s/m, no wind condition.

The average cooling power values (Table 14 to Table 16) can be used for back-of-the-envelope calculations. The final and simplified matrix in Section 6.3 will cover the average monthly cooling power values (W/m^2) for each climate as well as the percentage contribution of the canopy's transpiration to the total cooling effect of green walls.

6.2. Solar Interception Matrix—Heat Gain Reduction for Six Climate Scenarios

The predicted average heat gain reduction values (W/m^2 and %) for each summer month and for each climatic scenario are shown in Table 17 through Table 19. Each summer month has been broken down into south- and west-facing orientations and green wall designs with *LAI* values of 3, 4, and 5. The assumed extinction coefficient values, *k*, are noted for each month per climatic scenario. A detailed discussion of the *k* calculations can be found in Section 5.2.4. A detailed discussion of the trends of solar interception between various climates as they relate to summer month and latitude can be found in Section 5.2.

Note that the values in Table 17 through Table 19 represent idealized canopies with homogeneous and full coverage of the indicated *LAI* values for each unit area of canopy. In reality, however, the *LAI* varies continuously along the height of the canopy and during each summer month (Pérez et al., 2017; Schumann, 2007; Tilley et al., 2012). G. Preze et al. (2017) observed *LAI* values of 3.9, 3.2, and 2.1 for the lower, middle, and upper levels of an indirect green wall covered with *Boston ivy* in Lleida, Spain (latitude of 41° N).

Similar observations were made for an indirect green wall covered with *Virginia creeper* in Brighton, United Kingdom (latitude of 50° N) (Ip et al., 2010). In the same study, K. Ip et al. (2010) found that the shading effect of a green wall can be divided into three distinct periods (represented as a second order equation): growth phase, maximum growth phase, and leaf shedding phase. The maximum growth phase was associated with 5 leaf layers (months of August and early September). The other two phases were associated with 3 and 4 leaf layers. Note that Ip et al. (2010) evaluated the canopy density as number of leaf layers and not *LAI*.

A number of studies have demonstrated a positive correlation between *LAI* and a canopy's percentage of coverage and thickness (Schumann, 2007; Tilley et al., 2012). Every layer of *LAI* may reduce an exterior façade's temperature by 2 °C (Tilley et al., 2012).

Furthermore, *LAI* changes as canopies mature between growing seasons. D. Tilley et al. (2012) measured the *LAI* values of six vine species with four different training systems for two growing seasons in Maryland, United States (latitude of 39° N). They observed rapid growth for all the green walls in the first growing season, with similar *LAI* values ranging between 2.5 and 3.5 in the month of July. However, this range grew much larger, to approximately 1.5 to 6.5, by late August of the next growing season, with a mean *LAI* value of 4 in July.

A canopy becomes more homogeneous as a green wall matures (Pérez et al., 2017) and eventually its *LAI* value plateaus (Schumann, 2007). Most studies have observed *LAI* values of 3, 4, and 5 for both direct and indirect green walls (Hoelscher et al., 2016; Ip et al., 2010; Pérez et al., 2017; Tilley et al., 2012). Only a few studies have reported larger *LAI* values, such as 6.1, 7.2 (Šuklje et al., 2016), 7, and 8.51 (Wolter, Diebel, & Schroeder, 2008).

The values in Table 17 through Table 19 show reasonable agreement (5% to 10% margins of error) with the reported values from literature on the corresponding climates. Hoelscher et al. (2016) in Berlin, Germany (latitude of 52° N) in the months of August and early September observed 81.5% solar radiation interception for a west facing indirect green wall with an *LAI* value of 3. The predicted corresponding value from Table 17 shows a similar solar interception value of 80.21%.

Table 17. Solar radiation reduction (w/m^2 and %) for cool climates (latitude of 48°) for each summer month, for south- and west-facing orientations, and LAI values of 3, 4, and 5 (for a detailed discussion of the extinction coefficient, k, see Section 5.2.4)

Cool & Dry Climate (k Based on Latitude of 48°)

	June, K=0.49						July, K=0.5						August, , K=0.54					
	South Facing			West Facing			South Facing			West Facing			South Facing			West Facing		
Leaf Area Index	Initial Average Solar Gain [W/m^2]	Average Solar Radiation Reduction [W/m^2]	Average Solar Radiation Reduction [%]	Initial Average Solar Gain [W/m^2]	Average Solar Radiation Reduction [W/m^2]	Average Solar Radiation Reduction [%]	Initial Average Solar Gain [W/m^2]	Average Solar Radiation Reduction [W/m^2]	Average Solar Radiation Reduction [%]	Initial Average Solar Gain [W/m^2]	Average Solar Radiation Reduction [W/m^2]	Average Solar Radiation Reduction [%]	Initial Average Solar Gain [W/m^2]	Average Solar Radiation Reduction [W/m^2]	Average Solar Radiation Reduction [%]	Initial Average Solar Gain [W/m^2]	Average Solar Radiation Reduction [W/m^2]	Average Solar Radiation Reduction [%]
3	166.35	128.10	77.00	204.32	157.34	77.01	194.67	151.23	77.68	228.39	177.44	77.69	258.70	207.53	80.22	215.98	173.23	80.21
4	166.35	142.93	85.92	204.32	175.47	85.88	194.67	168.32	86.47	228.39	197.48	86.47	258.70	228.88	88.47	215.98	191.08	88.47
5	166.35	152.00	91.37	204.32	186.69	91.37	194.67	178.69	91.79	228.39	209.65	91.79	258.70	241.32	93.28	215.98	201.46	93.28

Cool & Humid Climate (k Based on Latitude of 48°)

	June, K=0.49						July, K=0.5						August, , K=0.54					
	South Facing			West Facing			South Facing			West Facing			South Facing			West Facing		
Leaf Area Index	Initial Average Solar Gain [W/m^2]	Average Solar Radiation Reduction [W/m^2]	Average Solar Radiation Reduction [%]	Initial Average Solar Gain [W/m^2]	Average Solar Radiation Reduction [W/m^2]	Average Solar Radiation Reduction [%]	Initial Average Solar Gain [W/m^2]	Average Solar Radiation Reduction [W/m^2]	Average Solar Radiation Reduction [%]	Initial Average Solar Gain [W/m^2]	Average Solar Radiation Reduction [W/m^2]	Average Solar Radiation Reduction [%]	Initial Average Solar Gain [W/m^2]	Average Solar Radiation Reduction [W/m^2]	Average Solar Radiation Reduction [%]	Initial Average Solar Gain [W/m^2]	Average Solar Radiation Reduction [W/m^2]	Average Solar Radiation Reduction [%]
3	144.97	112.60	77.67	185.98	143.21	77.00	169.15	131.42	77.69	200.89	156.06	77.68	218.31	175.10	80.21	189.60	152.08	80.21
4	144.97	124.54	85.91	185.98	159.79	85.92	169.15	146.27	86.47	200.89	173.71	86.47	218.31	193.12	88.46	189.60	167.73	88.47
5	144.97	132.07	91.10	185.98	169.93	91.37	169.15	155.26	91.79	200.89	184.40	91.79	218.31	203.63	93.28	189.60	172.10	90.77

Table 18. Solar radiation reduction (w/m^2) for warm climates (latitude of 40°) for each summer month, for south- and west-facing orientations, and LAI values of 3, 4, and 5 (for a detailed discussion of the extinction coefficient, k, see Section 5.2.4)

Warm & Dry Climate (k Based on Latitude of 40°)

	June, k=0.46						July k=0.47						August k=0.5					
	South Facing			West Facing			South Facing			West Facing			South Facing			West Facing		
Leaf Area Index	Initial Average Solar Gain [W/m^2]	Average Solar Radiation Reduction [W/m^2]	Average Solar Radiation Reduction [%]	Initial Average Solar Gain [W/m^2]	Average Solar Radiation Reduction [W/m^2]	Average Solar Radiation Reduction [%]	Initial Average Solar Gain [W/m^2]	Average Solar Radiation Reduction [W/m^2]	Average Solar Radiation Reduction [%]	Initial Average Solar Gain [W/m^2]	Average Solar Radiation Reduction [W/m^2]	Average Solar Radiation Reduction [%]	Initial Average Solar Gain [W/m^2]	Average Solar Radiation Reduction [W/m^2]	Average Solar Radiation Reduction [%]	Initial Average Solar Gain [W/m^2]	Average Solar Radiation Reduction [W/m^2]	Average Solar Radiation Reduction [%]
3	136.82	102.39	74.84	202.90	151.90	74.86	154.20	116.55	75.58	190.68	144.12	75.58	213.24	165.66	77.69	202.44	157.27	77.69
4	136.82	115.09	84.12	202.90	170.68	84.12	154.20	130.67	84.74	190.68	161.59	84.75	213.24	184.37	86.46	202.44	175.05	86.47
5	136.82	123.10	89.97	202.90	182.56	89.97	154.20	139.49	90.46	190.68	172.50	90.46	213.24	195.73	91.79	202.44	185.82	91.79

Warm & Humid Climate (k Based on Latitude of 40°)

	June, k=0.46						July k=0.47						August k=0.5					
	South Facing			West Facing			South Facing			West Facing			South Facing			West Facing		
Leaf Area Index	Initial Average Solar Gain [W/m^2]	Average Solar Radiation Reduction [W/m^2]	Average Solar Radiation Reduction [%]	Initial Average Solar Gain [W/m^2]	Average Solar Radiation Reduction [W/m^2]	Average Solar Radiation Reduction [%]	Initial Average Solar Gain [W/m^2]	Average Solar Radiation Reduction [W/m^2]	Average Solar Radiation Reduction [%]	Initial Average Solar Gain [W/m^2]	Average Solar Radiation Reduction [W/m^2]	Average Solar Radiation Reduction [%]	Initial Average Solar Gain [W/m^2]	Average Solar Radiation Reduction [W/m^2]	Average Solar Radiation Reduction [%]	Initial Average Solar Gain [W/m^2]	Average Solar Radiation Reduction [W/m^2]	Average Solar Radiation Reduction [%]
3	131.31	98.28	74.85	184.44	138.04	74.84	144.96	109.56	75.58	184.22	139.23	75.58	220.70	171.46	77.69	224.12	174.12	77.69
4	131.31	110.45	84.12	184.44	155.14	84.12	144.96	122.84	84.74	184.22	156.11	84.74	220.70	190.84	86.47	224.12	193.79	86.47
5	131.31	118.14	89.97	184.44	165.95	89.97	144.96	131.13	90.46	184.22	166.65	90.46	220.70	202.68	91.84	224.12	205.72	91.79

Table 19. Solar radiation reduction (w/m²) for hot climates (latitudes of 32° and 25°) for each summer month, for south- and west-facing orientations, and LAI values of 3, 4, and 5 (for a detailed discussion of the extinction coefficient, k, see Section 5.2.4)

Hot & Dry Climate (k Based on Latitude of 32°)																		
	June, k=0.44						**July, k=0.45**						**August, k=0.47**					
	South Facing			*West Facing*			*South Facing*			*West Facing*			*South Facing*			*West Facing*		
Leaf Area Index	Initial Average Solar Gain [W/m²]	Average Solar Radiation Reduction [W/m²]	Average Solar Radiation Reduction [%]	Initial Average Solar Gain [W/m²]	Average Solar Radiation Reduction [W/m²]	Average Solar Radiation Reduction [%]	Initial Average Solar Gain [W/m²]	Average Solar Radiation Reduction [W/m²]	Average Solar Radiation Reduction [%]	Initial Average Solar Gain [W/m²]	Average Solar Radiation Reduction [W/m²]	Average Solar Radiation Reduction [%]	Initial Average Solar Gain [W/m²]	Average Solar Radiation Reduction [W/m²]	Average Solar Radiation Reduction [%]	Initial Average Solar Gain [W/m²]	Average Solar Radiation Reduction [W/m²]	Average Solar Radiation Reduction [%]
3	110.23	80.79	73.29	254.30	186.37	73.29	129.78	96.14	74.08	241.10	178.60	74.08	200.00	151.17	75.59	270.61	204.54	75.59
4	110.23	91.26	82.80	254.30	210.56	82.80	129.78	108.33	83.47	241.10	201.24	83.47	200.00	169.48	84.74	270.61	229.31	84.74
5	110.23	98.01	88.92	254.30	226.13	88.92	129.78	116.10	89.46	241.10	215.68	89.46	200.00	180.93	90.46	270.61	244.81	90.47

Hot & Humid Climate (k Based on Latitude of 25°)																		
	June, k=0.43						**July, k=0.44**						**August, k=0.45**					
	South Facing			*West Facing*			*South Facing*			*West Facing*			*South Facing*			*West Facing*		
Leaf Area Index	Initial Average Solar Gain [W/m²]	Average Solar Radiation Reduction [W/m²]	Average Solar Radiation Reduction [%]	Initial Average Solar Gain [W/m²]	Average Solar Radiation Reduction [W/m²]	Average Solar Radiation Reduction [%]	Initial Average Solar Gain [W/m²]	Average Solar Radiation Reduction [W/m²]	Average Solar Radiation Reduction [%]	Initial Average Solar Gain [W/m²]	Average Solar Radiation Reduction [W/m²]	Average Solar Radiation Reduction [%]	Initial Average Solar Gain [W/m²]	Average Solar Radiation Reduction [W/m²]	Average Solar Radiation Reduction [%]	Initial Average Solar Gain [W/m²]	Average Solar Radiation Reduction [W/m²]	Average Solar Radiation Reduction [%]
3	85.89	62.24	72.47	155.77	112.89	72.47	100.59	73.72	73.29	185.60	136.04	73.30	139.30	103.18	74.08	195.94	145.15	74.08
4	85.89	70.51	82.09	155.77	127.89	82.10	100.59	83.29	82.79	185.60	153.67	82.80	139.30	116.27	83.47	195.94	163.55	83.47
5	85.89	75.88	88.35	155.77	137.63	88.35	100.59	89.45	88.92	185.60	165.04	88.92	139.30	124.61	89.46	195.94	175.28	89.46

In Lleida, Spain (latitude of 41° N), the reported summer average of solar interception of both south- and west-facing indirect green walls with mixed *LAI* values of 3.2 and 3.9 was 88% (Pérez et al., 2017). The predicted summer average value for south- and west-facing orientations with mixed *LAI* values shows 81% solar interception.

For a southeast-facing green wall in Maryland, United States (latitude of 39° N), Schumann (2007) measured solar radiation interception values of approximately 82% and 92% for *LAI* values of 3 and 5, respectively. The predicted values from Table 18 show approximately 6% and 2% overestimation for *LAI* values of 3 (75.59 % solar interception), and 5 (90.46% solar interception), respectively.

Although the percentages of solar interception for the south- and west-facing orientations are similar for all climates, the actual solar reduction value on the west-facing façade is greater. The difference in received radiation between the two orientations can range from 22% for a high latitude of 48°, to 80% for a low latitude of 25°. Therefore, the cooling effect from canopy shading is larger on the west-facing facade than the south-facing façade. This principle has been observed by other researchers at a latitude of 40° (Pérez et al., 2017; Tilley et al., 2012).

As is shown in Table 17 through Table 19, the cooling effect of a canopy's shading diminishes as *LAI* becomes larger than 5 for latitudes of 40° and above. This effect has been observed in field studies by both L. Schumann (2007) at a latitude of 40° and K. Ip et al. (2010) at a latitude of 50°. However, for latitudes of 30° and below, *LAI* values larger than 5 are recommended due to high incident solar radiation, especially for west-facing green walls.

The above findings show that the predicted values from Table 17 through Table 19 can be used to estimate average solar radiation interception with a ±10% margin of error. These values can be used for back-of-the-envelope calculations. Lastly, for more detailed calculations, it is recommended that designers consider *LAI* values of between 3 and 4 for the months of June and July, and an *LAI* value of 5 for the month of August, accounting for the growth patterns of the canopy (Ip et al., 2010).

6.3. A Simplified Matrix for Designers

Table 20 through Table 22 show the percentages of cooling power contributed by both solar interception reduction (shading) and transpiration for each summer month, for six climates, and for south- and west-facing orientations. These percentages are given relative to the total incident solar radiation received by the canopy. Note that the transpiration percentages for the hot and dry climate correspond with a 20% reduction from the values reported in Table 16, thus accounting for the overestimation of the Penman-Monteith model for this climate (Yunusa et al., 2000). (See section 6.1 for a detailed discussion.)

Detailed analyses of the cooling power produced from transpiration and shading were provided in Sections 6.1 and 6.2. The tables in those sections contain the actual cooling power values (W/m^2) for each canopy design for all climates and summer months. Those values can be used for simple back-of-the-envelope calculations.

Table 20. Percentage of cooling power from the transpiration and shading effects of various LAIs (3, 4, and 5) of south- and west-facing green walls for cool climates. Assumed variables: height of 3 m, average canopy resistance, no wind condition.

	Cool & Dry Climate											
	June				**July**				**August**			
	South Facing		*West Facing*		*South Facing*		*West Facing*		*South Facing*		*West Facing*	
Leaf Area Index	Average Transpiration Cooling Power Production [%]	Average Solar Radiation Reduction [%]	Average Transpiration Cooling Power Production [%]	Average Solar Radiation Reduction [%]	Average Transpiration Cooling Power Production [%]	Average Solar Radiation Reduction [%]	Average Transpiration Cooling Power Production [%]	Average Solar Radiation Reduction [%]	Average Transpiration Cooling Power Production [%]	Average Solar Radiation Reduction [%]	Average Transpiration Cooling Power Production [%]	Average Solar Radiation Reduction [%]
3		77.00		77.01		77.68		77.69		80.22		80.21
4	21.87	85.92	18.21	85.88	23.36	86.47	20.28	86.47	25.39	88.47	28.55	88.47
5		91.37		91.37		91.79		91.79		93.28		93.28

	Cool & Humid Climate											
	June				**July**				**August**			
	South Facing		*West Facing*		*South Facing*		*West Facing*		*South Facing*		*West Facing*	
Leaf Area Index	Average Transpiration Cooling Power Production [%]	Average Solar Radiation Reduction [%]	Average Transpiration Cooling Power Production [%]	Average Solar Radiation Reduction [%]	Average Transpiration Cooling Power Production [%]	Average Solar Radiation Reduction [%]	Average Transpiration Cooling Power Production [%]	Average Solar Radiation Reduction [%]	Average Transpiration Cooling Power Production [%]	Average Solar Radiation Reduction [%]	Average Transpiration Cooling Power Production [%]	Average Solar Radiation Reduction [%]
3		77.67		77.00		77.69		77.68		80.21		80.21
4	47.72	85.91	37.20	85.92	33.79	86.47	29.34	86.47	25.39	88.46	28.55	88.47
5		91.10		91.37		91.79		91.79		93.28		90.77

Table 21. Percentage of cooling power from the transpiration and shading effects of various LAIs (3, 4, and 5) of south-and west-facing green walls for warm climates. Assumed variables: height of 3 m, average canopy resistance, no wind condition.

	Warm & Dry Climate											
	June				**July**				**August**			
	South Facing		*West Facing*		*South Facing*		*West Facing*		*South Facing*		*West Facing*	
Leaf Area Index	Average Transpiration Cooling Power Production [%]	Average Solar Radiation Reduction [%]	Average Transpiration Cooling Power Production [%]	Average Solar Radiation Reduction [%]	Average Transpiration Cooling Power Production [%]	Average Solar Radiation Reduction [%]	Average Transpiration Cooling Power Production [%]	Average Solar Radiation Reduction [%]	Average Transpiration Cooling Power Production [%]	Average Solar Radiation Reduction [%]	Average Transpiration Cooling Power Production [%]	Average Solar Radiation Reduction [%]
3		74.84		74.86		75.58		75.58		77.69		77.69
4	60.05	84.12	41.87	84.12	60.76	84.74	48.86	84.75	39.26	86.46	38.44	86.47
5		89.97		89.97		90.46		90.46		91.79		91.79

	Warm & Humid Climate											
	June				**July**				**August**			
	South Facing		*West Facing*		*South Facing*		*West Facing*		*South Facing*		*West Facing*	
Leaf Area Index	Average Transpiration Cooling Power Production [%]	Average Solar Radiation Reduction [%]	Average Transpiration Cooling Power Production [%]	Average Solar Radiation Reduction [%]	Average Transpiration Cooling Power Production [%]	Average Solar Radiation Reduction [%]	Average Transpiration Cooling Power Production [%]	Average Solar Radiation Reduction [%]	Average Transpiration Cooling Power Production [%]	Average Solar Radiation Reduction [%]	Average Transpiration Cooling Power Production [%]	Average Solar Radiation Reduction [%]
3		74.85		74.84		75.58		75.58		77.69		77.69
4	40.79	84.12	30.44	84.12	37.20	84.74	30.48	84.74	30.10	86.47	29.72	86.47
5		89.97		89.97		90.46		90.46		91.84		91.79

Table 22. Percentage of cooling power from the transpiration and shading effects of various LAIs (3, 4, and 5) of south- and west-facing green walls for hot climates. Assumed variables: height of 3 m, average canopy resistance, no wind condition.

Hot & Dry Climate												
	June				**July**				**August**			
	South Facing		*West Facing*		*South Facing*		*West Facing*		*South Facing*		*West Facing*	
Leaf Area Index	Average Transpiration Cooling Power Production [%]	Average Solar Radiation Reduction [%]	Average Transpiration Cooling Power Production [%]	Average Solar Radiation Reduction [%]	Average Transpiration Cooling Power Production [%]	Average Solar Radiation Reduction [%]	Average Transpiration Cooling Power Production [%]	Average Solar Radiation Reduction [%]	Average Transpiration Cooling Power Production [%]	Average Solar Radiation Reduction [%]	Average Transpiration Cooling Power Production [%]	Average Solar Radiation Reduction [%]
3		73.29		73.29		74.08		74.08		75.59		75.59
4	134.82	82.80	61.41	82.80	105.73	83.47	59.70	83.47	64.22	84.74	48.77	84.74
5		88.92		88.92		89.46		89.46		90.46		90.47

Hot & Humid Climate												
	June				**July**				**August**			
	South Facing		*West Facing*		*South Facing*		*West Facing*		*South Facing*		*West Facing*	
Leaf Area Index	Average Transpiration Cooling Power Production [%]	Average Solar Radiation Reduction [%]	Average Transpiration Cooling Power Production [%]	Average Solar Radiation Reduction [%]	Average Transpiration Cooling Power Production [%]	Average Solar Radiation Reduction [%]	Average Transpiration Cooling Power Production [%]	Average Solar Radiation Reduction [%]	Average Transpiration Cooling Power Production [%]	Average Solar Radiation Reduction [%]	Average Transpiration Cooling Power Production [%]	Average Solar Radiation Reduction [%]
3		72.47		72.47		73.29		73.30		74.08		74.08
4	71.85	82.09	43.14	82.10	74.40	82.79	43.92	82.80	47.72	83.47	36.13	83.47
5		88.35		88.35		88.92		88.92		89.46		89.46

Table 20 through Table 22 provide a fast and simple method for designers to evaluate the efficacy of various green wall designs as a passive strategy for the climate corresponding with their project.

It is important to note that the reported percentages shown in the tables above can be misleading for performance comparisons between climates and orientations. For example, in July, for the warm and dry, and warm and humid, climates, an LAI of 4 corresponds with an approximately 84% solar radiation reduction for both south- and west-facing green walls.

However, when the actual values (W/m^2) for the two climates are compared, the cooling power from solar radiation reduction for the warm and dry climate is larger than that for the warm and humid climate. This is because the initial incident solar radiation value for the warm and dry climate is larger than for the warm and humid climate. Also, despite similar solar radiation reduction percentage values (84%) for the two orientations, for both climates the west-facing green wall provides greater solar radiation reduction than does the south-facing green wall.

Similarly, the percentage values for transpiration cooling power production can be misleading. For example, in July, in the warm and dry climate for canopies with an LAI of 4, the percentage of transpiration cooling power produced relative to solar radiation gain for the south-facing green wall is larger than that for the west-facing one (e.g., 61% for west- vs. 49% for south-facing green wall). However, the actual value of the cooling power (W/m^2) from the transpiration of the west-facing canopy is larger than that of the south-facing canopy (e.g., 184 W/m^2 for west- vs. 145 W/m^2 for south-facing green wall).

This is due to the slow rate (the shallow slope) of the linear relationship between the transpiration rate and solar radiation, which was discussed in Section 6.1. The difference between the transpiration of the west- and south-facing façades is minor compared to the amount of incident solar radiation. Therefore, it is advisable to further contextualize the percentages of cooling power from each category by looking up the actual cooling power values (W/m^2) from the tables in Sections 6.1 and 6.2.

This chapter provides designers with a series of tables to quickly and easily evaluate cooling effects from the transpiration and shading of various green wall designs as a percentage of the total incident solar radiation. This method provides an advantage for the early phase of a design project, where internal loads, thermal and spectral properties of the façade, and other variables are either unknown or still evolving.

A summary of the most important findings is as follows:

- To account for the monthly variations in LAI during the summer months, it is recommended to consider LAI values of between 3 and 4 for the months of June and July, and an LAI value of 5 for the month of August.
- For maximizing solar interception at latitudes of 40° and above LAI of 5 is recommended. For latitudes of 30° LAI and below larger than 5 is recommended.
- For maximizing transpiration cooling power canopies with LAI of 3 and larger, green wall height between 3 to 6 m, and vine species with stomatal resistance of 100 s/m or smaller is recommended.

- The impact of orientation (south- vs. west-facing) on canopy transpiration rates is limited at latitudes of 40° and above. However, for latitudes of 30° and below, the west-facing orientation has a more significant effect on transpiration rates. More research on this topic is required, as only one study has investigated the impact of orientation on the transpiration rates of green walls.

- Excepting the cool and dry climate, the percentage of transpiration cooling power from the dry climates is larger than that from the humid climates. The deviation of the cool and dry climate is due to the low transpiration rate of the associated vine species.

Note that the reported cooling performances assume idealized canopy geometries (e.g. full coverage and homogenous canopies) and well-water and optimal nutrient conditions. The last two variables are crucial for both performance and development of canopies.

7. Contributions and Discussion

The main goal of this dissertation is to close the gap between the worlds of academic research and practice. A series of matrices is introduced to provide designers with a simple and quick method for evaluating the cooling efficacy of a green wall as a passive design strategy during the early phase of a project.

These matrices provide designers with the estimated cooling from solar radiation reduction (shading) and transpiration as a percentage of total incident solar radiation for six climatic scenarios. Additionally, the expected cooling power values (W/m^2) achieved from canopy shading and transpiration are provided for several designs.

The results show that cooling power from transpiration accounts for 20% to 30% of the cooling effect of green walls for cool and dry climates, cool and humid climates, and warm and humid climates. The contribution from transpiration increases to 48% for warm and dry climates and 52% for hot and humid climates. The largest cooling effect from transpiration is associated with the hot and dry climate (99%) due to the oasis effect. Excepting sites in low latitudes, the cooling effect of solar radiation interception is approximately 70%, 80% and 90% for *LAI* values of 3, 4, and 5, respectively.

The chapters on Cooling from Canopy Transpiration and Cooling from Canopy Solar Interception provide a detailed discussion of the variables impacting each cooling mechanism.

In the section Cooling from Canopy Transpiration, a leaf resistance library for vine species for six climate conditions was introduced. A design investigation into how to achieve maximum cooling power from canopy transpiration was conducted for each climate. The results show that canopies with resistances lower than 100 s/m, heights of 3 m to 6 m, and *LAI* values of 3 or larger produce maximum cooling power. With the mentioned geometry design considerations and average stomatal resistances, it is estimated that the largest (300 W/m^2) and smallest (50 W/m^2) cooling powers corresponded with the hot and dry climate and the cool and dry climate, respectively.

In the section Cooling from Canopy Solar Interception, a technique was introduced for estimating extinction coefficient values, *k*, by combing empirical and statistical methods. The resultant solar interception calculations showed good agreement with field study measurements, with only ±10% margins of error. The results showed that—assuming vertical declination and random azimuth leaf angles—the largest cooling from shading by south-facing green walls occurs in locations with high latitudes, followed by mid latitudes and then low latitudes.

7.1. Areas for Further Investigations

This dissertation reveals several research gaps within the field of green wall design. First, although a wealth of information is available on ecology, plant morphology, and urban vine botany, there have been limited studies into the biophysical traits of urban vines, such as leaf and canopy resistance. Much of the information on vines consulted for this research came from studies of grapevines. Although these studies were adequate for this research, more detailed investigations into the biophysical traits of urban vines is required.

Second, further studies involving different climates, latitudes, and longer experimental periods are required to examine the impact of orientation on the transpiration rate of green walls. In contrast to the few other studies that have investigated the impact of orientation on green walls, this study shows that the impact of orientation on the transpiration of green walls is pronounced only for climates at latitudes of 30° or below.

Third, only a few researchers have considered—and even fewer have evaluated—the extinction coefficient, *k*, of green walls. As was highlighted in Chapter 5.2, the extinction coefficient is a function of leaf inclination and azimuth angles, solar altitude, and design of the training system. Quantifying *k* for various species, geographical locations, and design systems will improve the replicability of results and experiments.

Fourth, there have currently only been limited studies of the integrated design of green walls. In most studies, the cooling power produced from the transpiration of green walls has only been evaluated for its contribution to the reduction of heat flow into the building façade. This approach fails to fully account for the available free cooling power. One method of integrated design is to reimagine green walls as evaporative porous surfaces coupled with the natural ventilation of buildings to directly address cooling loads (Yazdanseta & Norford, 2017).

Ultimately, integrated design solutions provide a stronger incentive for practitioners, developers, and policy makers to push for and invest in green urban infrastructure.

7.2. Instructions for Use of Matrices

This section provides instructions for use of the matrices in Chapter 6. The Appendix section includes the early-phase design tool, which is comprised of a design steps flow chart, instructions, a case study as an example, and the matrices. The early-phase design tool is intended to further simplify the process by enabling practitioners to easily follow each design step without the need to refer to the manuscript.

A designer consulting the matrices should follow six simple steps:

1. Look up the latitude of your project, the average maximum temperature during the summer months (°C), and either the average minimum relative humidity range during the summer months (%) or the average precipitation during the summer months (mm).
2. Identify the climate category of your project using Table 1. For details on climatic scenarios and corresponding latitudes, see Table 5.
3. For the seasonal cooling performance for the south- and west-facing green walls, look up the percentage cooling power values from solar radiation reduction of green walls with LAI values of 4 for the month of July. Calculate the summer average percentage of transpiration cooling power production for the two orientations using Table 20 through Table 22.

   Note that these percentages are relative to the average monthly incident solar radiation at the site. Therefore, if the initial average monthly solar radiation gains at the south- and west-facing facades are known, you can further refine your estimation by considering the site specific values.
4. To compare the seasonal shading performance of the two orientations, look up the actual cooling power values for green walls with LAI values of 4 for the month July using Table 17 through Table 19. Similarly, compare the transpiration cooling power of the two orientations produced seasonally by calculating the average summer cooling power using Table 14 through Table 16.

5. For monthly performance evaluations, look up the average monthly contributions to cooling power, in percentage terms, from transpiration and solar radiation reduction for south- and west-facing orientations using Table 20 through Table 22. Note that these percentages are relative to the average monthly incident solar radiation at the site.

   While the percentages of cooling power from transpiration are similar for green walls with *LAI* values of 3, 4, and 5, the percentages of solar radiation reduction vary for each *LAI* value. It is recommended to assume *LAI* values of 3, 4, and 5 for the months of June, July, and August, respectively. For a conservative estimate of cooling power from solar radiation reduction, assume an *LAI* value of 4 for the months of July and August.

6. Use Table 17 through Table 19 to look up the cooling power values in W/m^2 from transpiration cooling and solar radiation reduction for the south- and west-facing orientations. These values are useful as simple back-of-the-envelope calculations to get a general understanding of the expected cooling effect of the canopy in the climate of your project.

7.2.1. A Case Study – Seasonal Cooling Performance Evaluation

As a case study, let's consider a project located in Boston, MA. First, look up the latitude and monthly summer climate conditions. The table below shows the values obtained from Climate Consultant, taken at Logan Airport in Boston, MA.

Table 23. Boston, MA summer months climate conditions.

Boston – Latitude. 42° N	June	July	August
Avg. Max. Temp. (°C)	32	35.5	31
Avg. Min. Relative Humidity (%)	59	55	60
Avg. Precipitation (mm)	93	87	85

Comparing the Boston's average maximum temperatures and average precipitation for the summer months with the climate categories listed in the Table 1, we see that the warm and humid climate scenario best represents the climatic condition of this project.

Let's assume we are interested in evaluating and comparing the seasonal cooling performances of south- and west-facing green walls for maximum cooling effect.

Use Table 18 and look up the seasonal percentage of cooling from solar radiation reduction for the two orientations by assuming that the green walls have LAI values of 4 of July. Calculate the percentage of the seasonal transpiration cooling power for the two orientations by taking the average of the monthly performances. The results show that the seasonal transpiration cooling power percentages for the south- and west-facing green walls are 36% and 30%, respectively.

At the first glance, it seems that the seasonal cooling performance of the south- is slightly better than that of the west-facing green wall. That is because both orientations provide similar percentages of solar radiation reduction (85%). However, the south provides 6% more cooling power compared to west-facing green wall.

The cooling power percentage values are very useful when solar radiation gains are known. Tools such as Climate Consultant, Diva for Rhino, and Ladybug can be used to obtain the initial solar radiation gains at the south- and west-facing facades.

However, for this example, let's assume that the initial solar radiation values for the south- and west-facades are not available. Use Table 15 and Table 18 to further evaluate and compare the performances of the two orientations based on actual cooling power values (W/m^2).

The cooling from the solar radiation reduction of the south- and west-facing green walls with LAI values of 4 in July are 123 W/m^2 and 156 W/m^2, respectively. Accordingly, the west provides 23% more solar radiation reduction compared to south-facing green wall.

Comparing the average seasonal transpiration cooling power (calculated from the average of monthly values) shows minimal performance difference (approximately 2%) between the two orientations.

The above investigation shows that for a project in Boston, a west-facing green wall can provide greater average seasonal cooling power compared to a south-facing one. The expected seasonal cooling power values from the solar radiation reduction and transpiration cooling power production for the west-facing green wall are 156 W/m^2 and 59 W/m^2, respectively.

In addition to evaluating and comparing the performances of the two orientations, practitioners can use this method to optimize for each cooling method. For example, if the goal is to produce the largest cooling power, either orientation is a valid choice. This is especially significant for integrated design investigations where the objective is to utilize the produced cooling power to directly address the cooling loads of the buildings.

Furthermore, the above evaluations can be used for energy modeling purposes. For example, by modeling the canopy as a plane with 15% porosity, the energy savings from the shading of the canopy can be estimated.

7.2.2. A Case Study – Monthly Cooling Performance Evaluation

For a more detailed performance evaluation of the mentioned Boston Project, conduct monthly studies for the south- and west-facing green walls.

Use Table 21 to look up the monthly percentages of cooling power from solar radiation reduction and transpiration cooling power production. To account for the changes in canopy geometry and its impact on solar radiation interception, use the percentage values for LAI values of 3 for June, 4 for July, and 5 for August. Note that for the monthly transpiration cooling power a single value is considered for various LAIs.

Accordingly, the percentages of solar radiation reduction for the two ordinations are identical throughout the summer months: 75% in June, 85% in July, and 92% in August. These percentage values can be used for the monthly thermal and daylight design performance evaluations. For example, by modeling planes with 25%, 15%, and 8% porosity (with randomly arranged openings) representing each summer month, the thermal and daylight impacts of green walls can be easily simulated.

The percentage of transpiration cooling power relative to solar radiation gains of the south-facing green wall is larger by 18% in June and 19% in July compared to the west-facing green wall. This indicates that the south-facing green wall is more efficient in converting solar radiation into cooling power. Interestingly, in August, the performances of the two ordinations are almost identical due to the reduction of solar elevation in that month.

Similar to the previous example, let's assume that the initial solar radiation received by the south- and west-facing facades is unknown. Use Table 18 to look up the solar radiation reduction cooling power values for each summer month.

In June and July, the west-facing green wall provides 41% (LAI of 3) and 27% (LAI of 4) more cooling power than does the the south-facing one. However, in August (LAI of 5), the performance difference between the two orientations is diminished.

Conventionally, as part of standard sustainable design considerations, it is recommended to avoid west-facing windows due to excess solar heat gains and glare problems during summer months. The above investigations illustrate that green walls can address these concerns by obstructing up to 92% of solar radiation gains. The early-design matrices allow practitioners to easily and confidently estimate the performance of their design.

Use Table 15 to look up the transpiration cooling power values (W/m^2) for the south- and west-facing green walls. The table shows that the monthly cooling power produced from the two orientations is similar throughout the summer. These cooling power values can be used as a good estimate for the cooling performances of green walls as integrated design options.

The design implication of the above findings is that a west-facing green wall provides the largest cooling from solar radiation reduction. However, to maximize the transpiration cooling power production, either orientation is a valid choice.

Below are lists of assumptions and limitations of the matrices:

Assumptions:

- Vertical declination and random azimuth leaf angles (See Section 5.2.4)
- Uniform canopy *LAI* distribution
- Well-watered canopy conditions (See Section 5.1.1)
- Average bulk stomatal resistance (See section 5.1.3)
- No wind condition (See Section 5.1.2.3.1 and 5.1.6)
- 3 m canopy height (See Section 5.1.6)

Limitations:

- The values represent open field conditions where a green wall is exposed to sunlight throughout the day.
- The matrices assume a uniform and full distribution of the canopy along the building façade. Depending on the vine species and trellis system design, it can take up to two growing seasons to see full results.
- The predicted values represent monthly averages. This scale of resolution is only appropriate for the early-design phase of a project. However, Chapter 5 explains how to model each cooling effect. These models can be used to perform more detailed analyses.

References

Akbari, H., Kurn, D. M., Bretz, S. E., & Hanford, J. W. (1997). Peak power and cooling energy savings of shade trees. *Energy and Buildings, 25*(2), 139-148. doi:http://dx.doi.org.ezp-prod1.hul.harvard.edu/10.1016/S0378-7788(96)01003-1

Alexandri, E., & Jones, P. (2008). Temperature decreases in an urban canyon due to green walls and green roofs in diverse climates. *Building and Environment, 43*(4), 480-493. doi:10.1016/j.buildenv.2006.10.055

Allen, R. G., Pereira, L. S., Raes, D., & Smith, M. (1998). Crop evaporation–Guidelines for computing crop water requirements–FAO irrigation and drainage paper 56. *Food and Agriculture Organization of the United Nations, Rome,*

Allen, R., & Walter, I. (2003). In Allen R., Clemmens A.(Eds.), *The ASCE standardized reference evapotranspiration equation*

American Society of, L. A. (1984). *Energy-conserving site design*. Washington, D.C.: American Society of Landscape Architects.

Antonyová, A., Antony, P., & Korjenic, A. (2017). Evaluation the hygrothermal effects of integration the vegetation into the building envelope. *Energy and Buildings, 136*, 121-138.

Barker, M. G., & Pérez-Salicrup, D. (2000). Comparative water relations of mature mahogany (swietenia macrophylla) trees with and without lianas in a subhumid, seasonally dry forest in bolivia. *Tree Physiology, 20*(17), 1167-1174.

Bell, D., Forseth, I., & Teramura, A. (1988). Field water relations of three temperate vines. *Oecologia, 74*(4), 537-545.

Bindi, M., Miglietta, F., Gozzini, B., Orlandini, S., & Seghi, L. (1997). A simple model for simulation of growth and development in grapevine (vitis vinifera L.). II. model validation. *Vitis-Geilweilerhof-, 36*, 73-76.

Bolton, C., Rahman, M., Armson, D., & Ennos, A. (2014). Effectiveness of an ivy covering at insulating a building against the cold in manchester, UK: A preliminary investigation. *Building and Environment,*

BOTA, B. J., Flexas, J., & Medrano, H. (2001). Genetic variability of photosynthesis and water use in balearic grapevine cultivars. *Annals of Applied Biology, 138*(3), 353-361.

Braun, P., & Schmid, J. (1999). Sap flow measurements in grapevines (vitis vinifera L.) 2. granier measurements. *Plant and Soil, 215*(1), 47-55.

Brown, G. Z. (2014). In DeKay M. (Ed.), *Sun, wind, and light: Architectural design strategies* (Third [edition]. ed.) Wiley.

Buccola, N., & Spolek, G. (2011). A pilot-scale evaluation of greenroof runoff retention, detention, and quality. *Water, Air, & Soil Pollution, 216*(1), 83-92. doi:10.1007/s11270-010-0516-8

Bucks, D., Erie, L., NAKAVAMA, F., & French, O. (1974). Trickle irrigation management for grapes.

Cameron, R. W., Taylor, J. E., & Emmett, M. R. (2014). What's ‘cool’in the world of green façades? how plant choice influences the cooling properties of green walls. *Building and Environment, 73*, 198-207.

Carter, G. A., & Teramura, A. H. (1988). Vine photosynthesis and relationships to climbing mechanics in a forest understory. *American Journal of Botany,* , 1011-1018.

Cavallo, P., Poni, S., & Rotundo, A. (2001). Ecophysiology and vine performance of cv.“Aglianico” under various training systems. *Scientia Horticulturae, 87*(1), 21-32.

Chaves, M. M., Harley, P. C., Tenhunen, J. D., & Lange, O. L. (1987). Gas exchange studies in two portuguese grapevine cultivars. *Physiologia Plantarum, 70*(4), 639-647.

Coma, J., Pérez, G., de Gracia, A., Burés, S., Urrestarazu, M., & Cabeza, L. F. (2017). Vertical greenery systems for energy savings in buildings: A comparative study between green walls and green facades. *Building and Environment, 111*, 228-237.

Correia, M., Pereira, J., Chaves, M., Rodrigues, M., & Pacheco, C. (1995). ABA xylem concentrations determine maximum daily leaf conductance of field-grown vitis vinifera L. plants. *Plant, Cell & Environment, 18*(5), 511-521.

Cox, J. (2015). *From vines to wines: The complete guide to growing grapes and making your own wine* Storey Publishing.

Cuevas, E., Baeza, P., & Lissarrague, J. (2006). Variation in stomatal behaviour and gas exchange between mid-morning and mid-afternoon of north–south oriented grapevines (vitis vinifera L. cv. tempranillo) at different levels of soil water availability. *Scientia Horticulturae, 108*(2), 173-180.

Darwin, C. (1865). On the movements and habits of climbing plants. *Journal of the Linnean Society of London, Botany, 9*(33-34), 1-118.

Darwin, C. (1888). *The movements and habits of climbing plants* J. Murray.

Davis, M. M., & Hirmer, S. (2015). The potential for vertical gardens as evaporative coolers: An adaptation of the ‘ penman monteith equation’. *Building and Environment, 92*, 135-141. doi:10.1016/j.buildenv.2015.03.033

Dixon, M., & Grace, J. (1984). Effect of wind on the transpiration of young trees. *Annals of Botany, 53*(6), 811-819.

Downton, W., Grant, W., & Loveys, B. (1987). Diurnal changes in the photosynthesis of field-grown grape vines. *New Phytologist, 105*(1), 71-80.

Dragoni, D., Lakso, A. N., Piccioni, R. M., & Tarara, J. M. (2006). Transpiration of grapevines in the humid northeastern united states. *American Journal of Enology and Viticulture, 57*(4), 460-467.

Drake, B. G., Raschke, K., & Salisbury, F. B. (1970). Temperature and transpiration resistances of xanthium leaves as affected by air temperature, humidity, and wind speed. *Plant Physiology, 46*(2), 324-330.

Eastham, J., & Gray, S. A. (1998). A preliminary evaluation of the suitability of sap flow sensors for use in scheduling vineyard irrigation. *American Journal of Enology and Viticulture, 49*(2), 171-176.

Edwards, W., & Warwick, N. (1984). Transpiration from a kiwifruit vine as estimated by the heat pulse technique and the penman-monteith equation. *New Zealand Journal of Agricultural Research, 27*(4), 537-543.

Erie, L., French, O. F., & Harris, K. (1965). Consumptive use of water by crops in arizona.

Erwin Elsner. (2014). *Wine grape training systems*. http://msue.anr.msu.edu/uploads/234/43701/Elsner.Training_Systems.pdf: Michigan State University.

Escalona, J. M., Flexas, J., & Medrano, H. (2000). Stomatal and non-stomatal limitations of photosynthesis under water stress in field-grown grapevines. *Functional Plant Biology, 27*(1), 87-87.

Eumorfopoulou, E. A., & Kontoleon, K. J. (2009). Experimental approach to the contribution of plant-covered walls to the thermal behaviour of building envelopes. *Building and Environment, 44*(5), 1024-1038. doi:10.1016/j.buildenv.2008.07.004

Evans, R., Spayd, S., Wample, R., Kroeger, M., & Mahan, M. (1993). Water use of vitis vinifera grapes in washington. *Agricultural Water Management, 23*(2), 109-124.

Fichtner, K., & Schulze, E. (1990). Xylem water flow in tropical vines as measured by a steady state heating method. *Oecologia, 82*(3), 355-361.

Forseth, I., & Teramura, A. (1987). Field photosynthesis, microclimate and water relations of an exotic temperate liana, pueraria lobata, kudzu. *Oecologia, 71*(2), 262-267.

Forseth, I. N., & Teramura, A. H. (1986). Kudzu leaf energy budget and calculated transpiration: The influence of leaflet orientation. *Ecology, 67*(2), 564-571.

Fuentes, S., Palmer, A. R., Taylor, D., Zeppel, M., Whitley, R., & Eamus, D. (2008). An automated procedure for estimating the leaf area index (LAI) of woodland ecosystems using digital imagery, MATLAB programming and its application to an examination of the relationship between remotely sensed and field measurements of LAI. *Functional Plant Biology, 35*(10), 1070-1079.

Gates, D. M. (1980). *Biophysical ecology*. New York: Springer-Verlag.

Graaf, R., & Ende, J. (1981). *Transpiration and evapotranspiration of the glasshouse crops*. In *III International Symposium on Water supply and Irrigation in the open and under Protected Cultivation 119* (pp. 147-158).

Grace, J. (. (1977). *Plant response to wind*. London ; New York: Academic Press.

Grant, O. M., Tronina, L., Jones, H. G., & Chaves, M. M. (2007). Exploring thermal imaging variables for the detection of stress responses in grapevine under different irrigation regimes. *Journal of Experimental Botany, 58*(4), 815-825. doi:erl153 [pii]

Green Roofs for Healthy Cities. (2008). *Introduction to green walls technology, benefits & design.* (). http://www.greenscreen.com/home.html: Green screens.

Green Screen. (2012). *Considerations for advanced green facade design.* (). http://www.greenscreen.com/home.html: Green screen.

Hacker, J. N., & Holmes, M. J. (2007). Thermal comfort: Climate change and the environmental design of buildings in the united kingdom. *Built Environment (1978-),* , 97-114.

Hoelscher, M., Nehls, T., Jänicke, B., & Wessolek, G. (2016). Quantifying cooling effects of facade greening: Shading, transpiration and insulation. *Energy and Buildings, 114*, 283-290.

Holm, D. (1989). Thermal improvement by means of leaf cover on external walls - a simulation-model. *Energy and Buildings; Energy Build., 14*(1), 19-30.

Hoyano, A. (1988). Climatological uses of plants for solar control and the effects on the thermal environment of a building. *Energy & Buildings, 11*(1), 181-199. doi:10.1016/0378-7788(88)90035-7

Huang, Y., Akbari, H., Taha, H., & Rosenfeld, A. H. (1987). The potential of vegetation in reducing summer cooling loads in residential buildings. *Journal of Climate and Applied Meteorology, 26*(9), 1103-1116.

Hunter, A. M., Williams, N. S. G., Rayner, J. P., Aye, L., Hes, D., & Livesley, S. J. (2014). Quantifying the thermal performance of green façades: A critical review. *Ecological Engineering, 63*, 102-113. doi:10.1016/j.ecoleng.2013.12.021

Iandolino, A., Pearcy, R., & Williams, L. (2013). Simulating three-dimensional grapevine canopies and modelling their light interception characteristics. *Australian Journal of Grape and Wine Research, 19*(3), 388-400.

Intrieri, C., Poni, S., Rebucci, B., & Magnanine, E. (1998). Row orientation effects on whole-canopy gas exchange of potted and field-grown grapevines. *Vitis-Geilweilerhof-, 37*, 147-154.

Intrigliolo, D., Lakso, A., & Piccioni, R. (2009). Grapevine cv.'Riesling'water use in the northeastern united states. *Irrigation Science, 27*(3), 253-262.

Ip, K., Lam, M., & Miller, A. (2010). Shading performance of a vertical deciduous climbing plant canopy. *Building and Environment, 45*(1), 81-88. doi:10.1016/j.buildenv.2009.05.003

Isnard, S., & Silk, W. K. (2009). Moving with climbing plants from charles darwin's time into the 21st century. *American Journal of Botany, 96*(7), 1205-1221. doi:10.3732/ajb.0900045 [doi]

Isobe, S. (1969). Theory of the light distribution and photosynthesis in canopies of randomly dispersed foliage area. *Tokyo Nat Inst Agr Sci Bull Ser A Phys Statist.*

Jackson, J., & Palmer, J. (1979). A simple model of light transmission and interception by discontinuous canopies. *Annals of Botany, 44*(3), 381-383.

Jaffe, M., & Galston, A. (1968). The physiology of tendrils. *Annual Review of Plant Physiology, 19*(1), 417-434.

Jim, C. (2015). Thermal performance of climber greenwalls: Effects of solar irradiance and orientation. *Applied Energy, 154*, 631-643.

Jones, H. G. (1992). *Plants and microclimate : A quantitative approach to environmental plant physiology* (2nd ed. ed.). Cambridge England] ; New York: Cambridge University Press.

JONNES, J. (2011). What is a tree worth? *The Wilson Quarterly (1976-), 35*(1), 34-41.

Köhler, M. (2008). Green facades—a view back and some visions. *Urban Ecosystems, 11*(4), 423-436. doi:10.1007/s11252-008-0063-x

Kontoleon, K. J., & Eumorfopoulou, E. A. (2010). The effect of the orientation and proportion of a plant-covered wall layer on the thermal performance of a building zone. *Building and Environment, 45*(5), 1287-1303. doi:10.1016/j.buildenv.2009.11.013

Koyama, T., Yoshinaga, M., Hayashi, H., Maeda, K., & Yamauchi, A. (2013). Identification of key plant traits contributing to the cooling effects of green facades using freestanding walls. *Building and Environment, 66*, 96-103.

Koyama, T., Yoshinaga, M., Maeda, K., & Yamauchi, A. (2015). Transpiration cooling effect of climber greenwall with an air gap on indoor thermal environment. *Ecological Engineering, 83*, 343-353.

Lascano, R., Baumhardt, R., & Lipe, W. (1992). Measurement of water flow in young grapevines using the stem heat balance method. *American Journal of Enology and Viticulture, 43*(2), 159-165.

Lebon, E., Schultz, H., & Dumas, V. (1995). Application d'un modèle d'interception du rayonnement solaire par la vigne pour la simulation du bilan hydrique et de la photosynthèse à l'échelle du couvert: Résultats préliminaires. *Compte Rendu, , 8* 31-39.

Leicht-Young, S. A., Hormaza, J. I., Boufford, D. E., & Rose, N. (2014). Seeing the lianas in the trees: Woody vines of the temperate zone. *Arnoldia, 72*(1), 2.

Lemeur, R., & Blad, B. L. (1974). A critical review of light models for estimating the shortwave radiation regime of plant canopies. *Agricultural Meteorology, 14*(1-2), 255-286.

Leuzinger, S., Hartmann, A., & Körner, C. (2011). Water relations of climbing ivy in a temperate forest. *Planta, 233*(6), 1087-1096.

Liu, W., Pool, R., Wenkert, W., & Kriedemann, P. (1978). Changes in photosynthesis, stomatal resistance and abscisic acid of vitis labruscana through drought and irrigation cycles. *American Journal of Enology and Viticulture, 29*(4), 239-246.

Liu, W., Wenkert, W., Allen Jr, L., & Lemon, E. (1978). Soil-plant water relations in a new york vineyard; resistances to water movement. *Journal American Society for Horticultural Science.*

Lu, P., Yunusa, I. A., Walker, R. R., & Müller, W. J. (2003). Regulation of canopy conductance and transpiration and their modelling in irrigated grapevines. *Functional Plant Biology, 30*(6), 689-698.

Mabrouk, H., Carbonneau, A., & Sinoquet, H. (1997). Canopy structure and radiation regime in grapevine. I. spatial and angular distribution of leaf area in two canopy systems. *Vitis-Geilweilerhof-, 36*, 119-124.

Magnanini, E., & Intrieri, C. (1987). Calcolo della intercettazione della radiazione solare in vigneti a controspalliera. *Vignevini, 14*(3), 47-52.

McPherson, E. G., Nowak, D. J., & Rowntree, R. A. (1994). Chicago's urban forest ecosystem: Results of the chicago urban forest climate project.

McPherson, E. G., Nowak, D., Heisler, G., Grimmond, S., Souch, C., Grant, R., & Rowntree, R. (1997). Quantifying urban forest structure, function, and value: The chicago urban forest climate project. *Urban Ecosystems, 1*(1), 49-61.

McPherson, E. G., & Rowntree, R. A. (1993). Energy conservation potential of urban tree planting. *Journal of Arboriculture, 19*, 321-321.

Meier, A. K. (1990). Strategic landscaping and air- conditioning savings: A literature review. *Energy & Buildings, 15*(3), 479-486. doi:10.1016/0378-7788(90)90024-D

Mitsch, W. (2012). What is ecological engineering? *Ecological Engineering; Ecol.Eng., 45*, 5-12. doi:10.1016/j.ecoleng.2012.04.013

Mitsch, W., & Jorgensen, S. (2003). Ecological engineering: A field whose time has come. *Ecological Engineering; Ecol.Eng., 20*(5), 363-377. doi:10.1016/j.ecoleng.2003.05.001

Moffat, A. S. (1981). In Schiler M. (Ed.), *Landscape design that saves energy* (1st ed. ed.). New York: Morrow.

Monteith, J., & Unsworth, M. (2013). *Principles of environmental physics: Plants, animals, and the atmosphere* Academic Press.

Monteith, J. L. (2008). In Unsworth M. H. (Ed.), *Principles of environmental physics* (3rd ed. ed.). Amsterdam ; Boston: Elsevier ;.

Moutinho-Pereira, J., Correia, C., Gonçalves, B., Bacelar, E., & Torres-Pereira, J. (2004). Leaf gas exchange and water relations of grapevines grown in three different conditions. *Photosynthetica, 42*(1), 81-86.

National Oceanic and Atmospheric Administration. (2017). NOAA solar position calculator. Retrieved from https://www.esrl.noaa.gov/gmd/grad/solcalc/azel.html

Nellis, G. (2009). In Klein S. A. (Ed.), *Heat transfer*. Cambridge ; New York: Cambridge University Press.

Nowak, D. J., Rowntree, R. A., McPherson, E. G., Sisinni, S. M., Kerkmann, E. R., & Stevens, J. C. (1996). Measuring and analyzing urban tree cover. *Landscape and Urban Planning, 36*(1), 49-57.

Ottelé, M., van Bohemen, H. D., & Fraaij, A. L. (2010). Quantifying the deposition of particulate matter on climber vegetation on living walls. *Ecological Engineering, 36*(2), 154-162.

Padgett-Johnson, M., Williams, L., & Walker, M. (2003a). Vine water relations, gas exchange, and vegetative growth of seventeen vitis species grown under irrigated and nonirrigated conditions in california. *Journal of the American Society for Horticultural Science, 128*(2), 269-276.

Padgett-Johnson, M., Williams, L., & Walker, M. (2003b). Vine water relations, gas exchange, and vegetative growth of seventeen vitis species grown under irrigated and nonirrigated conditions in california. *Journal of the American Society for Horticultural Science, 128*(2), 269-276.

Parker J.H. (1983). Landscaping to reduce the energy used in cooling buildings urban forestry]. *Journal of Forestry; Landscaping to Reduce the Energy used in Cooling Buildings Urban Forestry]., 81*(2)

Patakas, A., Noitsakis, B., & Chouzouri, A. (2005). Optimization of irrigation water use in grapevines using the relationship between transpiration and plant water status. *Agriculture, Ecosystems & Environment, 106*(2), 253-259.

Pearcy, R. W. (. (1989). *Plant physiological ecology : Field methods and instrumentation*. London ; New York: Chapman and Hall.

Pérez, G., Coma, J., Sol, S., & Cabeza, L. F. (2017). Green facade for energy savings in buildings: The influence of leaf area index and facade orientation on the shadow effect. *Applied Energy, 187*, 424-437.

Pérez, G., Rincón, L., Vila, A., González, J. M., & Cabeza, L. F. (2011). Green vertical systems for buildings as passive systems for energy savings. *Applied Energy, 88*(12), 4854-4859.

Perini, K., Ottelé, M., Haas, E., & Raiteri, R. (2011). Greening the building envelope, façade greening and living wall systems. *Open Journal of Ecology, 1*(01), 1.

Perini, K., Ottele, M., Fraaij, A., Haas, E., & Raiteri, R. (2011). Vertical greening systems and the effect on air flow and temperature on the building envelope. *Building and Environment, 46*(11), 2287-2294. doi:10.1016/j.buildenv2011.05.009

Poblete-Echeverría, C., & Ortega-Farias, S. (2013). Evaluation of single and dual crop coefficients over a drip-irrigated merlot vineyard (vitis vinifera L.) using combined measurements of sap flow sensors and an eddy covariance system. *Australian Journal of Grape and Wine Research, 19*(2), 249-260.

Price, J. W. (2010). *Green facade energetics* (Masters Desgree).

Putz, F. (2014,). Vine ecology: How lianas affect trees, arboreal animals, forests and ecological succession. *Trends in Ecology & Evolution, 17(5),* 223-230.

Putz, F. E. (1984). The natural history of lianas on barro colorado island, panama. *Ecology, 65*(6), 1713-1724.

Putz, F. E. (1983). Liana biomass and leaf area of a " tierra firme" forest in the rio negro basin, venezuela. *Biotropica, 15*(3), 185-189.

Putz, F. E., & Mooney, H. A. (1991). *The biology of vines*. Cambridge ; New York: Cambridge ; New York : Cambridge University Press, 1991.

Quick, W., Chaves, M., Wendler, R., David, M., Rodrigues, M., Passaharinho, J., . . . Stitt, M. (1992). The effect of water stress on photosynthetic carbon metabolism in four species grown under field conditions. *Plant, Cell & Environment, 15*(1), 25-35.

Rana, G., & Katerji, N. (2000). Measurement and estimation of actual evapotranspiration in the field under mediterranean climate: A review. *European Journal of Agronomy; Eur.J.Agron., 13*(2-3), 125-153.

Raschke, K. (1975). *Stomatal action* doi:10.1146/annurev.pp.26.060175.001521

Reynolds, A. G., & Heuvel, J. E. V. (2009). Influence of grapevine training systems on vine growth and fruit composition: A review. *American Journal of Enology and Viticulture, 60*(3), 251-268.

Rogiers, S. Y., Greer, D. H., Hutton, R. J., & Clarke, S. J. (2011). Transpiration efficiency of the grapevine cv. semillon is tied to VPD in warm climates. *Annals of Applied Biology, 158*(1), 106-114.

Rose, C. W., & Sharma, M. L. (1984). *Summary and recommendations of the workshop on " evapotranspiration from plant communities"* doi:10.1016/B978-0-444-42250-7.50023-9

Rowe, D. (2011). Green roofs as a means of pollution abatement. *Environmental Pollution; Environ.Pollut., 159*(8-9), 2100-2110. doi:10.1016/j.envpol.2010.10.029

Sanches, M., & Válio, I. (2008). Photosynthetic response of two tropical liana species grown under different irradiances. *Photosynthetica, 46*(4), 557-566.

Schultz, H. (1995). Water relations and photosynthetic responses of two grapevine cultivars of different geographical origin during water stress. *Strategies to Optimize Wine Grape Quality 427,* , 251-266.

Schumann, L. M. (2007). *Ecologically inspired design of green roof retrofit* ProQuest.

Smart, R. (1974). Aspects of water relations of the grapevine (vitis vinifera). *American Journal of Enology and Viticulture, 25*(2), 84-91.

Smart, R., & Lang, A. (1973). A field method for estimating sun-leaf angles in productivity studies. *Agricultural Meteorology, 11*, 445-450.

Smart, R. E. (1973). Sunlight interception by vineyards. *American Journal of Enology and Viticulture, 24*(4), 141-147.

Smart, R. E. (1985). Principles of grapevine canopy microclimate manipulation with implications for yield and quality. A review. *American Journal of Enology and Viticulture, 36*(3), 230-239.

Stec, W. J., van Paassen, A. H. C., & Maziarz, A. (2005). Modelling the double skin façade with plants. *Energy & Buildings, 37*(5), 419-427. doi:10.1016/j.enbuild.2004.08.008

Šuklje, T., Medved, S., & Arkar, C. (2016). On detailed thermal response modeling of vertical greenery systems as cooling measure for buildings and cities in summer conditions. *Energy, 115*, 1055-1068.

Susorova, I., Angulo, M., Bahrami, P., & Stephens, B. (2013). A model of vegetated exterior facades for evaluation of wall thermal performance. *Building and Environment, 67*, 1-13.

Susorova, I., Azimi, P., & Stephens, B. (2014). The effects of climbing vegetation on the local microclimate, thermal performance, and air infiltration of four building facade orientations. *Building and Environment, 76*, 113-124.

Tan, C. L., Wong, N. H., Tan, P. Y., Ismail, M., & Wee, L. Y. (2017). Growth light provision for indoor greenery: A case study. *Energy and Buildings, 144*, 207-217.

Thom, A., & Oliver, H. (1977). On penman's equation for estimating regional evaporation. *Quarterly Journal of the Royal Meteorological Society, 103*(436), 345-357.

Tilley, D., Price, J., Matt, S., & Marrow, B. (2012). Vegetated walls: Thermal and growth properties of structured green facades. *Final Report to Green Roofs for Healthy Cities.*

Tyree, M. T., & Ewers, F. W. (1991). The hydraulic architecture of trees and other woody plants. *New Phytologist, 119*(3), 345-360.

Vogel, S. (1968). " Sun leaves" and " shade leaves": Differences in convective heat dissipation. *Ecology, 49*(6), 1203.

Wang, H. F. D., D.N. (1999). Cooling effect of ivy on a wall. *Experimental Heat Transfer, 12*(3), 235-245. doi:10.1080/089161599269708

Wermelinger, B., Baumgärtner, J., & Gutierrez, A. (1991). A demographic model of assimilation and allocation of carbon and nitrogen in grapevines. *Ecological Modelling, 53*, 1-26.

Wermelinger, B., & Koblet, W. (1990). Seasonal growth and nitrogen distribution in grapevine leaves, shoots and grapes. *Vitis, 29*(1), 15-26.

White, R. F. (1954). *Effects of landscape development on the natural ventilation of buildings and their adjacent areas*. College Station: Texas Engineering Experiment Station.

Winkel, T., & Rambal, S. (1990). Stomatal conductance of some grapevines growing in the field under a mediterranean environment. *Agricultural and Forest Meteorology, 51*(2), 107-121.

Wolter, S., Diebel, J., & Schroeder, F. (2008). Development of hydroponic systems for urban façade greenery. *International Symposium on Soilless Culture and Hydroponics 843,* 393-402.

Wong, E., Akbari, H., Bell, R., & Cole, D. (2011). Reducing urban heat islands: Compendium of strategies. *Environmental Protection Agency, Retrieved May, 12*, 2011.

Wong, N. H., Kwang Tan, A. Y., Chen, Y., Sekar, K., Tan, P. Y., Chan, D., . . . Wong, N. C. (2010). Thermal evaluation of vertical greenery systems for building walls. *Building and Environment, 45*(3), 663-672. doi:10.1016/j.buildenv.2009.08.005

Yazdanseta, A., & Norford, L. (2017). Estimating the untapped cooling power of green walls as evaporative coolers. *Building Physics 03: Innovative Envelopes.*

Yin, H., Kong, F., Middel, A., Dronova, I., Xu, H., & James, P. (2017). Cooling effect of direct green façades during hot summer days: An observational study in nanjing, china using TIR and 3DPC data. *Building and Environment, 116*, 195-206.

Yunusa, I., Walker, R., Loveys, B., & Blackmore, D. (2000). Determination of transpiration in irrigated grapevines: Comparison of the heat-pulse technique with gravimetric and micrometeorological methods. *Irrigation Science, 20*(1), 1-8.

Appendix

Arta Yazdanseta
66 Dana St. #2
Cambridge, MA 02138

June.24.2017

Dear Professor Elsner,

I am completing a doctoral dissertation at the Harvard University entitled "Designing green walls: An early-design framework to estimate the cooling impact of indirect green walls on buildings in different climates" I would like your permission to reprint in my dissertation the images from your conference presentation:

ERWIN ELSNER, 2014. *Wine Grape Training Systems.* http://msue.anr.msu.edu/uploads/234/43701/Elsner.Training_Systems.pdf: Michigan State University.

The excerpts to be reproduced are:

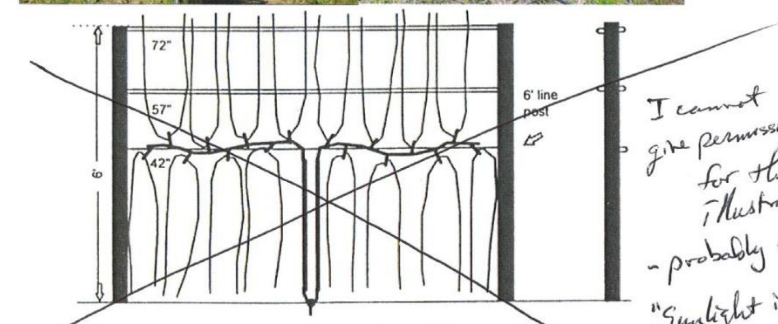

Fig. 11. The Smart-Dyson training system which has a vertically divided canopy and is shoot positioned

I cannot give permission for the illustration
- probably from "Sunlight into Wine" by Richard Smart
- I'll keep looking

The requested permission extends to any future revisions and editions of my dissertation, including non- exclusive world rights in all languages, and to the prospective publication of my dissertation by ProQuest through its ProQuest® Dissertation Publishing business. ProQuest may produce and sell copies of my dissertation on demand and may make my dissertation available for free internet download at my request. These rights will in no way restrict republication of the material in any other form by you or by others authorized by you. Your signing of this letter will also confirm that you own [or your company owns] the copyright to the above described materials.

If these arrangements meet with your approval, please sign this letter where indicated below and return it to me in the enclosed return envelope. Thank you very much.

Sincerely,
Arta Yazdanseta

PERMISSION GRANTED FOR THE USE REQUESTED ABOVE: [signature]

Date: Jun 26, 2017

Estimating Independent Vining Green Wall's Summer Cooling Performance

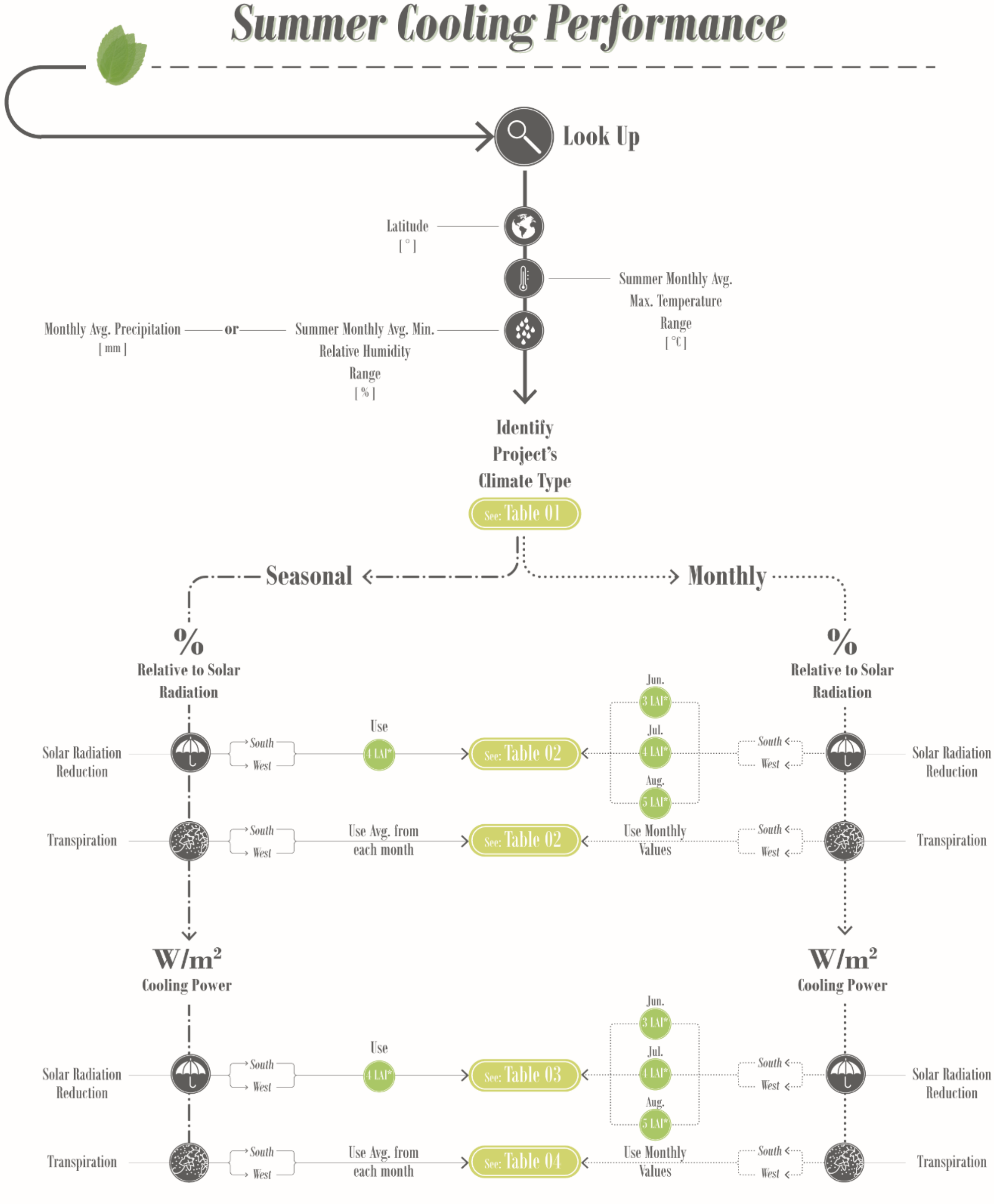

*Leaf Area Index: Ratio of the Projected Leaf Area to Wall Area

How to Use:

Step 1. Look up the latitude of your project, the average maximum temperature during the summer months (°C), and either the average minimum relative humidity range during the summer months (%) or the average precipitation during the summer months (mm).[1]

Step 2. Identify the climate category of your project using Table 01.

Seasonal Performance

Step 1. For the seasonal cooling performance for the south- and west-facing green walls, use Table 02 to look up the percentage cooling power values from solar radiation reduction of green walls with LAI[2] values of 4 for the month of July.

Calculate the summer average percentage of transpiration cooling power production for the two orientations using Table 02.

Note that these percentages are relative to the average monthly incident solar radiation at the site. Therefore, if the initial average monthly solar radiation gains at the south- and west-facing facades are known, you can further refine your estimation by considering the site specific values.

Step 2. To compare the seasonal shading performance of the two orientations, look up the actual cooling power values for green walls with LAI values of 4 for the month July using Table 03.

Similarly, compare the transpiration cooling power of the two orientations produced seasonally by calculating the average summer cooling power using Table 04.

Monthly Performance

Step 1. Look up the average monthly contributions to cooling power, in percentage terms, from transpiration and solar radiation reduction for south- and west-facing orientations using Table 02. Note that these percentages are relative to the average monthly incident solar radiation at the site.

While the percentages of cooling power from transpiration are similar for green walls with LAI values of 3, 4, and 5, the percentages of solar radiation reduction vary for each LAI value. It is recommended to assume LAI values of 3, 4, and 5 for the months of June, July, and August, respectively. For a conservative estimate of cooling power from solar radiation reduction, assume an LAI value of 4 for the months of July and August.

Step 2. Use Table 03 and Table 04 to look up the cooling power values in W/m^2 from solar radiation reduction and transpiration cooling for the south- and west-facing orientations.

These values are useful as simple back-of-the-envelope calculations to get a general understanding of the expected cooling effect of the canopy in the climate of your project.

Assumptions

Open field conditions where a green wall is exposed to sunlight throughout the day

Uniform and full distribution of the canopy

No water limits

1. Some of the useful resources for finding the needed weather data are the U.S. Climate Data website *https://www.usclimatedata.com*, and Climate Consultant tool *http://www.energy-design-tools.aud.ucla.edu*.

2. LAI: Leaf Area Index defines the ratio of the projected leaf area to wall area

Example:

As a case study, let's consider a project located in Boston, MA.

Step 1. look up the latitude and monthly summer climate conditions. The table below shows the values obtained from Climate Consultant, taken at Logan Airport in Boston, MA.

Boston – Latitude. 42° N	June	July	August
Avg. Max. Temp. (°C)	32	35.5	31
Avg. Min. Relative Humidity (%)	59	55	60
Avg. Precipitation (mm)	93	87	85

Step 2. Comparing the Boston's average maximum temperatures and average precipitation for the summer months with the climate categories listed in the Table 01, we see that the warm and humid climate scenario best represents the climatic condition of this project.

Let's assume we are interested in evaluating and comparing the seasonal cooling performances of south- and west-facing green walls for maximum cooling effect.

Seasonal Performance

Step 1. Use Table 02 and look up the seasonal percentage of cooling from solar radiation reduction for the two orientations by assuming that the green walls have LAI values of 4 of July.

Use Table 02 calculate the percentage of the seasonal transpiration cooling power for the two orientations by taking the average of the monthly performances.

The results show that the seasonal transpiration cooling power percentages for the south- and west-facing green walls are 36% and 30%, respectively.

At the first glance, it seems that the seasonal cooling performance of the south- is slightly better than that of the west-facing green wall.

That is because both orientations provide similar percentages of solar radiation reduction (85%). However, the south provides 6% more cooling power compared to west-facing green wall.

The cooling power percentage values are very useful when solar radiation gains are known. Tools such as Climate Consultant, Diva for Rhino, and Ladybug can be used to obtain the initial solar radiation gains at the south- and west-facing facades.

However, for this example, let's assume that the initial solar radiation values for the south- and west-facades are not available.

Step 2. Use Table 03 and Table 04 to further evaluate and compare the performances of the two orientations based on actual cooling power values (W/m^2).

The cooling from the solar radiation reduction of the south- and west-facing green walls with LAI values of 4 in July are 123 W/m^2 and 156 W/m^2, respectively.

Accordingly, the west provides 23% more solar radiation reduction compared to south-facing green wall.

Comparing the average seasonal transpiration cooling power (calculated from the average of monthly values) shows minimal performance difference (approximately 2%) between the two orientations.

The above investigation shows that for a project in Boston, a west-facing green wall can provide greater average seasonal cooling power compared to a south-facing one. The expected seasonal cooling power values from the solar radiation reduction and transpiration cooling power production for the west-facing green wall are 156 W/m^2 and 59 W/m^2, respectively.

In addition to evaluating and comparing the performances of the two orientations, practitioners can use this method to optimize for each cooling method.

For example, if the goal is to produce the largest cooling power, either orientation is a valid choice. This is especially significant for integrated design investigations where the objective is to utilize the produced cooling power to directly

1. Some of the useful resources for finding the needed weather data are the U.S. Climate Data website *https://www.usclimatedata.com*, and Climate Consultant tool *http://www.energy-design-tools.aud.ucla.edu*.

2. LAI: Leaf Area Index defines the ratio of the projected leaf area to wall area

address the cooling loads of the buildings.

Furthermore, the above evaluations can be used for energy modeling purposes. For example, by modeling the canopy as a plane with 15% porosity, the energy savings from the shading of the canopy can be estimated.

Monthly Performance

For a more detailed performance evaluation of the mentioned Boston Project, conduct monthly studies for the south- and west-facing green walls.

Step 1. Use Table 02 to look up the monthly percentages of cooling power from solar radiation reduction and transpiration cooling power production.

To account for the changes in canopy geometry and its impact on solar radiation interception, use the percentage values for LAI values of 3 for June, 4 for July, and 5 for August. Note that for the monthly transpiration cooling power a single value is considered for various LAIs.

Accordingly, the percentages of solar radiation reduction for the two ordinations are identical throughout the summer months: 75% in June, 85% in July, and 92% in August.

These percentage values can be used for the monthly thermal and daylight design performance evaluations. For example, by modeling planes with 25%, 15%, and 8% porosity (with randomly arranged openings) representing each summer month, the thermal and daylight impacts of green walls can be easily simulated.

The percentage of transpiration cooling power relative to solar radiation gains of the south-facing green wall is larger by 18% in June and 19% in July compared to the west-facing green wall.

This indicates that the south-facing green wall is more efficient in converting solar radiation into cooling power. Interestingly, in August, the performances of the two ordinations are almost identical due to the reduction of solar elevation in that month.

Similar to the previous example, let's assume that the initial solar radiation received by the south- and west-facing facades is unknown.

Step 2. Use Table 03 to look up the solar radiation reduction cooling power values for each summer month. In June and July, the west-facing green wall provides 41% (LAI of 3) and 27% (LAI of 4) more cooling power than does the the south-facing one. However, in August (LAI of 5), the performance difference between the two orientations is diminished.

Conventionally, as part of standard sustainable design considerations, it is recommended to avoid west-facing windows due to excess solar heat gains and glare problems during summer months.

The above investigations illustrate that green walls can address these concerns by obstructing up to 92% of solar radiation gains. The early-design matrices allow practitioners to easily and confidently estimate the performance of their design.

Step 3. Use Table 04 to look up the transpiration cooling power values (W/m^2) for the south- and west-facing green walls. The table shows that the monthly cooling power produced from the two orientations is similar throughout the summer.

These cooling power values can be used as a good estimate for the cooling performances of green walls as integrated design options.

The design implication of the above findings is that a west-facing green wall provides the largest cooling from solar radiation reduction. However, to maximize the transpiration cooling power production, either orientation is a valid choice.

Table 01 - Six climate catagories

Climate Type	***Monthly Average Maximum Temperature [°c]***	***Monthly Average Minimum Relative Humidity [%]***	***Monthly Average Precipitation [mm]***
Cool & Humid	20 to 26	50 to 55	> 50
Cool& Dry	21 to 26	30 to 40	< 50
Warm & Humid	27 to 32	55 to 60	> 50
Warm & Dry	28 to 32	20 to 30	< 50
Hot & Humid	32 to 40	60 to 65	> 50
Hot & Dry	33 to 40	10 to 20	< 50

Table 02 - Percentage of Cooling Power from the Transpiration and Shading of Various LAIs* (3, 4, and 5) of South- and West-Facing Green Walls For Six Climates. Assumed variables: height of 3 m, average canopy resistance, no wind condition.

Cool & Dry Climate												
	June				July				August			
	South Facing		West Facing		South Facing		West Facing		South Facing		West Facing	
Leaf Area Index	Average Transpiration Cooling Power Production [%]	Average Solar Radiation Reduction [%]	Average Transpiration Cooling Power Production [%]	Average Solar Radiation Reduction [%]	Average Transpiration Cooling Power Production [%]	Average Solar Radiation Reduction [%]	Average Transpiration Cooling Power Production [%]	Average Solar Radiation Reduction [%]	Average Transpiration Cooling Power Production [%]	Average Solar Radiation Reduction [%]	Average Transpiration Cooling Power Production [%]	Average Solar Radiation Reduction [%]
3		77.00		77.01		77.68		77.69		80.22		80.21
4	21.87	85.92	18.21	85.88	23.36	86.47	20.28	86.47	25.39	88.47	28.55	88.47
5		91.37		91.37		91.79		91.79		93.28		93.28

Cool & Humid Climate												
	June				July				August			
	South Facing		West Facing		South Facing		West Facing		South Facing		West Facing	
Leaf Area Index	Average Transpiration Cooling Power Production [%]	Average Solar Radiation Reduction [%]	Average Transpiration Cooling Power Production [%]	Average Solar Radiation Reduction [%]	Average Transpiration Cooling Power Production [%]	Average Solar Radiation Reduction [%]	Average Transpiration Cooling Power Production [%]	Average Solar Radiation Reduction [%]	Average Transpiration Cooling Power Production [%]	Average Solar Radiation Reduction [%]	Average Transpiration Cooling Power Production [%]	Average Solar Radiation Reduction [%]
3		77.67		77.00		77.69		77.68		80.21		80.21
4	47.72	85.91	37.20	85.92	33.79	86.47	29.34	86.47	25.39	88.46	28.55	88.47
5		91.10		91.37		91.79		91.79		93.28		90.77

Warm & Dry Climate												
	June				July				August			
	South Facing		West Facing		South Facing		West Facing		South Facing		West Facing	
Leaf Area Index	Average Transpiration Cooling Power Production [%]	Average Solar Radiation Reduction [%]	Average Transpiration Cooling Power Production [%]	Average Solar Radiation Reduction [%]	Average Transpiration Cooling Power Production [%]	Average Solar Radiation Reduction [%]	Average Transpiration Cooling Power Production [%]	Average Solar Radiation Reduction [%]	Average Transpiration Cooling Power Production [%]	Average Solar Radiation Reduction [%]	Average Transpiration Cooling Power Production [%]	Average Solar Radiation Reduction [%]
3		74.84		74.86		75.58		75.58		77.69		77.69
4	60.05	84.12	41.87	84.12	60.76	84.74	48.86	84.75	39.26	86.46	38.44	86.47
5		89.97		89.97		90.46		90.46		91.79		91.79

Warm & Humid Climate												
	June				July				August			
	South Facing		West Facing		South Facing		West Facing		South Facing		West Facing	
Leaf Area Index	Average Transpiration Cooling Power Production [%]	Average Solar Radiation Reduction [%]	Average Transpiration Cooling Power Production [%]	Average Solar Radiation Reduction [%]	Average Transpiration Cooling Power Production [%]	Average Solar Radiation Reduction [%]	Average Transpiration Cooling Power Production [%]	Average Solar Radiation Reduction [%]	Average Transpiration Cooling Power Production [%]	Average Solar Radiation Reduction [%]	Average Transpiration Cooling Power Production [%]	Average Solar Radiation Reduction [%]
3		74.85		74.84		75.58		75.58		77.69		77.69
4	40.79	84.12	30.44	84.12	37.20	84.74	30.48	84.74	30.10	86.47	29.72	86.47
5		89.97		89.97		90.46		90.46		91.84		91.79

Hot & Dry Climate												
	June				July				August			
	South Facing		West Facing		South Facing		West Facing		South Facing		West Facing	
Leaf Area Index	Average Transpiration Cooling Power Production [%]	Average Solar Radiation Reduction [%]	Average Transpiration Cooling Power Production [%]	Average Solar Radiation Reduction [%]	Average Transpiration Cooling Power Production [%]	Average Solar Radiation Reduction [%]	Average Transpiration Cooling Power Production [%]	Average Solar Radiation Reduction [%]	Average Transpiration Cooling Power Production [%]	Average Solar Radiation Reduction [%]	Average Transpiration Cooling Power Production [%]	Average Solar Radiation Reduction [%]
3		73.29		73.29		74.08		74.08		75.59		75.59
4	134.82	82.80	61.41	82.80	105.73	83.47	59.70	83.47	64.22	84.74	48.77	84.74
5		88.92		88.92		89.46		89.46		90.46		90.47

Hot & Humid Climate												
	June				July				August			
	South Facing		West Facing		South Facing		West Facing		South Facing		West Facing	
Leaf Area Index	Average Transpiration Cooling Power Production [%]	Average Solar Radiation Reduction [%]	Average Transpiration Cooling Power Production [%]	Average Solar Radiation Reduction [%]	Average Transpiration Cooling Power Production [%]	Average Solar Radiation Reduction [%]	Average Transpiration Cooling Power Production [%]	Average Solar Radiation Reduction [%]	Average Transpiration Cooling Power Production [%]	Average Solar Radiation Reduction [%]	Average Transpiration Cooling Power Production [%]	Average Solar Radiation Reduction [%]
3		72.47		72.47		73.29		73.30		74.08		74.08
4	71.85	82.09	43.14	82.10	74.40	82.79	43.92	82.80	47.72	83.47	36.13	83.47
5		88.35		88.35		88.92		88.92		89.46		89.46

*Leaf Area Index: Ratio of the Projected Leaf Area to Wall Area

Table 03 - Solar Radiation Reduction (w/m²) for Six Climates for Each Summer Month, for South- and West-Facing Orientations, and LAIs* of 3, 4, and 5 .

Cool & Dry Climate (k Based on Latitude of 48°)												
	June, K=0.49				July, K=0.5				August, , K=0.54			
	South Facing		West Facing		South Facing		West Facing		South Facing		West Facing	
Leaf Area Index	Initial Average Solar Gain $[W/m^2]$	Average Solar Radition Reduction $[W/m^2]$	Initial Average Solar Gain $[W/m^2]$	Average Solar Radition Reduction $[W/m^2]$	Initial Average Solar Gain $[W/m^2]$	Average Solar Radition Reduction $[W/m^2]$	Initial Average Solar Gain $[W/m^2]$	Average Solar Radition Reduction $[W/m^2]$	Initial Average Solar Gain $[W/m^2]$	Average Solar Radition Reduction $[W/m^2]$	Initial Average Solar Gain $[W/m^2]$	Average Solar Radition Reduction $[W/m^2]$
3	166.35	128.10	204.32	157.34	194.67	151.23	228.39	177.44	258.70	207.53	215.98	173.23
4	166.35	142.93	204.32	175.47	194.67	168.32	228.39	197.48	258.70	228.88	215.98	191.08
5	166.35	152.00	204.32	186.69	194.67	178.69	228.39	209.65	258.70	241.32	215.98	201.46

Cool & Humid Climate (k Based on Latitude of 48°)												
	June, K=0.49				July, K=0.5				August, , K=0.54			
	South Facing		West Facing		South Facing		West Facing		South Facing		West Facing	
Leaf Area Index	Initial Average Solar Gain $[W/m^2]$	Average Solar Radition Reduction $[W/m^2]$	Initial Average Solar Gain $[W/m^2]$	Average Solar Radition Reduction $[W/m^2]$	Initial Average Solar Gain $[W/m^2]$	Average Solar Radition Reduction $[W/m^2]$	Initial Average Solar Gain $[W/m^2]$	Average Solar Radition Reduction $[W/m^2]$	Initial Average Solar Gain $[W/m^2]$	Average Solar Radition Reduction $[W/m^2]$	Initial Average Solar Gain $[W/m^2]$	Average Solar Radition Reduction $[W/m^2]$
3	144.97	112.60	185.98	143.21	169.15	131.42	200.89	156.06	218.31	175.10	189.60	152.08
4	144.97	124.54	185.98	159.79	169.15	146.27	200.89	173.71	218.31	193.12	189.60	167.73
5	144.97	132.07	185.98	169.93	169.15	155.26	200.89	184.40	218.31	203.63	189.60	172.10

Warm & Dry Climate (k Based on Latitude of 40°)												
	June, k=0.46				July k=0.47				August k=0.5			
	South Facing		West Facing		South Facing		West Facing		South Facing		West Facing	
Leaf Area Index	Initial Average Solar Gain $[W/m^2]$	Average Solar Radition Reduction $[W/m^2]$	Initial Average Solar Gain $[W/m^2]$	Average Solar Radition Reduction $[W/m^2]$	Initial Average Solar Gain $[W/m^2]$	Average Solar Radition Reduction $[W/m^2]$	Initial Average Solar Gain $[W/m^2]$	Average Solar Radition Reduction $[W/m^2]$	Initial Average Solar Gain $[W/m^2]$	Average Solar Radition Reduction $[W/m^2]$	Initial Average Solar Gain $[W/m^2]$	Average Solar Radition Reduction $[W/m^2]$
3	136.82	102.39	202.90	151.90	154.20	116.55	190.68	144.12	213.24	165.66	202.44	157.27
4	136.82	115.09	202.90	170.68	154.20	130.67	190.68	161.59	213.24	184.37	202.44	175.05
5	136.82	123.10	202.90	182.56	154.20	139.49	190.68	172.50	213.24	195.73	202.44	185.82

Warm & Humid Climate (k Based on Latitude of 40°)												
	June, k=0.46				July k=0.47				August k=0.5			
	South Facing		West Facing		South Facing		West Facing		South Facing		West Facing	
Leaf Area Index	Initial Average Solar Gain $[W/m^2]$	Average Solar Radition Reduction $[W/m^2]$	Initial Average Solar Gain $[W/m^2]$	Average Solar Radition Reduction $[W/m^2]$	Initial Average Solar Gain $[W/m^2]$	Average Solar Radition Reduction $[W/m^2]$	Initial Average Solar Gain $[W/m^2]$	Average Solar Radition Reduction $[W/m^2]$	Initial Average Solar Gain $[W/m^2]$	Average Solar Radition Reduction $[W/m^2]$	Initial Average Solar Gain $[W/m^2]$	Average Solar Radition Reduction $[W/m^2]$
3	131.31	98.28	184.44	138.04	144.96	109.56	184.22	139.23	220.70	171.46	224.12	174.12
4	131.31	110.45	184.44	155.14	144.96	122.84	184.22	156.11	220.70	190.84	224.12	193.79
5	131.31	118.14	184.44	165.95	144.96	131.13	184.22	166.65	220.70	202.68	224.12	205.72

Hot & Dry Climate (k Based on Latitude of 32°)												
	June, k=0.44				July, k=0.45				August, k=0.47			
	South Facing		West Facing		South Facing		West Facing		South Facing		West Facing	
Leaf Area Index	Initial Average Solar Gain $[W/m^2]$	Average Solar Radition Reduction $[W/m^2]$	Initial Average Solar Gain $[W/m^2]$	Average Solar Radition Reduction $[W/m^2]$	Initial Average Solar Gain $[W/m^2]$	Average Solar Radition Reduction $[W/m^2]$	Initial Average Solar Gain $[W/m^2]$	Average Solar Radition Reduction $[W/m^2]$	Initial Average Solar Gain $[W/m^2]$	Average Solar Radition Reduction $[W/m^2]$	Initial Average Solar Gain $[W/m^2]$	Average Solar Radition Reduction $[W/m^2]$
3	110.23	80.79	254.30	186.37	129.78	96.14	241.10	178.60	200.00	151.17	270.61	204.54
4	110.23	91.26	254.30	210.56	129.78	108.33	241.10	201.24	200.00	169.48	270.61	229.31
5	110.23	98.01	254.30	226.13	129.78	116.10	241.10	215.68	200.00	180.93	270.61	244.81

Hot & Humid Climate (k Based on Latitude of 25°)												
	June, k=0.43				July, k=0.44				August, k=0.45			
	South Facing		West Facing		South Facing		West Facing		South Facing		West Facing	
Leaf Area Index	Initial Average Solar Gain $[W/m^2]$	Average Solar Radition Reduction $[W/m^2]$	Initial Average Solar Gain $[W/m^2]$	Average Solar Radition Reduction $[W/m^2]$	Initial Average Solar Gain $[W/m^2]$	Average Solar Radition Reduction $[W/m^2]$	Initial Average Solar Gain $[W/m^2]$	Average Solar Radition Reduction $[W/m^2]$	Initial Average Solar Gain $[W/m^2]$	Average Solar Radition Reduction $[W/m^2]$	Initial Average Solar Gain $[W/m^2]$	Average Solar Radition Reduction $[W/m^2]$
3	85.89	62.24	155.77	112.89	100.59	73.72	185.60	136.04	139.30	103.18	195.94	145.15
4	85.89	70.51	155.77	127.89	100.59	83.29	185.60	153.67	139.30	116.27	195.94	163.55
5	85.89	75.88	155.77	137.63	100.59	89.45	185.60	165.04	139.30	124.61	195.94	175.28

*Leaf Area Index: Ratio of the Projected Leaf Area to Wall Area

Table 04 - Monthly Average Transpiration Cooling Power for Six Climates for Well-Watered, South- and West-Facing Green Walls. Assumed design variables: LAI* of 3, height of 3 m, no wind condition, and average stomata resistances (r_l s/m) for each climate.

Cool & Humid Climate, r_l = 115 s/m											
Jun				July				August			
South		West		South		West		South		West	
Average Cooling Power [W/m^2]	Monthly Average Solar Radition [W/m^2]	Average Cooling Power [W/m^2]	Monthly Average Solar Radition [W/m^2]	Average Cooling Power [W/m^2]	Monthly Average Solar Radition [W/m^2]	Average Cooling Power [W/m^2]	Monthly Average Solar Radition [W/m^2]	Average Cooling Power [W/m^2]	Monthly Average Solar Radition [W/m^2]	Average Cooling Power [W/m^2]	Monthly Average Solar Radition [W/m^2]
69.18	144.97	69.18	185.98	57.15	169.15	58.94	200.89	55.42	218.31	54.14	189.60

Cool & Dry Climate, r_l = 255.71 s/m											
Jun				July				August			
South		West		South		West		South		West	
Average Cooling Power [W/m^2]	Monthly Average Solar Radition [W/m^2]	Average Cooling Power [W/m^2]	Monthly Average Solar Radition [W/m^2]	Average Cooling Power [W/m^2]	Monthly Average Solar Radition [W/m^2]	Average Cooling Power [W/m^2]	Monthly Average Solar Radition [W/m^2]	Average Cooling Power [W/m^2]	Monthly Average Solar Radition [W/m^2]	Average Cooling Power [W/m^2]	Monthly Average Solar Radition [W/m^2]
36.38	166.35	37.21	204.32	45.47	194.67	46.33	228.39	44.31	258.70	43.41	215.98

Warm & Dry Climate, r_l = 151.62 s/m											
Jun				July				August			
South		West		South		West		South		West	
Average Cooling Power [W/m^2]	Monthly Average Solar Radition [W/m^2]	Average Cooling Power [W/m^2]	Monthly Average Solar Radition [W/m^2]	Average Cooling Power [W/m^2]	Monthly Average Solar Radition [W/m^2]	Average Cooling Power [W/m^2]	Monthly Average Solar Radition [W/m^2]	Average Cooling Power [W/m^2]	Monthly Average Solar Radition [W/m^2]	Average Cooling Power [W/m^2]	Monthly Average Solar Radition [W/m^2]
82.16	136.82	84.96	202.90	88.08	144.96	90.00	184.22	86.64	220.70	86.16	224.12

Warm & Humid Climate, r_l = 128.45 s/m											
Jun				July				August			
South		West		South		West		South		West	
Average Cooling Power [W/m^2]	Monthly Average Solar Radition [W/m^2]	Average Cooling Power [W/m^2]	Monthly Average Solar Radition [W/m^2]	Average Cooling Power [W/m^2]	Monthly Average Solar Radition [W/m^2]	Average Cooling Power [W/m^2]	Monthly Average Solar Radition [W/m^2]	Average Cooling Power [W/m^2]	Monthly Average Solar Radition [W/m^2]	Average Cooling Power [W/m^2]	Monthly Average Solar Radition [W/m^2]
53.56	131.31	56.14	184.44	53.92	144.96	56.14	184.22	66.44	220.70	66.60	224.12

Hot & Dry Climate, r_l = 125.09 s/m											
Jun				July				August			
South		West		South		West		South		West	
Average Cooling Power [W/m^2]	Monthly Average Solar Radition [W/m^2]	Average Cooling Power [W/m^2]	Monthly Average Solar Radition [W/m^2]	Average Cooling Power [W/m^2]	Monthly Average Solar Radition [W/m^2]	Average Cooling Power [W/m^2]	Monthly Average Solar Radition [W/m^2]	Average Cooling Power [W/m^2]	Monthly Average Solar Radition [W/m^2]	Average Cooling Power [W/m^2]	Monthly Average Solar Radition [W/m^2]
148.61	110.23	156.16	254.30	137.22	129.78	143.94	241.10	128.45	200.00	131.97	270.61

Hot & Humid Climate, r_l = 91.55 s/m											
Jun				July				August			
South		West		South		West		South		West	
Average Cooling Power [W/m^2]	Monthly Average Solar Radition [W/m^2]	Average Cooling Power [W/m^2]	Monthly Average Solar Radition [W/m^2]	Average Cooling Power [W/m^2]	Monthly Average Solar Radition [W/m^2]	Average Cooling Power [W/m^2]	Monthly Average Solar Radition [W/m^2]	Average Cooling Power [W/m^2]	Monthly Average Solar Radition [W/m^2]	Average Cooling Power [W/m^2]	Monthly Average Solar Radition [W/m^2]
61.71	85.89	67.19	155.77	74.84	100.59	81.52	185.60	66.47	139.30	70.80	195.94

*Leaf Area Index: Ratio of the Projected Leaf Area to Wall Area